EXPERIMENTAL STUDIES OF ELECTRONIC, VIBRONIC AND EXCITONIC EFFECTS IN SOME MOLECULAR CRYSTALS

by

DAVID H. SPIELBERG

A dissertation submitted to the Graduate Faculty in Physics in partial fulfillment of the requirements for the degree of Doctor of Philosophy, The City University of New York.

1970

This manuscript has been read and accepted for the Graduate Faculty in Physics in satisfaction of the dissertation requirement for the degree of Doctor of Philosphy.

Mar 24 1970
date

Arthur C. Damask
Chairman of Executive Committee

March 26 1970
date

Executive Officer

Professor Milton Furst
Professor Mark Miksic
Professor William Miller
Doctor I. Lefkowitz

Supervisory Committee

The City University of New York

TABLE OF CONTENTS

TABLES

FIGURES

CHAPTER ONE

1. Introduction

Interest in the study of organic compounds has been stimulated during the past ten years by several factors. The first is the advance in the techniques for obtaining single crystals of reproducible purity and perfection. The fact that organic materials are for the most part bound by the relatively weak van der Waal forces required special care in order to purify without ruining the sample.

Secondly, organic materials have become important because of industrial interest in finding new materials for use as scintillators, semiconductors, thermoelectrics, and piezoelectrics.

Of major concern to us was the problem of purity. In the literature, there was ample evidence of the ambiguity of results which can follow from insufficient consideration of the necessity of dealng with specified purities. The case of the specific heat anomaly in phenanthrene ($C_{10}H_{22}$) is an example of this problem. In 1950, Ueberreiter and Orthmann reported an anomalous heat absorption of about 600 calories/mole with phenanthrene of unspecified purity.[1] In 1966, specifying the method of purification, Arndt and Damask reported the value at about 380 calories/mole.[2] Again in 1967, Ringel, Arndt, and Damask studied the anomaly in deuterated material as a function of purity.[3] They found that the effect was suppressed by impurities, with the "as received" material giving a value of about 150 calories/mole,

as compared with their purified material which gave a value of 310 calories /mole.

Thus the question of reproduceability demands the routine indication of at least the purification procedure, if not the actual purity itself.

Concerning the use of single crystals rather than powdered or pollycrystalline samples, when dealing with anisotropic materials, there is no question but that studies on single crystals, made in the various crystallographic directions is the only correct way to proceed. Yet the difficulty in obtaining large single crystals has until recently been only occasionally overcome. The advent of a whole series of techniques, useful for the purification of organic materials, has made the growth of single crystals meaningful. Among these techniques are liquid chromatography, vacuum sublimation, and zone refining, and are amply described in the literature.[4]

Previously, growing large single crystals from solution ran the risk of incorporating the solvent molecules within the crystal lattice as an impurity. Growth from the melt does not present this problem. However, one must be very careful to check that the material has not been changed upon melting, due to the high thermal instability of many organic materials. This may be monitored using a gas chromatograph.

2. The Reported Heat Capacity Anomaly in Phenanthrene

As can be seen in Fig.1.1, the phenanthrene molecule is made up of three benzene rings fused together. The name derives from the fact that it contains a diphenyl group (Fig.1.1b) and is isomeric with anthracene (Fig.1.1c). The molecule is slightly non planar in the crystal, the 2,3 and 6,7 carbons being displaced inopposite directions from the plane of the center ring by about 0.04 Å. It is believed that intramolecular overcrowding of the hydrogen atoms in the 4,5 positions is the result of this distortion.[5] The hydrogen atoms are not shown in the Figure.

The position of the phenanthrene molecule in the unit cell is shown in Fig.1.2. The crystal is monoclinic, face-centered-cubic with two molecules per unit cell.

The melting temperature of phenanthrene is about 98°C. It is colorless and has a room temperature dark resistivity of about 10^{17} ohms-cm.[6] The melting point of phenanthrene and its high resistivity are typical of the aromatic hyrocarbons.

A large percentage of organic materials exhibit a thermal anomaly of some kind or another.[7] The heat capacity anomaly reported by Arndt and Damask, referred to above, was detected using a differential, isochronal, microcalorimeter developed by Arndt and Fujita[8]. The phenomenon did not appear to be an isothermal process. No latent heat was observed to

a)

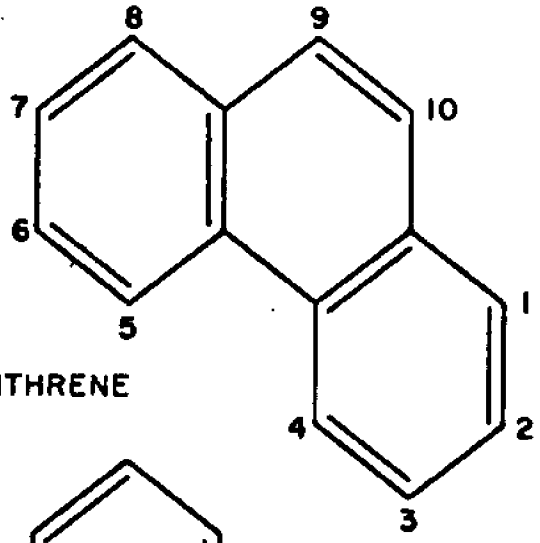

PHENANTHRENE

b)

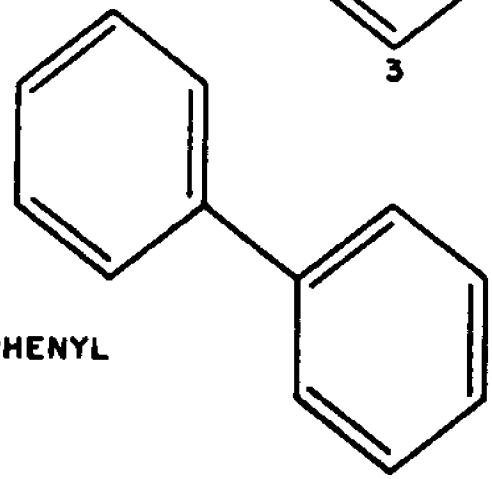

DIPHENYL

c)

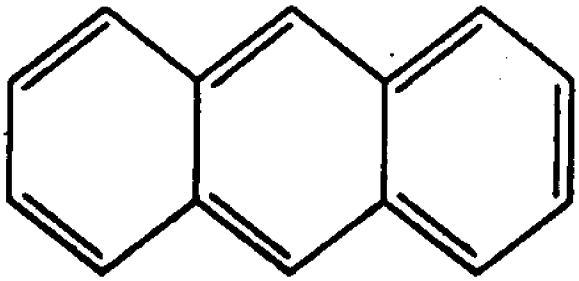

ANTHRACENE

FIG. I.I

(a) The Molecular Structure of Phenanthrene and its Relationship to (b) Diphenyl and (c) Anthracene.

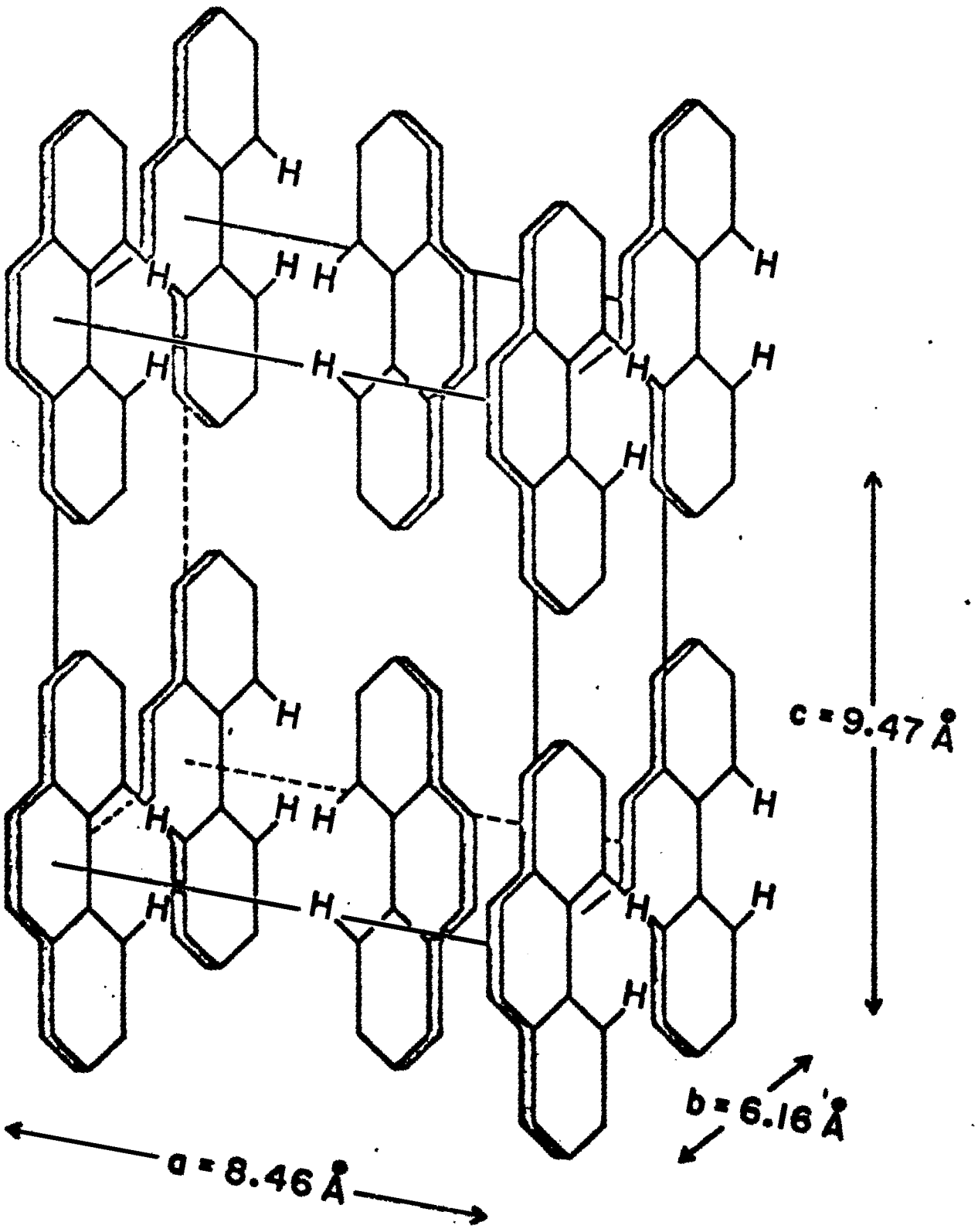

FIG. 1.2

The Crystal Structure of Phenanthrene Indicating the Positions of the Molecules in the Unit Cell.

be associated with the process, nor was a satisfactory model presented to explain the anomaly.

Theoretical models correlating the thermodynamic properties of ideal gases with real gases have been relatively successful. However, when dealing with the highly interdependent components of organic solids, few useful correlations with the ideal gas model emerge. Changes in the crystal structure and the phase changes of organic solids, which are often caused by relatively minor differences in molecular structure, have a profound effect on the heat capacity of an organic solid[9]. Furthermore, deviations of experimental results from ideal behavior can be attributed to impurity effects, internal strains, and failure to obtain thermodynamic equilibrium during the taking of a measurement.

Characterizing a transition as first-order or of some higher order is made difficult due to the slow rate of equilibration of the system under investigation. Although usually not so long, it may take as long as a day or more for the system to equilibrate thermally in the vicinity of a transition. Thus, for example, accurate measurements of the heat capacity in the transition region are prejudiced, since it may be impossible to unambiguously determine whether or not a process is isothermal.

The shape of the curve presented by Arndt and Damask[2] does, however, suggest a higher order transition is being observed because of the temperature interval of several degrees over which the transition takes place.

A good test for a polymorphic, solid-solid transformation is to observe the heating of the crystalline solid on the hot stage of a polarizing microscope. Evidence for a transition is observed by a darkening of the crystal or a change in the color. This is due to to breaking up of the crystal and light scattering off the consequent new air-crystal interfaces.[10] Second order transitions, however, will frequently be missed on heating due to their subtlety, since they may involve only a very small distortion of the atomic network. This test was performed by Arndt and Damask[2] and resulted in no evidence for a polymorphic first-order transformation.

3.The Reported Electrical Conductivity Anomaly in Phenanthrene

Phenanthrene has been observed to exhibit complex and anomalous electrical conductivity properties.[6] It was found that phenanthrene has properties dependent on its electrical history. It was observed that phenanthrene can be characterized by three conditions, identified as follows: the virgin state, the reversibly polarized state, and the irreversibly polarized state.

The virgin state is described as being associated with cleaved crystals which have not been raised above room temperature after being cooled from the melt. In this condition, an order of magnitude increase in the dark conductivity is noted

at about 70°C. Similarly, an anomalous conductivity increase of about two orders of magnitude occurs in the photoconductivity of phenanthrene.

The reversibly polarized state obtains after a crystal has been heated above 72 degrees centigrade and then cooled in the presence of an electric field. In this condition, charge releases, independent of the thickness of the crystal, were observed at the anomaly temperature, when the crystals were heated and cooled in a field. Changing the sign of the field completely reversed the sign of the charge release. With no field present, no charge release was observed.

The irreversibly polarized state is obtained by illuminating a crystal with intense white light for several minutes and then heating the crystal in the biasing field. Crystals in this state have been heated and cooled through the anomaly temperature many times with the bias field opposite in sense to the initial cooling bias after illumination, and even with zero field. For this case the charge release (even with zero bias!) was always polarized in the initial polarization direction. Also, irreversibly polarized crystals will cling to a dielectric, indicating that the internal polarization is largely in one direction.

Some speculation concerning charge trapping was advanced, but the interpretation of the irreversibly polarized state was deferred in the hope that future experimentation would provide additional information.

4. Thesis Objectives

It was shown that phenanthrene is a molecular semiconductor, exhibiting the gross characteristics of the organic solid state. At the same time it possesses certain anomalous properties, which, owing to the complexities of organic compounds, are not easily related to any model.

In order to formulate a mechanism for these irregular properties additional experimental data is required. In this respect the static dielectric constant of phenanthrene was determined as a function of temperature. These measurements were performed on high purity single crystals, in the three crystallographic directions, the a, the b, and the c' (normal to the a,b plane).

The linear coefficients of thermal expansion in these three directions were also determined.

The results of the above work suggested that an inelastic neutron scattering analysis should be performed, to check for new modes of vibration in going through the anomaly temperature, as well as to check for signs of lattice instabilities. This work was performed on polycrystalline material.

The anomalous behavior of the conductivity in phenanthrene suggested that an examination of charge transport properties should be investigated. The photo-Hall effect being a valuable method for choosing between band theory analysis and hopping theory analysis for charge transport, it was chosen as an area for investigation. Unfortunately, the photo-current in

in phenanthrene was just outside the range of sensitivity of our instruments. For this reason it was decided to investigate the photo-Hall effect in naphthalene, another typical aromatic hydrocarbon ($C_{10}H_8$), and similar to phenanthrene in symmetry.

A final effort to characterize the phase transition observed in phenanthrene involved a phosphorescence study of hexamethylbenzene. The motivation for this rests in the fact that hexamethylbenzene undergoes a low temperature phase transition at about 111°K which is ascribed to the onset of a new degree of rotational freedom.[11] Describing work performed on phenanthrene, Whitten, Arndt, and Damask[12] determined the rate of monomolecular triplet exciton decay over a limited range of temperatures, including the anomaly temperature. No irregular behavior was observed at the transition temperature. This did not allow for the creation of a mechanism for transition involving new degrees of freedom.

Performing the experiment on hexamethylbenzene with its recognized new degree of freedom allows for a comparison with the phananthrene results. Anomalous behavior in the triplet decay rate for hexamethylbenzene can be attributed to the onset of the new degree of freedom. The fact that no irregular behavior occured in phenanthrene would then indicate that the phenanthrene anomaly does not involve a new degree of freedom. If negative results are observed in hexamethylbenzene, one can draw no firm conclusions one way or the other.

References - Chapter 1

1. K. Ueberreiter and H.Z.Orthmann, Naturforschung 5a,101 (1950).

2. R.A.Arndt and A.C.Damask, J.Chem.Phys. 45, 755 (1966).

3. H.Ringel, R.A.Arndt, and A.C.Damask, Molecular Crystals 3, 145 (1967).

4. F.Gutmann and L.Lyons, Organic Semiconductors (John Wiley and Sons, Inc., New York, 1967), chapter 3.

5. J.Trotter,Acta Crst.16, 605 (1963).

6. R.A.Arndt and A.C.Damask, J.Chem.Phys. 45, 4627 (1966).

7. P.A.Andrews, A.F.Armington, and B.Rubin, Applied Phys. Letters 7, 86 (1965).

8. R.A.Arndt and F.E.Fujita, Rev.Sci.Instr. 34, 868 (1963).

9. G.J.Janz, Estimation of the Thermodynamic Properties of Organic Compounds (Academic Press,Inc.,New York, 1958).

10. W.C.McCrone, Polymorphism in D.Fox, M.M.Labes, and A. Weisberger eds., Physics and Chemistry of the Organic Solid State (Interscience, New York, 1967), Vol.3, ch.8.

11. J.J.Rush and J.I.Taylor,J.Chem.Phys. 44,2749 (1966).

12. W.Whitten, R.A.Arndt, A.C.Damask, Mol.Cryst.9, 239 (1969).

CHAPTER TWO

1. Introduction

Ordinary change of phase processes are most commonly characterized by a discontinuous change of properties such as volume and entropy. This discontinuity occurs at what is referred to as the transition temperature. These discontinuous changes in volume and entropy result in a latent heat.

On the other hand, transitions have been observed in which the changes in volume and entropy have not been discontinuous, but were merely rapid. This continuous change in volume and entropy, within an interval of only a few degrees, results in an unusual increase in the specific heat, but no latent heat.

Frequently, the specific heat distinguishes itself by rising to a peak, and then rapidly falling to a lower value. This is the phenomenon referred to as the lambda anomaly.

It was originally useful to separate the phase changes into categories. They were either first order or second order. The transitions were first order if the entropy changed discontinuously, resulting in a latent heat. The shape of the specific heat curve near the anomaly temperature was often used to characterize a transtion as either first order or second order.

The advent of detailed thermodynamic analysis of organic materials brought chaos to the problem of classifying phase

transitions. By 1942, Deffet[1] listed almost 1200 organic compounds in which polymorphism had been detected. Crystals underwent transformations exhibiting a variety of peaks and shapes in the specific heat curve.

In 1933, Ehrenfest[2] proposed a classification of phase transitions according to the mathematical nature of F, the free-energy curve of a substance. He defined a transition of the n^{th} order as one for which $(\partial^n F/\partial T^n)_p$ is discontinuous, F and all lower derivatives being continuous. Using this criterion, a first-order transition is characterized by a continuous free energy curve and a discontinuous entropy, enthalpy, and specific heat. A second-order transition is characterized by continuous free energy, entropy, and enthalpy curves, but a discontinuous specific heat.

Ehrenfest's method of classification is applicable only with transitions that occur discontinuously, with two distinct phases in equilibrium at the transition temperature. With a great number of transitions occuring continuously, this method of classification is severely limited.

Because of the difficulty involved in classifying phase transitions, a purely empirical system, based on the shape of the specific heat curve was developed.[3,4]

Finally, a phenomenological classification, indicating the model used for explaining the transition, is commonly used. These include the order-disorder transitions, including orientational, conformational, and positional disorders, electronic and magnetic transitions, and finally dipole transitions as in ferroelectrics.

At first glance, these various models for second-order phase transitions seem rather different from each other. The anomalous behavior of their thermodynamic quantities such as specific heat, expansion coefficients, and dielectric constants, are not particularly similar between ordered alloys, ferroelectrics, superconductors, or ferromagnetic materials. Yet these differences are probably due to a lack of understanding of the real mechanisms of second-order, or continuous phase transitions. It is this lack of a clear general theory of phase transitions which prompts the periodic attempts, which we see in the literature, to form a general theoretical description of the process.

From a phenomenological approach, the order-disorder effect was invoked by Bragg and Williams[5] to explain lambda transitions in alloys. A long-range order parameter was defined so that the entropy could be defined for various degrees of order or disorder. It was a simple matter to relate the various thermodynamic quantities through the changes in the entropy. Such phenomena as the excess specific heat at the transition temperature were explained in this way.

Indeed, it is seen that in a phase transition the fundamental role is played by the entropy. As the temperature increases, a particular phase, unstable at low temperatures, may become stable above a certain temperature, if in spite of an unfavorable internal energy, its entropy becomes high enough.

Another theory, by Bethe[6], based on short-range order effects, is used to explain in more detail the second-order transitions in alloys. Cowley[7] related the order parameter to coefficients of the Fourier series determining the intensity of scattered x-rays. This made direct comparisons between the theory and experiment possible.

Other materials exhibit the phenomena of a critical temperature and anomalous specific heat behavior. The general interpretation of this phenomenon in terms of the sudden onset of free ions or molecules forming the lattice was given by Pauling[8] in 1930.

According to Pauling's theory, the anomalous specific heats are associated with a transition from libration to free rotation for the ions or molecules in question. This phenomenon has been referred to by Frenkel[9] as "rotational melting."

Fowler[10] developed a classical theory for this so-called hindered molecular rotation, which gave good qualitative agreement with experiment.

Kirkwood[11] developed an improved theory of hindered molecular rotation, based on developing a set of functions specifying the distribution in orientation of the molecules. Further improvements were suggested by Nakamura[12].

Models based on what Fowler[10] referred to as "cooperative phenomena" kept appearing in the literature, with various refinements and improvements, and a variety of potentials hindering the molecular motion, producing a variety of partition functions.

The phenomenon of ferroelectricity is of interest to the phase

transition problem because of the interesting anomalous behavior of the thermodynamic properties of ferroelectrics. Many of the properties, such as polarization and dielectric constant, are interpreted by a purely thermodynamic model.

A study of ferroelectric properties has lead to new attempts at a general theory of phase transitions in terms of lattice dynamics. This will be discussed in Chapter Three.

It turns out that an investigation of the properties of phenanthrene indicates some ferroelectric-likebehavior for this material. In this chapter, ferroelectric-like anomalies in the static dielectric constant are reported. Appendix A also indicates the existence of anomalous behavior in the expansion coefficients, which will be discussed in terms of lattice dynamics. The next chapter will describe an investigation of the cold neutron inelastic scattering properties of phenanthrene and relate this to the lattice dynamical theory of phase transitions.

But first, a thermodynamical theory of ferroelectric-like behavior is presented to indicate the connection between the properties of phenanthrene and those of typical ferroelectrics.

2. Thermodynamic Theory of Second Order Transitions in Ferroelectric - Like Materials

The thermodynamical approach given here is basically that of Devonshire's[13].

The differential dU of the internal energy of a body subject

to internal stress and an electric field is

$$dU = TdS - \sum_i X_i dx_i + \vec{E} \cdot d\vec{P} \tag{2.1}$$

where S is the entropy, T is the absolute temperature, x_i and X_i are the strain and stress components, respectively, $\vec{E}$ is the electric field, and $\vec{P}$ is the polarization.

One now defines a potential function in terms of the entropy, internal energy, etc., called the elastic Gibbs function, as

$$G = U + \sum_i X_i x_i - TS \tag{2.2}$$

Upon differentiating Eqt.2.2 and substituting from Eqt.2.1 we obtain

$$dG = -SdT + \sum_{i=1}^{3} x_i dX_i + \vec{E} \cdot d\vec{P} \tag{2.3}$$

If we assume the stress to be zero, then G can be expanded in powers of the polarization, with the coefficients supplying the temperature dependency. If the crystal has a center of symmetry above the transition temperature only even terms are significant. Therefore G can be expanded in terms of P^2 as

$$\begin{aligned} G = G_0 &+ \tfrac{1}{2} g_1 (P_x^2 + P_y^2 + P_z^2) + \tfrac{1}{4} g_2 (P_x^4 + P_y^4 + P_z^4) + \\ &+ \tfrac{1}{2} g_3 (P_x^2 P_y^2 + P_z^2 P_x^2 + P_y^2 P_z^2) + \tfrac{1}{6} g_4 (P_x^6 + P_y^6 + P_z^6) + \\ &+ \tfrac{1}{6} g_5 (P_x^2 P_y^2 P_z^2 + \cdots) + \cdots \end{aligned} \tag{2.4}$$

where G_0 is the mean free energy for zero polarization and the g's are the temperature dependent coefficients.

One may apply Eqt.2.4 to the whole temperature range since the polarized phase below the transition temperature is considered as only a slight distortion from the unpolarized state above the transition temperature.

If one assumes that in the ferroelectric phase the spontaneous polarization lies along the z-direction and the electric fields

are only applied along this direction then $P_x=P_y=0$ and $E_x=E_y=0$. Therefore, Eqt.2.4 becomes

$$G = G_0 + \frac{1}{2}\alpha P^2 + \frac{1}{4}\gamma P^4 + \frac{1}{6}\delta P^6 \qquad (2.5)$$

where α, γ, and δ are the new temperature dependent coefficients commonly used instead of the g's.

Differentiating Eqt.2.5 with respect to the polarization, and using Eqt.2.3, one obtains

$$\frac{\partial G}{\partial P} = E = \alpha P + \gamma P^3 + \delta P^5 \qquad (2.6)$$

Neglecting saturation effects, the electric susceptibility above the transition temperature is defined by $\frac{\partial E}{\partial P} \equiv \frac{1}{\chi}$ for zero polarization. Therefore by differentiating Eqt.2.6 with respect to P, and setting P=0 one gets

$$\frac{\partial^2 G}{\partial P^2} = \frac{\partial E}{\partial P} \equiv \frac{1}{\chi} = \alpha + 3\gamma P^2 + 5\delta P^4$$

or

$$\alpha = \frac{1}{\chi} \qquad (2.7)$$

In order for the dielectric constant to obey a Curie-Weiss dependence (i.e., a $1/(T-T_0)$ dependence), the Devonshire theory requires that α be approximated by the linear temperature function

$$\alpha = \beta (T - T_0) \qquad (2.8)$$

while γ and δ are considered constant in the first approximation. The free energy then becomes

$$G = G_0 + \frac{1}{2}\beta(T-T_0)P^2 + \frac{1}{4}\gamma P^4 + \frac{1}{6}\delta P^6 \qquad (2.9)$$

In all known ferroelectrics, β and δ are positive. However, γ can be either positive or negative. Therefore the dependence of the free energy on temperature and polarization is strongly dependent on the sign of γ. If γ is negative, the free energy describes a ferroelectric with a discontinuity in the polarization at the transition temperature. This represents a first-order

transition with a latent heat and a discontinuous specific heat. If γ is positive, Eqt.2.9 describes a ferroelectric with no discontinuity in the polarization at the transition temperature. This represents a second-order transition, characterized by no latent heat and a continuous peak in the specific heat. Only the second-order case will be considered.

2a. The Dielectric Constant

According to the above, for the second-order case β, γ, and δ are all considered positive. Assuming this consider the G versus P curve shown in Fig.2.1. Since stable states are those with a minimum free energy, this curve must have either one minimum at P=0 or a pair of minima symmetrically on either side. This can be seen from Eqt.2.7 that if α is positive there will be a minimum at P=0, if it is negative, a maximum, which implies a pair of minima on either side. The case for a single minimum at P=0 for ferroelectrics corresponds to the situation for $T > T_0$. (See Fig.2.1.) The spontaneous polarization may have either of two values, $+P_s$ or $-P_s$ corresponding to the situation for $T<T_0$.

In order to observe qualitatively the behavior of the dielectric constant near the transition temperature, one uses Eqt.2.6 to obtain

$$E = \beta(T-T_0)P + \gamma P^3 + \delta P^5 \qquad (2.10)$$

The dielectric stiffness is defined as the reciprocal of the electric susceptibility and is obtained by differentiating Eqt.2.10 with respect to P, and using Eqt.2.7 to obtain

$$\alpha \equiv \frac{1}{\chi} = \frac{\partial E}{\partial P} = \beta(T-T_0) + 3\gamma P^2 + 5\delta P^4 \qquad (2.11)$$

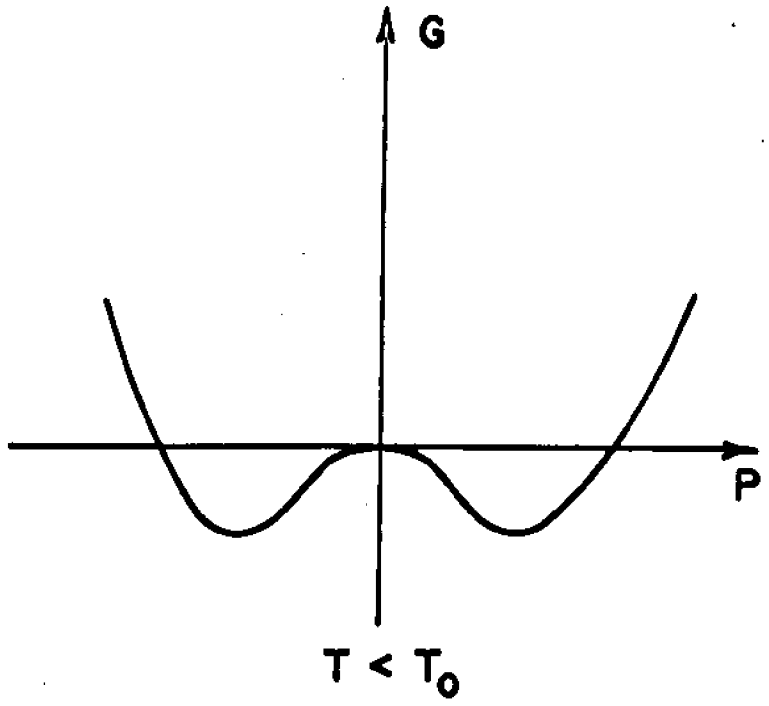

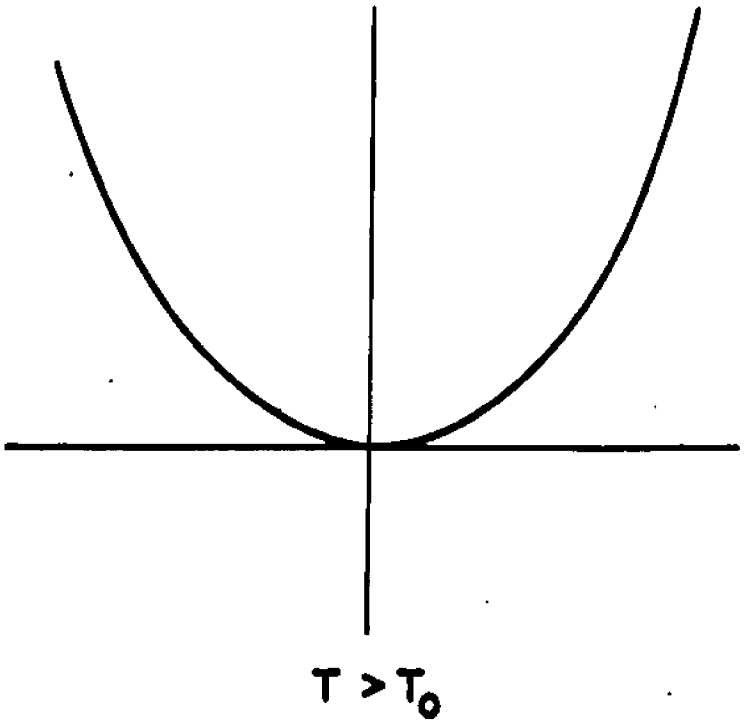

FIG. 2.1

The Free Energy as a Function of the Internal Polarization for a Second-Order Phase Transition (a) Below the Transition Temperature and (b) Above the Transition Temperature.

Since the electric susceptibility is directly proportional to the dielectric constant, the stiffness constant χ is consequently inversely proportional to the dielectric constant.

The spontaneous polarization is obtained by setting E=0 in Eqt.2.10, solving for P, and accepting only the real solutions. Examining the results for the different temperature intervals, we see that for $T<T_0$, where it was shown that two solutions for P exist, one obtains

$$P_S = \mp\left\{\frac{\gamma}{2\delta}\left[\left\{1-4\frac{\delta\beta}{\gamma^2}(T-T_0)\right\}^{1/2}-1\right]\right\}^{1/2} \qquad (2.12)$$

If $T>T_0$ there is one real solution, which is equal to zero.

It is to be noted that if all three coefficients β, γ, and δ are positive the terms in P^5 in Eqt.2.10 and the terms in P^4 in Eqt.2.11 can be neglected near the transition point, since here $P \to 0$. Therefore Eqt.2.10 becomes

$$E = \beta(T-T_0)P + \gamma P^3 \qquad (2.13)$$

and Eqt.2.11 becomes

$$\chi = \beta(T-T_0) + 3\gamma P^2 \qquad (2.14)$$

From Eqt.2.13 the spontaneous polarization may be approximated by

$$P_s = \left[\frac{\beta}{\gamma}(T-T_0)\right]^{1/2} \qquad (2.15)$$

Eqt.2.15 that as the temperature approaches T_0, P_s gradually goes to zero. Since there is no discontinuous change in P_s, there can be no latent heat associated with the ferroelectric-paraelectric transition. This describes what is called a second-order transition.

For the case where $T>T_0$

$$\chi_> = \beta(T-T_0) \qquad (2.16)$$

since P=0.

For the case where $T<T_0$, substituting Eqt.2.15 into 2.14 gives

$$\mathcal{K}_< = -2\beta(T-T_0) \tag{2.17}$$

Thus, no matter which way the transition point is approached, from below the transition temperature or above it, at $T=T_0$ the dielectric stiffness vanishes, resulting in an infinite dielectric constant. Although the experimental dielectric constant of most ferroelectrics measured has been shown to increase, it always remains finite. The infinity results from a lack of a completely correct model.

2b. The Specific Heat

From Eqt.2.3 we can obtain an expression for the entropy of the ferroelectric material

$$S = -\left(\frac{\partial G}{\partial T}\right)_{X,P} \tag{2.18}$$

Using Eqt.2.9 we can determine the change in entropy between states with polarization and states with no polarization

$$\Delta S = S_0 - S = \frac{1}{2}P^2\frac{\partial}{\partial T}\left[\beta(T-T_0)\right] + \frac{1}{4}P^4\left(\frac{\partial \gamma}{\partial T}\right) + \frac{1}{6}P^6\left(\frac{\partial \delta}{\partial T}\right) \tag{2.19}$$

where $S_0 = -\left(\frac{\partial G_0}{\partial T}\right)_{X,P}$ is the entropy for zero polarization.

In most ferroelectrics δ and ζ do not vary much with temperature,[13] giving for the entropy change

$$\Delta S = \frac{1}{2}\beta P^2 \tag{2.20}$$

Below the transition temperature, P is the spontaneous polarization, P_s given by Eqt.2.12. Therefore

$$S = S_0 - \frac{\beta\gamma}{4\delta}\left\{\left[1 + \frac{4\delta\beta}{\gamma^2}(T_0 - T)\right]^{1/2} - 1\right\} \tag{2.21}$$

Below the transition temperature, but near it, P_s is given by Eqt.2.15. Therefore the entropy near the transition point becomes

$$S = S_0 - \frac{1}{2}\frac{\beta^2}{\gamma}(T - T_0) \qquad \text{(near } T_0\text{)} \tag{2.22}$$

Now the specific heat is given by

$$C = T\left(\frac{\partial S}{\partial T}\right) \tag{2.23}$$

Using Eqt.2.21

$$\Delta C = C - C_P = \frac{1}{2}\frac{\beta^2 T}{\gamma}\left[1 + \frac{4\delta\beta}{\gamma^2}(T_0 - T)\right]^{-1/2} \tag{2.24}$$

where $c_p = T(\partial S_P/\partial T)$ is the specific heat at constant polarization, and Δc is the excess specific heat due to the temperature variation of the polarization. From Eqt.2.24 we see that Δc

increases as the temperature approaches T_o, at which point, using Eqt.2.22, it has the value:

$$\Delta C = \frac{1}{2}\frac{\beta^2 T_o}{\gamma} \qquad (\text{at } T=T_o) \tag{2.25}$$

Above the transition temperature, Δc is zero, from Eqt.2.20, since the polarization is zero. This gives the typical lambda transition of the second-orderphase change.

It is noted that the thermodynamic theory of ferroelectricity does not attempt to relate any of the macroscopic properties of ferroelectrics, such as specific heat, and dielectric constant to a microscopic model. It merely relates macroscopic properties to each other, describing them in terms of parameters, such as α, γ, and δ which must be determined experimentally. To attempt a microscopic description at this point would be futile since none exist which are free from serious objection. The most common theory, the dipole theory, fails to account for many experimentally observed features, such as the two Curie temperatures of Rochelle salt[14]. Other models have correspondingly serious defects. A microscopic theory will be described in the next chapter, in terms of lattice dynamics.

In any event, phenanthrene does exhibit one of the features of a ferroelectric-like material. It possesses a second-order or lambda transition in its specific heat.[15] It will be seen in the remainder of this chapter, that in seeking additional ferroelectric-like behavior, an anomalous peak in the static dielectric constant was observed. Phenanthrene thus exhibits another ferroelectric-like property.

3. Experimental Techniques

The dielectric constant of a material may be determined by using the substance as the dielectric material for a parallel plate capacitor. The standard equation for such a capacitor, neglecting edge effects (which are smaller than the other sources of error present in the experiment) is

$$C = \frac{A\varepsilon}{d} \tag{2.26}$$

Using electrodes made by painting opposite sides of an oriented crystal sample we can measure A, the area of the electrodes, and d the separation between the electrodes (i.e. the crystal thickness). The capacitance, C is determined by using a sensitive capacitance bridge. In this way Eqt.2.26 may be solved for ε, the dielectric constant.

The simplest form of Debye equation relating the dielectric constant of the material to its dipolar properties is [16]

$$\frac{\varepsilon - 1}{\varepsilon + 2} = \frac{4N_1\pi}{3}\left(\alpha_o + \frac{\mu^2}{3kT}\right) \tag{2.27}$$

where N_1 is the number of molecules per unit volume, α_o is the polarizability, μ is the permanent dipole moment of the molecule, k is Boltzmann's constant, and T is the absolute temperature.

A more useful form of the equation is obtained by multiplying both sides of Eqt.2.27 by M/d, where M is the molecular weight and d is the density. This gives the molar polarization

$$P = \frac{4N\pi}{3}\left(\alpha_o + \frac{\mu^2}{3kT}\right) \tag{2.28}$$

where N is Avogadro's number.

The second term in the parentheses represents the average

electric dipole moment per molecule in the direction of the field produced by the orienting influence of the applied field. For this term to contribute to Eqt.2.28, the molecule must possess some rotational freedom.

Since α_o and μ are usually temperature independent, P is the sum of a temperature independent induced polarization P_I and a temperature dependent orientation polarization P_M. Also, P_I is made up of the sum of the electronic polarization, P_E, and the atomic polarization P_A. Therefore,

$$P = P_E + P_A + P_M \qquad (2.29)$$

where only P_M is temperature dependent. If the molecular dipole moment is zero, or if the molecule is so hindered in the crystal that it is not free to orient itself with the field, then $P_M = 0$.

The polarization of a material by electronic displacement occurs in about 10^{-16} seconds. Atomic displacements require from 10^{-14} to 10^{-16} seconds. However, molecular orientation may take from 10^{-12} to 10^{-10} seconds or longer.[16] Therefore, if a field is used which has a frequency greater than 10^{12} cycles per second, the molecule can not move rapidly enough to follow the changing field. This results in the so-called optical dielectric constant. For fields having a frequency less than 10^{10} cycles per second, the molecules will see an essentially static field, resulting in what may be called the static dielectric constant.

3a. The Crystal Sample

The sample material was research grade phenanthrene, further purified using now standard techniques of liquid chromatography, vacuum sublimation, and zone refining.[17,18] The phenanthrene was also treated with maleic anhydride and KOH to remove any anthracene and fluorine impurities.[19] The resulting impurity level was of the order of 0.1 part per million of anthracene and less than 5 parts per million total impurity, as determined by spectrophotometric analysis. This analysis was performed using a Cary 14 Recording Spectrophotometer.

Single crystals were grown from the melt using the standard Bridgeman-type furnace.[20] The growing time for a five inch boule was about five days. The temperature of the furnace was then dropped to room temperature over a period of about seven days in order to prevent cracking the crystal. The boule was then slipped out of the growing tube, which had been coated with a silicone release agent.

The crystal boule usually showed small cleavage planes when tilted at various angles to the light. Using a razor blade, one can easily cleave the boule by holding the blade parallel to one of these planes. This exposes the a,b plane. The a and b directions may be determined by observing the double refraction, according to the method proposed by Nakada[21].

Samples were prepared which were about five to ten millimeters on a side and about one millimeter thick. The sample preparation involved polishing the crystal on a fine tissue paper soaked in

ethanol.

To make the sides as parallel as possible the crystal sample was glued to a glass slide, using "Duco" cement, and taking care not to get any cement under the crystal. Walls were then built up on either side of the crystal using thin cover slides, until the height of the walls was just below that of the crystal. A razor blade was then used to shave the crystal flat. Turning the crystal up-side-down and shaving the new side insured parallelism for the two sides.

Using "Dupont #4817" silver conducting paint, thinned with butyl acetate, two opposite sides of the oriented crystal were painted to form the electrodes of a parallel plate capacitor. The crystal thus acted as the dielectric material for the capacitor.

3b. The Sample Holder

The sample holder is shown in Fig.2.2. It consists basically of a nylon block, with spring-loaded electrical leads at one end for connection to the crystal. At the other end, the spring-loaded wires were connected to low capacitance coaxial cable, leading to the capacitance bridge. The shielding around the cables was joined and connected to the grounded shield around the sample container in the water bath.(See next section.)

The spring-loaded leads were cemented to the painted electrodes using unthinned "Dupont #4817" paint.

A chromel-alumel thermocouple was introduced through the nylon block as close as possible to the crystal, to monitor the local crystal temperature.

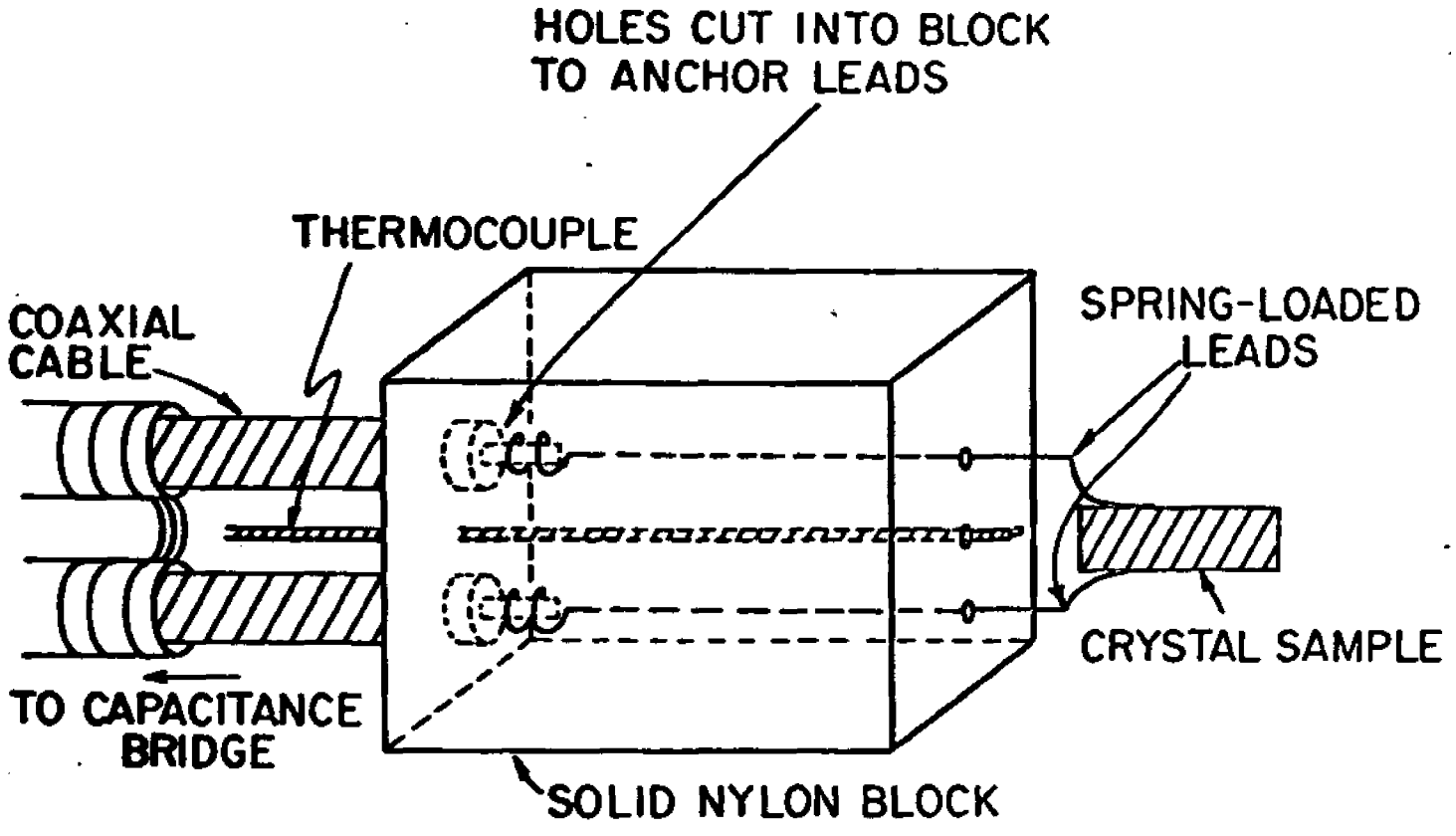

FIG. 2.2

The Sample Holder for the Dielectric Constant Experiment. Approximately 2X Actual Size.

3c.The Temperature Bath

The sample holder was placed in a shielded sample container, which was in turn immersed in the temperature bath, see Fig.2.3. It is to this shielded container that the coaxial cable shielding is connected.

The open top of the shielded container was closed with aluminum foil after the sample was placed inside. This helped to maintain stable thermal conditions.

Since the temperature was not to exceed 85 °C, a water bath was used. Going above this temperature ran the risk of accidentally melting the crystal.

A knifeblade heater was used to heat the bath. A mechanical stirrer was used to maintain a uniform temperature throughout the bath. A glass thermometer provided crude determinations of the bath temperature. A more accurate value for the bath temperature was obtained using the chromel-alumel thermocouple associated with the bath temperature controller.

The bath container was a 1500 milliliter Dewar. A styrofoam plug was used to seal the top of the Dewar and provide thermal insulation. The appropriate holes were cut in the plug to allow the necessary wires to pass out of the Dewar.

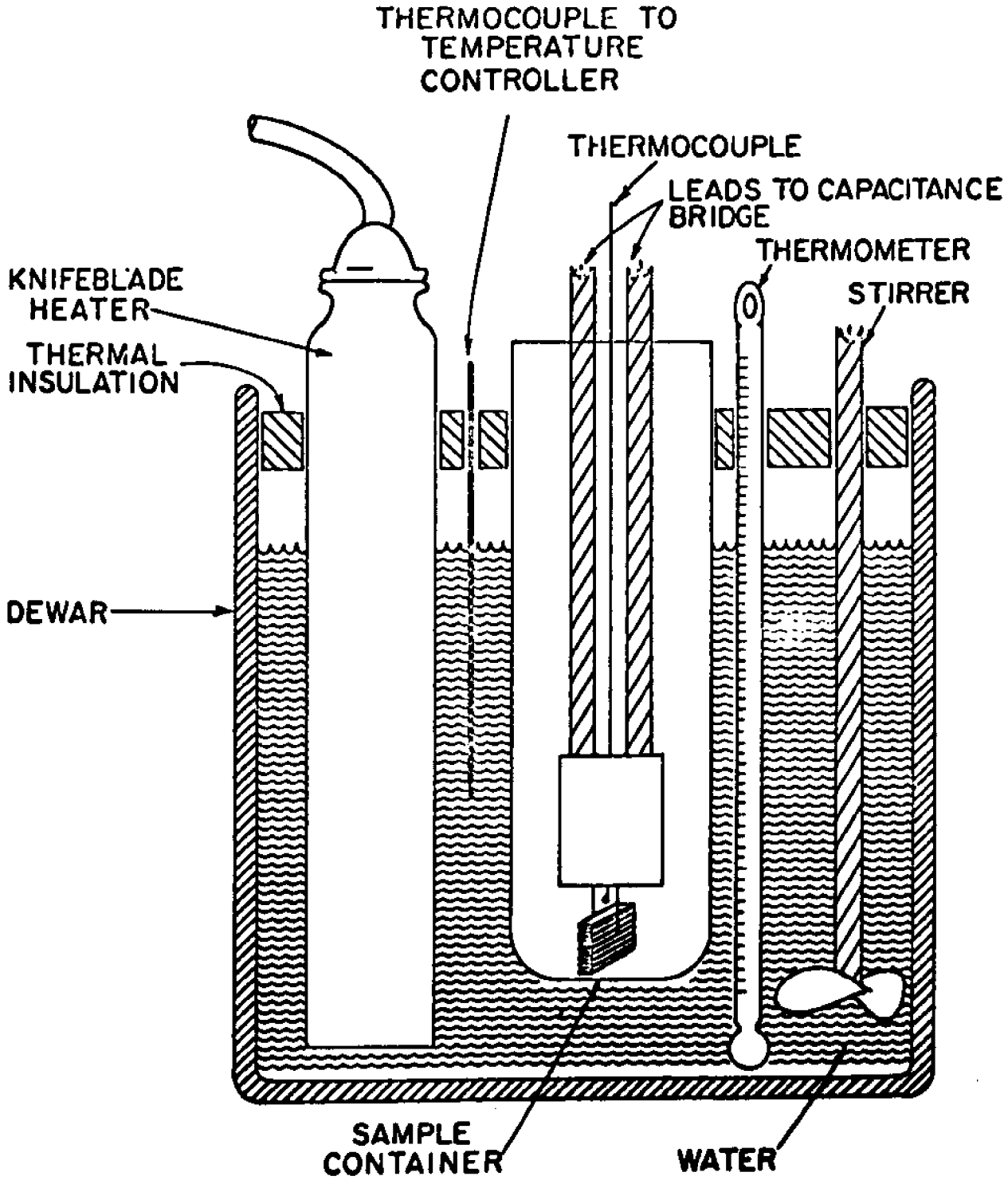

FIG. 2.3

The Hot Water Temperature Bath.

3d. The Electronics

The measurement was made using a General Radio, three wire capacitance bridge, Type 1616-A, along with the General Radio Adio Oscillator, Type 1311-A, and the General Radio Tuned Amplifier and Null Detector, Type 1232-A.

A wide range of capacitances can be measured with this apparatus. The lower limit on the capacitance bridge is 10μpicofarads (10^{-5} picofarads). The null detector also provided an extra preamplifier when dealing with a very high impedance sample. This was especially useful for the high impedances exhibited by phenanthrene.

The temperature controller used was the Precision Temperature Controller, Model 104, Bayley Instrument Company.

A Honeywell-Brown Electronik Potentiometer Recorder with a range of 0 - 10.1 millivolts, was used to monitor the local crystal temperature.

3e. Techniques and Results

The temperature was increased in increments of 0.05 to 0.10 millivolts at a time, using a chromel-alumel thermocouple to monitor the sample region temperature. The system was allowed to equilibrate by waiting ten to fifteen minutes after each new temperature was reached, before a reading of the sample capacitance was made.

It was possible to adjust the rate of heating to a relatively slow value (about 0.3 degrees centigrade per minute while the heater was on) so that there was no detectable thermal overshoot.

As a result, the temperature was controlled to within ±0.1 degrees centigrade, or about ±0.005 millivolts on the chromel-alumel thermocouple.

The measurements were made at a frequency of one thousand cycles per second, with a field strength of 150 volts/centimeter across the crystal.

The results of the capacitance measurements, for a temperature interval including the anomalous region, in the three crystallographic directions, a, b, and c', are shown in Fig.2.4. The data points represent the measured capacitances. It is noted that there is anomalous behavior around 70 degrees centigrade.

The solid curve represents the capacitances corrected for the thermal expansion of the crystal.

Anomalous changes in the temperature dependence of the static dielectric constant (the static dielectric constant is directly related to the measured capacitance through Eqt.2.26) is observed in all three directions, although a peak is exhibited in the a direction.

3f. Correcting For Thermal Expansion

As the crystal dielectric expands with increasing temperature, the painted electrodes move further apart, accounting for some of the variation in the value of the measured capacitance with temperature. To correct for this one must examine the standard equation for a parallel plate capacitor, where we consider the

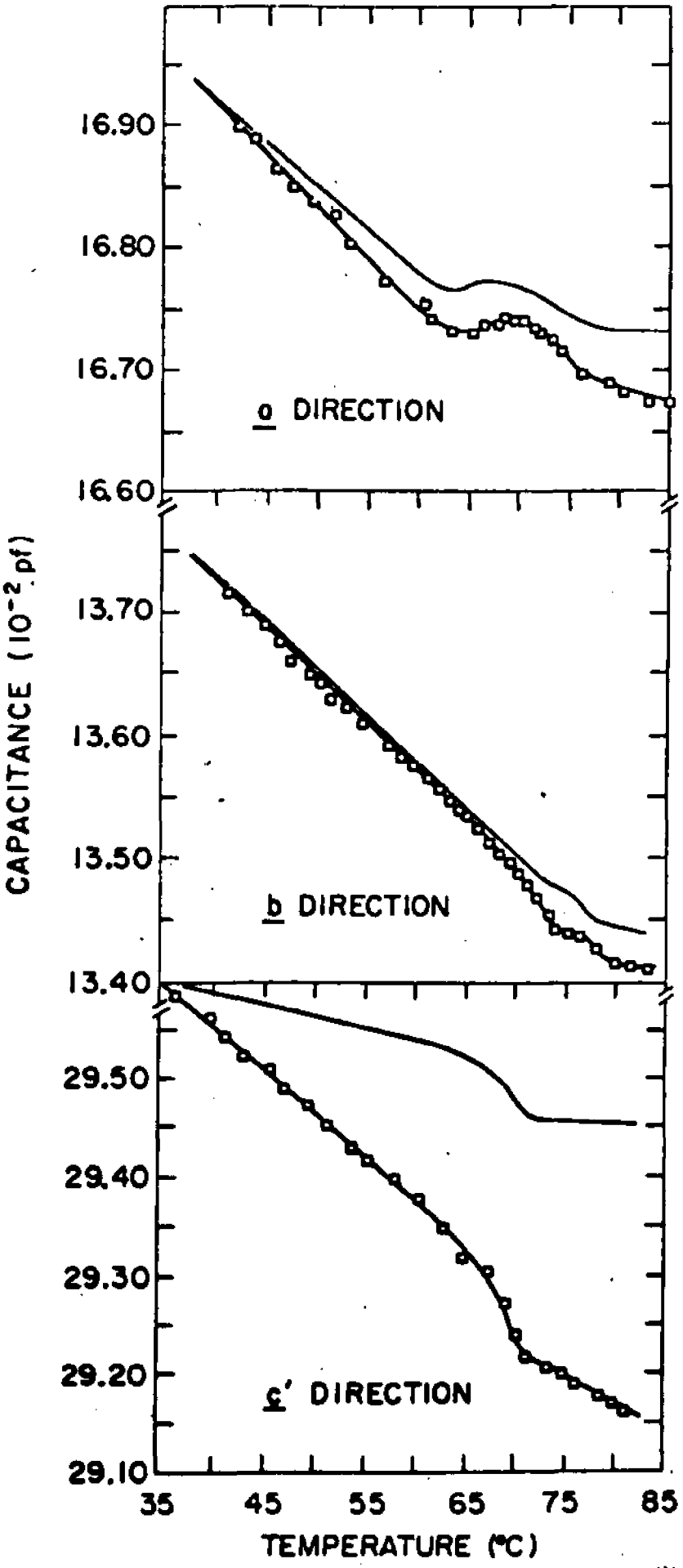

FIG. 2.4. The Measured Capacitance as a Function of Temperature of the Parallel Plate Capacitor With a Phenanthrene Single Crystal Dielectric, in the Three Crystallographic Directions.

parameters that are temperature dependent. This equation is:

$$C(T) = \frac{0.08842 \cdot A \cdot \epsilon(T)}{d(T_0)[1+\alpha(T-T_0)]} \qquad (2.30)$$

where A is the area of the painted electrodes, in centimeters, ϵ is the static dielectric constant, d is the separation of the painted electrodes, in centimeters, α is the linear coefficient of thermal expansion, the T's are the various temperatures, and C is the measured capacitance, in picofarads.

Therefore, the capacitance we measure is too small, due to the expansion of the crystal, by a factor of $1/[1+\alpha(T-T_0)]$. To correct for this, we must multiply C(T) by the reciprocal of the above factor, giving:

$$C_T(T) = C(T)\,[1+\alpha(T-T_0)] \qquad (2.31)$$

The results of these corrections are the solid curves in Fig.2.4.

The method for obtaining the anisotropic linear coefficients of thermal expansion of phenanthrene is explained in Appendix A.

4. Discussion

As would be expected from the thermodynamic theory of ferroelectrics, presented in Section 2 of this chapter, the static dielectric constant should show an anomalous increase, and indeed, the results, as seen in Fig.2.4, agree with this prediction. This occurred in the temperature region already singled out for inspection because of the anomalous specific heat peak in this temperature region.

The fact that an anomalous increase in the static dielectric constant was observed adds new incentive for investigating other properties that a ferroelectric-like material might be predicted to have. This leads to a study of phenanthrene from the lattice dynamical point of view, which will be reviewed in the next chapter.

However, some attempt at a microscopic model to explain the ferroelectric-like behavior exhibited by phenanthrene will be made here.

It has been indicated earlier that cooling a phenanthrene crystal from above 72 degrees centigrade in a d.c. field induces a bulk polarization which cannot be reversed,[22] a behavior similar to that of electrets. This polarization has been found in three crystallographic directions, with an effective dipole moment of 10^{-3}D per molecule in the c' direction. Structure work by both x-ray[23] and neutrons[24] at room temperature have shown the crystal class of phenanthrene to be $P2_1$, indicating a two-fold screw axis. With such a space group, if any permanent dipole moment were present in the molecule, it would have to be in the b direction, since any permanent dipoles associated with the molecules would cancel out in the other directions, as can be seen from Fig.1.2. The phenanthrene molecule is ordinarily slightly distorted from a plane, with the outer two rings being displaced in opposite directions from the plane of the plane of the central ring.[23] It may be conjectured that the overcrowded hydrogen atoms in the 4,5 positions of the molecule can undergo

a hindered libration above the anomaly temperature. In Fig.2.5a, the side view of the phenanthrene moleculeis seen in the normal configuration in the crystal at room temperature, as suggested by Trotter[23], and confirmed by Kay[24] using neutron diffraction techniques. Kay has, in fact, shwn the 4,5 hydrogen atoms to be on opposite sides of the central ring. The angles in Fig.2.5 are grossly exaggerated, and are actually of the order of one degree. There cannot be an effective dipole moment in the molecule which arises from this configuration, because of its two-fold symmetry. On increasing the temperature of a crystal, i.e. going through the anomaly region, thermal expansion could lower the barrier which hinders the motion of the 4,5 hydrogen atoms and permit the new configuration shown in Fig.2.5b. This configuration can give rise to a permanent dipole moment in the $\underline{a}$ direction, in agreement with the observed peak in the dielectric constant. This configuration could be stabilized in cooling through the anomaly temperature by applying an electric field.

The above configuration implies that phenanthrene polarized in such a way would no longer belong to the $P2_1$ space group. An investigation of this would be interesting as a check of this model.

It is also noted that an increase in the configurational entropy is suggested here, indicating an anomalous increase in the specific heat, as was reported.

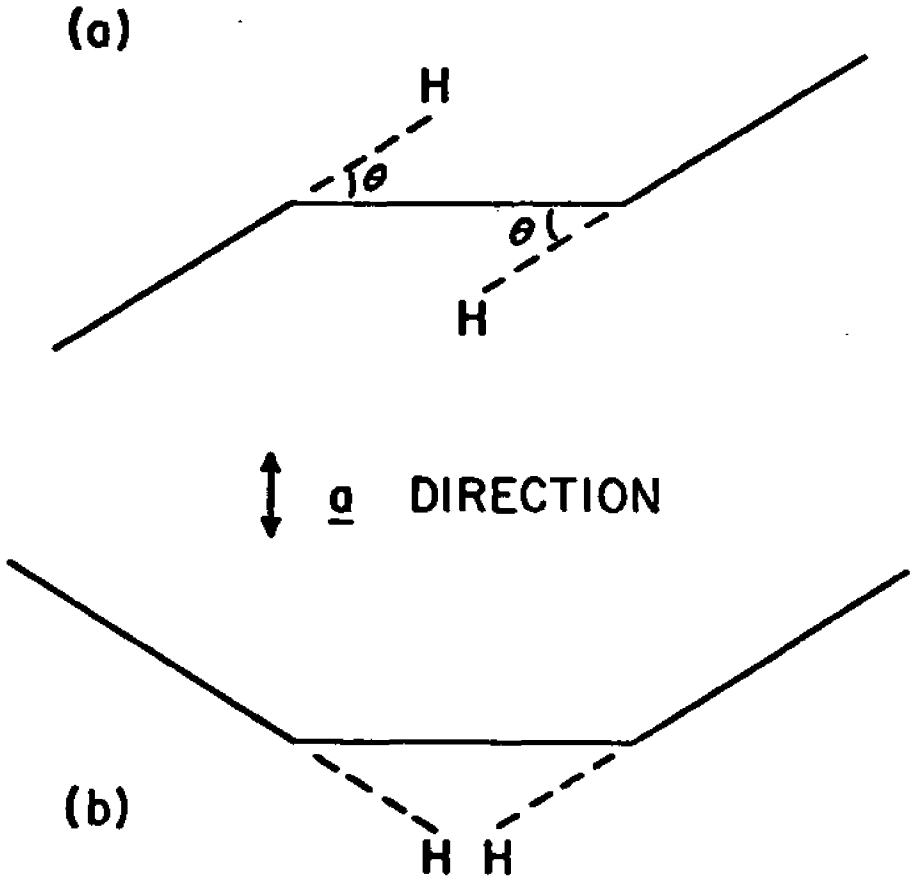

FIG.2.5. Side View of the Phenanthrene Molecule in the (a) Room Temperature Configuration and (b) in the Proposed High Temperature Configuration. The Angle is of the Order of One Degree. The Lines represent the Planes of the Three Benzene Rings.

References - Chapter 2

1. L. Deffet, Réportoire des Composés Organiques Polymorphes, (Edition Desoer, Liege,1942).

2. P.Ehrenfest, Leiden Comm. Suppl. 756 (1933).

3. J.P.McCullough, Pure and Applied Chem. 2, 221 (1961).

4. J.Joffray, Ann.Phys. 3, 5 (1948).

5. W.L.Bragg and E.J.Williams, Proc.Roy.Soc.(London) A145, 699(1934).

6. H.A.Bethe, Proc. Roy. Soc.(London) A150, 552 (1935).

7. J.M.Cowley, Phys. Rev. 77, 669 (1950).

8. L.Pauling, Phys. Rev. 36, 430 (1930)

9. J.Frenkel, Acta Physica Chem. USSR 1, 97 (1934)

10. R.H.Fowler, Statistical Mechanics,(Cambridge Press,London, 1936), Ch.21.

11. J.G.Kirkwood, J.Chem. Phys. 8, 205 (1940).

12. T.Nakamura, J.Phys.Soc. of Japan 7, 264 (1952).

13. A.F.Devonshire, Advances in Physics 3, 85 (1954).

14. A.J.Dekker, Solid State Physics,(Prentice Hall,Inc., New York, 1965),p.195.

15. R.A.Arndt and A.C.Damask, J.Chem.Phys. 45, 755 (1966).

16. C.P.Smyth, Dielectric Phenomena in D.Fox,M.M.Labes,A.Weissberger, eds.,Physics and Chemistry of the Organic Solid State, (Interscience Publishers, New York, 1963).

17. C.F.Reynolds, Crystal Growth in D.fox, M.M.Labes, and A.Weissberger, eds., Physics and Chemistry of the Organic Solid State, (Interscience Publishers, New York, 1963).

18. J.N.Sherwood, Purification and Growth of Large Anthracene Crystals in M.Zeif, ed., Methods and Techniques of Fractional Solidification, (M.Dekker, New York, 1969).

19. H.Ringel, Ph.D. Thesis, City University of New York (Unpublished, 1969).

20. F.Gutmann and L.Lyons, Organic Semiconductors,(John Wiley & Sons, Inc., New York,1967), p.158.

21. I.Nakada, J.Phys. Soc. of Japan 17, 113 (1962).

22. R.A.Arndt and A.C.Damask, J.Chem.Phys. 45, 4627 (1966).

23. J.Trotter, Acta Cryst. 16, 605 (1963).

24. M.Kay, (To be published).

CHAPTER THREE

1. Introduction

Experimental work on second order transitions have been primarily directed towards investigating the macroscopic properties of the various materials. Specific heat, dielectric constants and elastic constants typically recieved special attention. (See Chapter 2.) Anomalies in any or all of these properties provide initial evidence for the existence of phase transitions.

More recently, due to some theoretical work by Cochran[1,2], the suggestion was advanced that some second order phase transitions resulting in a structural modification may be considered from the point of view of lattice dynamics.

The essence of Cochran's theory was that the structure should be unstable against a particular mode of vibration. By the usual criteria for stability, this meant that the frequency of this mode should vanish at the transition point. Furthermore, Cochran showed that the static dielectric constant should be related to an anomaly in the transverse optic mode, in the case of a ferroelectric transition, in accordance with the Lyddane-Sachs-Teller relationship[3], $\varepsilon_s/\varepsilon_\infty = \omega_{LO}^2/\omega_{TO}^2$, where ε_s is the static or low frequency dielectric constant, ε_∞ is the optical dielectric constant, ω_{LO} is the frequency of a longitudinal optic mode and ω_{TO} is the frequency of a transverse optic mode of vibration.

In Cochran's theory, the coefficients of the dynamical matrix are allowed to vary with the temperature in such a way that the

transverse optical frequency vanishes at the transition temperature directly as $(T-T_c)$. Using the Lyddane-Sachs-Teller (LST) relationship one can see that if

$$\omega_{TO}^2 \propto T - T_c$$

this implies that

$$\varepsilon_s \propto \frac{1}{T-T_c}$$

in agreement with experimental results for ferroelectric transitions.

Cowley[4] attempted to derive the temperature variation of the phonon frequencies using a microscopic theory. In his theory, Cowley attributed the temperature variation of the frequencies of the modes of vibration to the anharmonic terms of the interaction potential. Using the expansion of the potential in terms of atomic displacements, including the third and fourth order terms, he calculated the shift and damping of the vibrational frequencies using perturbation techniques. He used the frequencies that he calculated (at a given temperature) from this perturbation technique in a thermodynamic theory of the actual transition. He did this by expanding the free energy of the lattice in powers of distortion parameters. The coefficients of this new expansion depended on the frequencies of vibration calculated earlier.

The theory is compromised by using a perturbation method if the shift in frequencies is not small.[5] In the case of certain phase transitions, it is observed that the phonon dispersion curves undergo drastic variations at the critical temperature.[6]

The actual three-dimensional problem must be considered as a difficult many-body problem, strongly dependent on the actual form of the interaction potential.

2. Lattice Dynamics

It is the purpose of this chapter, after first establishing the vocabulary of lattice dynamics, to indicate the particular relevance of cold neutron inelastic scattering as a probe for investigating the lattice and molecular vibrations of solid phenathrene. The results of such an investigation will be discussed and further evidence of ferroelectric-like behavior of phenanthrene will be presented.

For a model, a simple Bravais lattice will be assumed, with the lattice points given by

$$\vec{R}_{i0} = \alpha_i \hat{r}_1 + \beta_i \hat{r}_2 + \gamma_i \hat{r}_3 \qquad (3.1)$$

where α_i, β_i and γ_i are integers and the $\hat{r}_\nu$ are the unit lattice vectors. All combinations of α, β, γ correspond to lattice points.

2a. The Three Dimensional Dispersion Relationship [7]

The assumed three dimensional crystal lattice has N atoms, whose equilibrium positions are given by $\vec{R}_{io}$. The interaction potential is given by $V(\vec{R}_i - \vec{R}_j)$, where $\vec{R}_i = \vec{R}_{io} + \vec{\delta R}_i$. The Hamiltonian for the system is given by

$$H = \sum_i p_i^2/2m + \sum_{i \neq j} \tfrac{1}{2} V(\vec{R}_i - \vec{R}_j) \qquad (3.2)$$

where the factor $\frac{1}{2}$ enters since pairs of interactions are counted twice.

We may expand the potential in a series about the equilibrium

positions of the atoms:[8]

$$\sum_{\substack{i,j \\ i\neq j}} V(\vec{R}_i-\vec{R}_j) = \sum_{\substack{i,j \\ i\neq j}} \Big[V(\vec{R}_{io}-\vec{R}_{jo}) + \cdots + \Big\{ (\delta\vec{R}_i\cdot\nabla_i)(\delta\vec{R}_i\cdot\nabla_i) + \cdots + (\delta\vec{R}_i\cdot\nabla_i)(\delta\vec{R}_j\cdot\nabla_j) \Big\} V(\vec{R}_{io}-\vec{R}_{jo}) \Big] \tag{3.3}$$

The linear term in the expansion does not contribute since the force on any atom vanishes atthis equilibrium position. The anharmonic cubic and quartic terms are not included.

If the potential energy is well behavod, it may be expanded as a Fourier series. Thus,

$$V(\vec{R}_i-\vec{R}_j) = \sum_k V_k\, e^{i\,\vec{k}\cdot(\vec{R}_i-\vec{R}_j)} \tag{3.4}$$

where we sum over all values of the wavevector k. Using Eqt.3.4 one may evaluate the second term on the right hand side of Eqt.3.3. We get

$$\begin{aligned}(\delta\vec{R}_i\cdot\nabla_i)(\delta\vec{R}_i\cdot\nabla_i V) &= (\delta\vec{R}_i\cdot\nabla_i)\Big(\delta\vec{R}_i\cdot\Big[\textstyle\sum_k i\vec{k}\,V_k e^{i\vec{k}\cdot(\vec{R}_i-\vec{R}_j)}\Big]_o\Big) \\ &= (\delta\vec{R}_i\cdot\nabla_i)\Big(\Big[\textstyle\sum_k i\vec{k}\,V_k e^{i\vec{k}\cdot(\vec{R}_i-\vec{R}_j)}\Big]_o\cdot\delta\vec{R}_i\Big) \\ &= \delta\vec{R}_i\cdot\Big[\textstyle\sum_k -\vec{k}\vec{k}\,V_k e^{i\vec{k}\cdot(\vec{R}_i-\vec{R}_j)}\Big]_o\cdot\delta\vec{R}_i\end{aligned} \tag{3.5}$$

The expression in brackets is a dyadic[8] and is defined as

$$Q_{ij} = -\sum_k \vec{k}\vec{k}\,V_k\, e^{i\vec{k}\cdot(\vec{R}_i-\vec{R}_j)} \qquad i\neq j \tag{3.6}$$

Similarly, the last term on the right hand side of Eqt.3.3 may be evaluated as follows:

$$\begin{aligned}(\delta\vec{R}_i\cdot\nabla_i)(\delta\vec{R}_j\cdot\nabla_j)V &= (\delta\vec{R}_i\cdot\nabla_i)\Big(\delta\vec{R}_j\cdot\Big[\textstyle\sum_k i\vec{k}\,V_k e^{i\vec{k}\cdot(\vec{R}_i-\vec{R}_j)}\Big]_o\Big) \\ &= (\delta\vec{R}_i\cdot\nabla_i)\Big(\Big[\textstyle\sum_k -i\vec{k}\,V_k e^{i\vec{k}\cdot(\vec{R}_i-\vec{R}_j)}\Big]_o\cdot\delta\vec{R}_j\Big) \\ &= \delta\vec{R}_i\cdot\Big[\textstyle\sum \vec{k}\vec{k}\,V_k e^{i\vec{k}\cdot(\vec{R}_i-\vec{R}_j)}\Big]_o\cdot\delta\vec{R}_j\end{aligned} \tag{3.7}$$

The expression in parentheses is again a dyadic, defined as

$$Q_{ij} = \sum_k \vec{k}\vec{k} V_k e^{i\vec{k}\cdot(\vec{R}_{i0} - \vec{R}_{j0})} \qquad (i \neq j) \tag{3.8}$$

We may now rewrite Eqt.3.3 as

$$\sum_{\substack{i,j \\ i \neq j}} V(\vec{R}_i - \vec{R}_j) = \text{constant} + \sum_{i,j} \delta\vec{R}_i \cdot Q_{ij} \cdot \delta\vec{R}_j \tag{3.9}$$

One can now also rewrite the expression for the system Hamiltonian. Eqt.3.2 becomes

$$H = \sum_i P_i^2/2m + \frac{1}{2} \sum_{\substack{i,j \\ i \neq j}} V(\vec{R}_{i0} - \vec{R}_{j0}) + \frac{1}{2} \sum_{i,j} \delta\vec{R}_i \cdot Q_{ij} \cdot \delta\vec{R}_j \tag{3.10}$$

The equation of motion for the i^{th} atom is then

$$\dot{\vec{P}} = M \ddot{\delta\vec{R}}_i = -\nabla_i H \tag{3.11}$$

or

$$M \ddot{\delta\vec{R}}_i = -\sum_j Q_{ij} \cdot \delta\vec{R}_j \tag{3.12}$$

Considering the solution to be oscillatory, let

$$\delta\vec{R}_i = \delta\vec{R}_{i0} e^{-i\omega t} \tag{3.13}$$

where $\delta\vec{R}_{i0}$ is the time independent displacement of the i^{th} atom and ω is the circular frequency.

Substituting this into Eqt.3.12 gives

$$M\omega^2 \delta\vec{R}_{i0} = \sum_j Q_{ij} \cdot \delta\vec{R}_{j0} \tag{3.14}$$

Because of the periodic nature of the crystal array, there is nothing to distinguish the motion of the i^{th} atom from that of its neighbor. Consequently,

$$\delta\vec{R}_{(n+1)0} = e^{i\vec{k}\cdot\vec{r}} \delta\vec{R}_{n0} \tag{3.15}$$

where the atoms are separated by integral multiples of the elementary

lattice vector $\vec{r}$. (See Eqt.3.1.) Eqt.3.15 is essentially the form of Floquet's theorem[9] which says that the solutions of the Hamiltonian equation for the system with a periodic potential are plane waves modified by a function which has the same periodicity as the potential. This allows us to write for the time independent displacement:

$$\delta\vec{R}_{i0} = \hat{\varepsilon}_k Q_k e^{i\vec{k}\cdot\vec{R}_{i0}} \tag{3.16}$$

where $\hat{\varepsilon}_k$ is the unit polarization vector for the plane wave, and Q_k is the magnitude of the displacement and has the periodicity of the lattice.

Substituting Eqt.3.16 into Eqt.3.14 gives us finally

$$M\omega_{k\lambda}^2 \hat{\varepsilon}_{k\lambda} = \sum_j a_{ij} \cdot \hat{\varepsilon}_{k\lambda} e^{i\vec{k}\cdot(\vec{R}_{j0}-\vec{R}_{i0})} \tag{3.17}$$

which is the dispersion relationship, expressing ω in terms of wavevector, $\vec{k}$. The subscript λ is introduced to indicate that corresponding to a given direction of propogation and wavelength there are three polarizations and frequencies. The three polarization eigenvectors are orthonormal.

The actual solution of the dispersion relationship between ω and $\vec{k}$ is a difficult many-body problem. Fortunately, its solution is not required in order to discuss qualitatively the behavior of the dispersion relationship, which will be useful in explaining the results of the neutron scattering experiment, described later in this chapter.

It is further noted that the cubic and quartic terms were

omitted in the expansion of interaction potential. These anharmonic terms give rise to macroscopic phenomena such as thermal expansion and a linear term in the specific heat at higher temperatures.[10] From a microscopic point of view, these higher-order terms give rise to the possibility of interaction between phonons. It becomes possible to have phonon-phonon scattering take place, which will obviously become a factor in thermal conductivity. This added complexity is, however, not relevant to this discussion and will not be pursued.

2b. The Number of Independent Modes

It is to be noted that not all the $\vec{k}$ vectors are independent. This can be seen by considering the Laue conditions for wave diffraction[11], which state that wavevectors must obey the relationships

$$\left.\begin{aligned} \hat{a}\cdot\vec{\Delta}k &= 2\pi q \\ \hat{b}\cdot\vec{\Delta}k &= 2\pi r \\ \hat{c}\cdot\vec{\Delta}k &= 2\pi s \end{aligned}\right\} \quad \text{or} \quad \vec{r}\cdot\vec{\Delta}k = (\text{integer})\times 2\pi \tag{3.18}$$

where q, r, and s are integers, and

$$\vec{r} = n_1\hat{a} + n_2\hat{b} + n_3\hat{c} \tag{3.19}$$

is the lattice displacement vector in configuration space, with n_1, n_2, and n_3 being integers also.

To relate this to the space dependence of the $\vec{k}$ vectors, one must introduce the concept of reciprocal vectors. These

reciprocal lattice vectors are defined as[11]

$$\vec{A} = 2\pi \frac{\hat{b}\times\hat{c}}{\hat{a}\cdot\hat{b}\times\hat{c}}$$
$$\vec{B} = 2\pi \frac{\hat{c}\times\hat{a}}{\hat{a}\cdot\hat{b}\times\hat{c}} \qquad (3.20)$$
$$\vec{C} = 2\pi \frac{\hat{a}\times\hat{b}}{\hat{a}\cdot\hat{b}\times\hat{c}}$$

and have the units of (length)$^{-1}$.

Any arbitrary vector in the reciprocal lattice may be formed as

$$\vec{G} = h\vec{A} + k\vec{B} + l\vec{C} \qquad (3.21)$$

where h, k, andl are integers.

Forming the scalar product between $\vec{G}$ and $\vec{r}$ will demonstrate the significance of $\vec{G}$. Performing this product, we have:

$$\begin{aligned}\vec{r}\cdot\vec{G} &= (n_1\hat{a} + n_2\hat{b} + n_3\hat{c})\cdot(h\vec{A} + k\vec{B} + l\vec{C}) \\ &= 2\pi(hn_1 + kn_2 + ln_3) \\ &= 2n(\text{integer})\end{aligned} \qquad (3.22)$$

Comparing Eqts.3.18 and 3.22, we see that if $\vec{\Delta k}$ is equal to any reciprocal lattice vector $\vec{G}$, then the Laue conditions are satisfied. Therefore,

$$\vec{\Delta k} = \vec{G} \quad \text{or} \quad \vec{k'} = \vec{k} + \vec{G} \qquad (3.23)$$

This states that the wavevector $\vec{k}$ is unchanged if it is replaced by $\vec{k} + \vec{G}$. The restriction is therefore made that all the independent $\vec{k}$ vectors lie within the volume contained within the parallelpiped defined by the reciprocal vectors of smallest moduli, $\vec{A}$, $\vec{B}$, and $\vec{C}$. This is defined as the first three-dimensional Brillouin

zone, and is equal in volume to:

$$\vec{A} \cdot \vec{B} \times \vec{C} = \frac{(2\pi)^3}{\hat{a} \cdot \hat{b} \times \hat{c}} = \frac{(2\pi)^3}{V_o} \tag{3.24}$$

where V_o is the volume per atom in configuration space. This volume calculated in Eqt.3.24 represents the range of the vector $\vec{k}$. It is an obvious generalization of the one-dimensional range of k which is $2\pi / a$.

Again generalizing from the one dimensional case, where there is one allowed k for each volume $(2\pi/L)$ in k-space, we get for the density of points in $\vec{k}$-space:

$$\mathcal{N}_k = \left(\frac{L}{2\pi} \right)^3 \tag{3.25}$$

where L is the length of the side of the cubic sample, with periodic boundary conditions.

The number of points in $\vec{k}$-space (i.e., the number of independent modes of vibration) is then obtained from Eqts.3.24 and 3.25, and is

$$\left(\frac{L}{2\pi} \right)^3 \frac{(2\pi)^3}{V_o} = N \tag{3.26}$$

since $L^3 = NV_o$. The number of independent modes is thus equal to the number of atoms in the sample. Since each mode may exist in any of three polarizations, this leads to 3N phonons for the system.

Frequently, as in the case for this investigation, one is more interested in the number of states per frequency range.

The density of states for a particular frquency ω is obtained as follows:

$$\frac{dn}{d\omega} = \mathcal{D}(\omega) = w_k \frac{dk}{d\omega} = \frac{w_k}{\frac{d\omega}{dk}} \tag{3.27}$$

or

$$\mathcal{D}(\omega) = \frac{w_k}{|\nabla_k \omega|} \tag{3.28}$$

We can obtain $|\nabla_k \omega|$ from the dispersion relationship, Eqt.3.17, once the interaction potential is known. It is also to be noted that

$$v_g = |\nabla_k \omega| \tag{3.29}$$

where v_g is the magnitude of the group velocity.

Eqt.3.28 is important because it is essentially $\mathcal{D}(\omega)$ which will be observed by the neutron scattering experiment to be described later in this chapter.

2c.The Lattice With a Basis[13]

Consider a one-dimensional solid composed of two atoms per unit cell. Instead of obtaining one equation of motion as in Eqt.3.12, one obtains two equations, one for each atom in the unit cell.These are,

$$m_1 \ddot{u}_{n,1} = \beta(u_{n,2} + u_{n-1,2} - 2u_{n,1})$$
$$m_2 \ddot{u}_{n,2} = \beta(u_{n,1} + u_{n+1,1} - 2u_{n,2})$$

where u is the displacement, and n labels the unit cell. The two equations cannot be satisfied by a single plane wave, so two waves are assumed, one passing through atom n,1, and the other through atom n,2,

$$u_{n,1} = q_1 e^{i(\omega t + kr_{n,1})}$$
$$u_{n,2} = q_2 e^{i(\omega t + kr_{n,2})}$$

where the r's are the actual positions of the atoms, and the q's are amplitudes. Substituting these solutions into the equations of motion results in two simultaneous equations for the displacements of the two atoms,

$$-\omega^2 m_1 q_1 = \beta q_2 (e^{ika} + e^{-ika}) - 2\beta q_1$$
$$-\omega^2 m_2 q_2 = \beta q_1 (e^{ika} + e^{-ika}) - 2\beta q_2$$

where $r_{n,1} = na$. By the standard analysis, these two equations can give nontrivial values for the displacements only if the determinant of the coefficients of the displacements is set equal to zero,

$$\begin{vmatrix} 2\beta - m_1\omega^2 & -2\beta\cos ka \\ -2\beta\cos ka & 2\beta - m_2\omega^2 \end{vmatrix} = 0$$

Evaluating the secular determinant results in a second order equation for ω^2 in terms of k. The equation has two sets of solutions,

$$\omega^2 = \beta\left(\frac{1}{m_1} + \frac{1}{m_2}\right) \pm \beta\left[\left(\frac{1}{m_1} + \frac{1}{m_2}\right) - \frac{4\sin^2 ka}{m_1 m_2}\right]^{1/2}$$

Thus for each value of k there are two distinct modes of vibration. The modes in which the two atoms in a given cell are in phase with each other are called the acoustic modes. The modes in which the two atoms are out of phase with each other are called the optic modes. (See Fig.3.1 for the case of ionic basis elements under transverse polarization.) Intuitively, one can see that for a given k, the optic modes will have a considerably higher frequency than the acoustic modes, since the out-of-phase motion of the two neighboring atoms can give rise to a higher frequency of vibration than

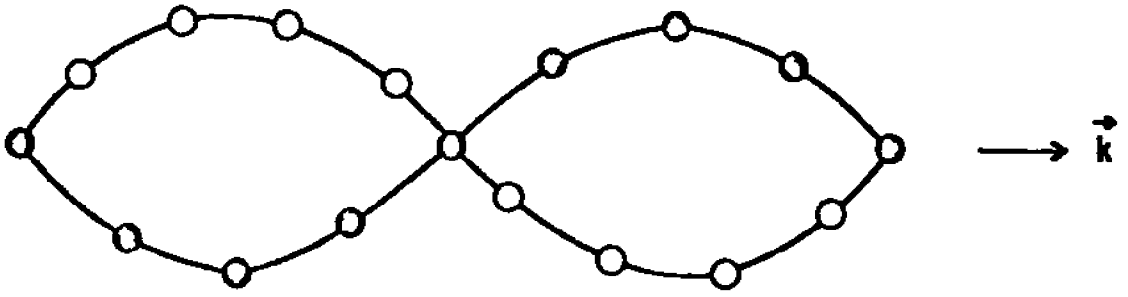

TRANSVERSE OPTIC MODE

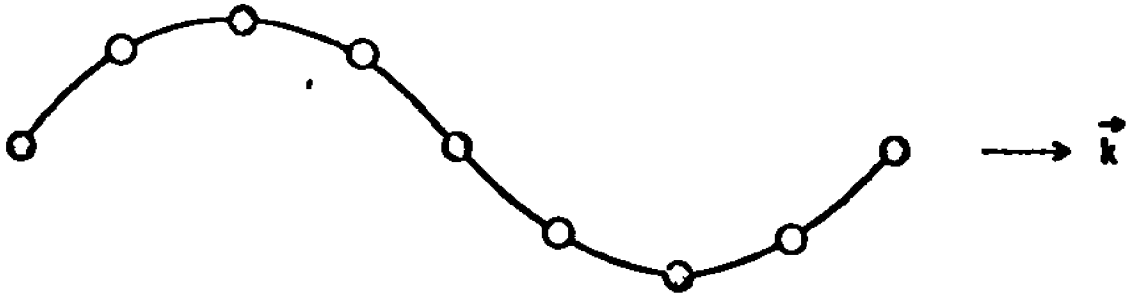

TRANSVERSE ACOUSTIC MODE

FIG. 3.1

One Dimensional Ionic Basis Elements Undergoing Transverse Polarization. (a) The Optic Mode. (b) The Acoustic Mode.

the in-phase motion.

Fig.3.2 shows the result for the one-dimensional dispersion relation of the lattice with a basis.[13] Waves within the forbidden region, indicated in Fig.3.2, are damped and will not propogate. Both the acoustic and optic branches are shown for the first Brillouin zone. It is to be noted that the two branches intersect the zone boundaries perpendicularly. This is equivalent to saying that the group velocity, $v_g=d\omega/dk$, is zero. The lattice will therefore support only standing waves at $k=\pi/2a$. (The basis dimension in this case is 2a.)

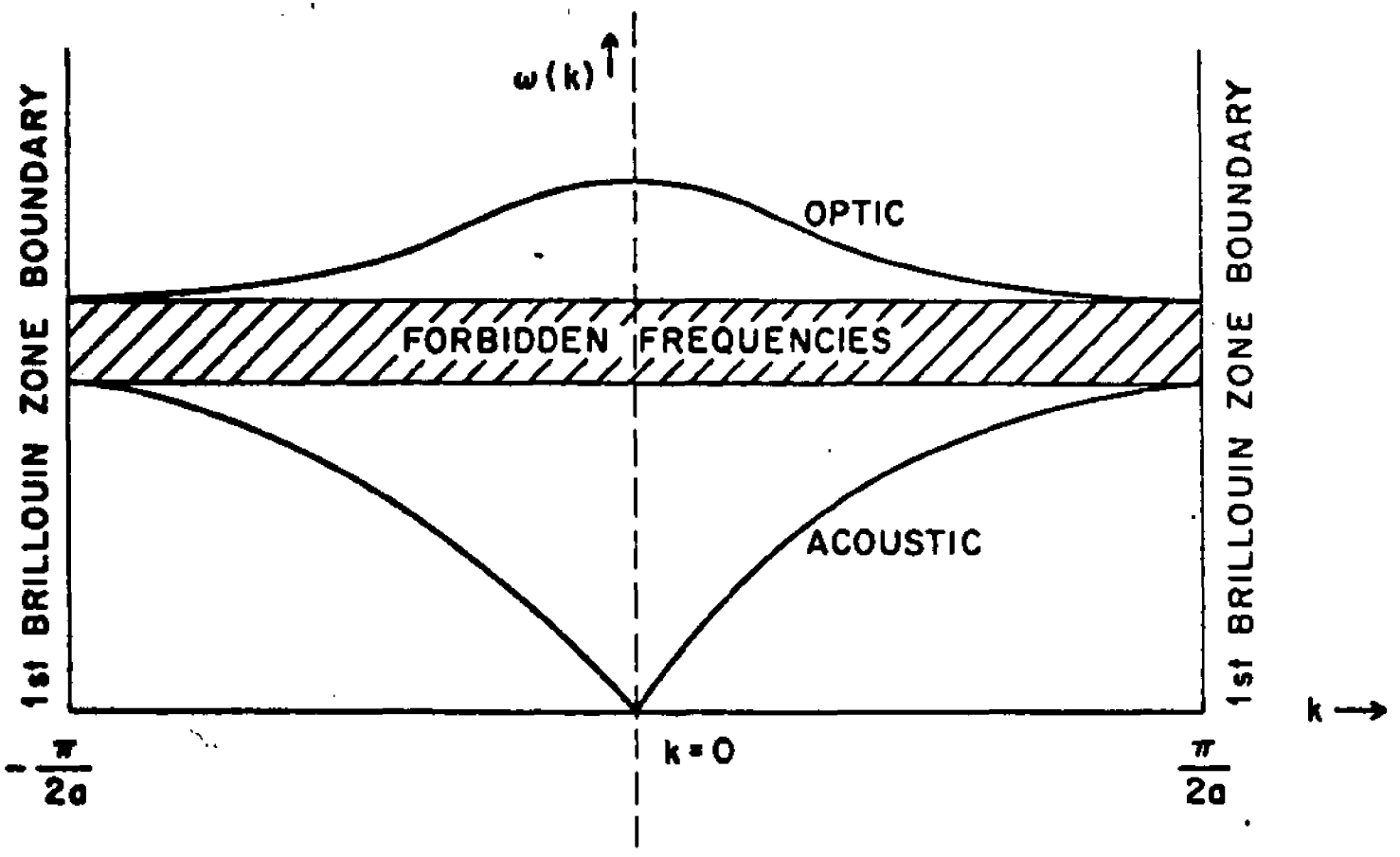

FIG. 3.2

The One Dimensional Dispersion Curve Over the Entire First Brillouin Zone.

2d. The Lyddane-Sachs-Teller Relationship[14]

In deriving the LST relationship, it is helpful first to consider the differences between longitudinal and transverse polarizations. We will also be concerned with the long wavelength ($k \to 0$) or continuous limit. We may therefore use Maxwell's equations for continuous media.

Let the polarization per unit volume be given by

$$\vec{P} = \vec{P}_0 e^{-i(\vec{k}\cdot\vec{r} - \omega t)} \tag{3.30}$$

This polarization is associated with a time varying $\vec{E}$ and $\vec{D}$ fields,

$$\vec{E} = \vec{E}_0 e^{-i(\vec{k}\cdot\vec{r} - \omega t)} \tag{3.31}$$

and

$$\vec{D} = \vec{D}_0 e^{-i(\vec{k}\cdot\vec{r} - \omega t)} \tag{3.32}$$

using the standard expression,

$$\vec{D} = \vec{E} + 4\pi \vec{P} \tag{3.33}$$

Maxwell's first equation may be evaluated using Eqt.3.33 by taking the divergence of $\vec{D}$,[15]

$$\nabla\cdot\vec{D} = \nabla\cdot\vec{E} + 4\pi\,\nabla\cdot\vec{P} = 4\pi\rho = 0 \tag{3.34}$$

if there is no free charge density present. This gives for the divergence of $\vec{E}$,

$$\nabla\cdot\vec{E} = -4\pi\,\nabla\cdot\vec{P} \tag{3.35}$$

For the case of <u>transverse</u> polarization, $\vec{k}$ and $\vec{P}$ are perpendicular, so Eqt.3.35 becomes, using Eqt.3.30,

$$\nabla\cdot\vec{E} = -4\pi(i\vec{k}\cdot\vec{P}) = 0 \tag{3.36}$$

To sovle this equation for $\vec{E}$, one sees that $\vec{E}$ is either a

constant, which may be set equal to zero, or $\vec{E}=(\text{constant})\vec{P}$. If there are no sources for transverse $\vec{E}$, $\vec{E}$ and $\vec{P}$ cannot be parallel and the latter possibility is not correct. Therefore one finds that

$$\vec{E}=0 \qquad \text{(Transverse)} \tag{3.37}$$

In the case of a time varying <u>longitudinal</u> polarization, $\vec{P}$ and $\vec{k}$ are parallel so Eqt.3.35 must be evaluated. To a constant term, we may express the field then, using Eqt.3.35 as,

$$\vec{E}=4\pi\vec{P} \qquad \text{(Longitudinal)} \tag{3.38}$$

where a longitudinal polarization is then associated with a longitudinal electric field.

Consider now the case for positive and negative ions, displaced in opposite directions by x_+ and x_-, respectively.

The ionic polarization per unit volume becomes

$$P = \frac{e\,x}{2a^3} = \frac{e\,x}{\Omega} \tag{3.39}$$

where a is the lattice spacing and $\Omega = 2a^3$, the volume per ion pair.

The equation of motion for the displacement is given by

$$\ddot{x} = \frac{F}{\mu} \tag{3.40}$$

where F is the restoring force and μ is the reduced mass of the ion pair.

In the transverse case, ignoring the damping terms, the restoring force may be rewritten as:

$$F_T = -\beta x = -\mu\omega_T^2 x \tag{3.41}$$

corresponding to free harmonic oscillations, where β is the force constant, and ω_T is the transverse vibrational frequency.

Eqt.3.40 becomes

$$\ddot{X} + \omega_T^2 X = 0 \qquad \text{(Transverse)} \tag{3.42}$$

In the longitudinal case, the restoring force is given by

$$F_L = -\mu\omega_T^2 x + eE \tag{3.43}$$

The first term on the right hand side of the equation is identical with that in Eqt.3.41 and arises from the overlap of the displaced ions. The second term is due to the longitudinal electric field associated with the longitudinal vibration. Thus the equation of motion becomes:

$$\ddot{X} + \omega_T^2 X - \frac{eE}{\mu} = 0 \qquad \text{(Longitudinal)} \tag{3.44}$$

As we saw in Chapter 2, the polarization $\vec{P}$ must include both ionic and electronic contributions,

$$P = P_I + P_e \tag{3.45}$$

At optical frequencies, the ionic contribution vanishes since the ions cannot follow the changes in the field. P_e may then be written in terms of the high frequency dielectric constant, ε_∞, by rearranging Eqt.3.33 and remembering that $\vec{D} = \varepsilon\vec{E}$ we get

$$P_e = \frac{(\varepsilon_\infty - 1)E}{4\pi} \tag{3.46}$$

Therefore, using Eqt.3.39

$$P = \frac{ex}{\Omega} + \frac{(\varepsilon_\infty - 1)E}{4\pi} \tag{3.47}$$

or using Eqt.3.38

or using Eqt.3.38

$$E = -4\pi\left[\frac{ex}{\Omega} + \frac{(\varepsilon_\infty - 1)E}{4\pi}\right] \tag{3.48}$$

Solving Eqt.3.48 for E, one gets

$$E = -\frac{4\pi e x}{\Omega \varepsilon_\infty} \tag{3.49}$$

so that Eqt.3.44 takes the form

$$\ddot{x} + \left(\omega_T^2 + \frac{4\pi e^2}{\mu \Omega \varepsilon_\infty}\right) x = 0 \tag{3.50}$$

This has the same form as Eqt.3.42 if the longitudinal frequency ω_L is defined as

$$\omega_L^2 = \omega_T^2 + \frac{4\pi e^2}{\mu \Omega \varepsilon_\infty} \tag{3.51}$$

In evaluating this, one must consider the two solutions to Eqt.3.44, one for each ion. They are

$$x_- = -\frac{e}{m_1}\left(\frac{E}{\omega_T^2 - \omega^2}\right)$$
$$x_+ = \frac{e}{m_2}\left(\frac{E}{\omega_T^2 - \omega^2}\right) \tag{3.52}$$

where plane wave solutions were substituted into Eqt.3.44.

At very low frequencies, where the ions are able to follow the field, the maximum displacement is:

$$X = x_+ - x_- = \frac{eE}{\mu \omega_T^2} \tag{3.53}$$

Therefore the ionic contribution to the polarization becomes, using Eqt.3.39,

$$\Delta P = \frac{e^2 E}{\Omega \mu \omega_T^2} \tag{3.54}$$

Also, since $(\varepsilon - 1) = 4\pi P/E$, we get:

$$\Delta\varepsilon = \frac{4\pi}{E}\Delta P = \varepsilon_s - \varepsilon_\infty \tag{3.55}$$

where ε_s is the low frequency or static dielectric constant. Substituting Eqt.3.54 into 3.55 gives

$$\omega_T^2(\varepsilon_s - \varepsilon_\infty) = \frac{4\pi e^2}{\Omega \mu} \tag{3.56}$$

Substituting this into Eqt.3.51 gives

$$\omega_L^2 = \omega_T^2 + \omega_T^2(\varepsilon_s - \varepsilon_\infty)/\varepsilon_\infty \tag{3.57}$$

which may be further simplified to read:

$$\frac{\omega_L^2}{\omega_T^2} = \frac{\varepsilon_s}{\varepsilon_\infty} \qquad (k \to 0) \tag{3.58}$$

This is the Lyddane-Sachs-Teller relationship[16]. Since this relation was derived using the continuous limit, it applies for wavevectors near zero and for optic frequencies.

3. Motivation For a Cold Neutron Inelastic Scattering Investigation of Phenanthrene

Eqt.3.58, the Lyddane-Sachs-Teller relationship, represents the primary reason for performing the cold neutron inelastic scattering study of phenanthrene. In view of the results of Chapter 2, in which an anomalous increase in the static dielectric constant was observed, Eqt.3.58 predicts that a diminishing of a transverse mode of vibration should occur at the same anomaly temperature. Such a "softening" of low lying ($k \to 0$) modes has been observed in some ferroelectric materials at their transition temperatures.[17]

If one were to perform a coherent scattering experiment on an oriented single crystal, one might hope to obtain experimentally the dispersion relationship between ω and $\vec{k}$. This would provide us with a picture similar to that in Fig.3.2, but for three dimensions, where the behavior of low lying modes of vibration could be observed.

Unfortunately, for most hydrogenous material, the scattering is essentially entirely incoherent. This makes it impossible to determine the particular values for $\vec{k}$. One cannot then obtain data directly on the shape of the dispersion curve.

It will be shown later in this chapter that in the experiment that was performed one observes essentially the density of modes per frequency, $\mathcal{D}(\omega)$. However, we may relate this to the low-lying modes by using Eqt.3.28. A decrease in the number of low-lying modes of vibration, determined by comparing density of state spectra at different temperatures, is associated with an increase in the slope of the small $\vec{k}$ end of the dispersion curve through this equation. Furthermore, Fig.3.3 indicates how this increase in the slope of the dispersion curve is related to a decrease in the value of low lying modes, ω_{T_0}. This in turn is of significance when viewed in light of the LST relatic

Since the range in energy of the scattered neutron spectra in this experiment is about from $5x10^{-3}$ electron volts to about $5x10^{-1}$ electron volts, the frequencies corresponding to these limits go from about 10^{12} to 10^{14} cycles per second, which is within the optical region.

4. Cold Neutron Scattering in Solids: Essential Properties[18]

With the development of high flux reactors, the use of cold neutrons as a probe of lattice and molecular vibrations has become increasingly common. There are several features about cold neutrons (energy less than 1 ev) which make them particularly suitable as a probe. First, the neutron-phonon coupling is weak, insuring that the probe does not materially influence what it is monitoring. Secondly, the de Broglie wavelength of

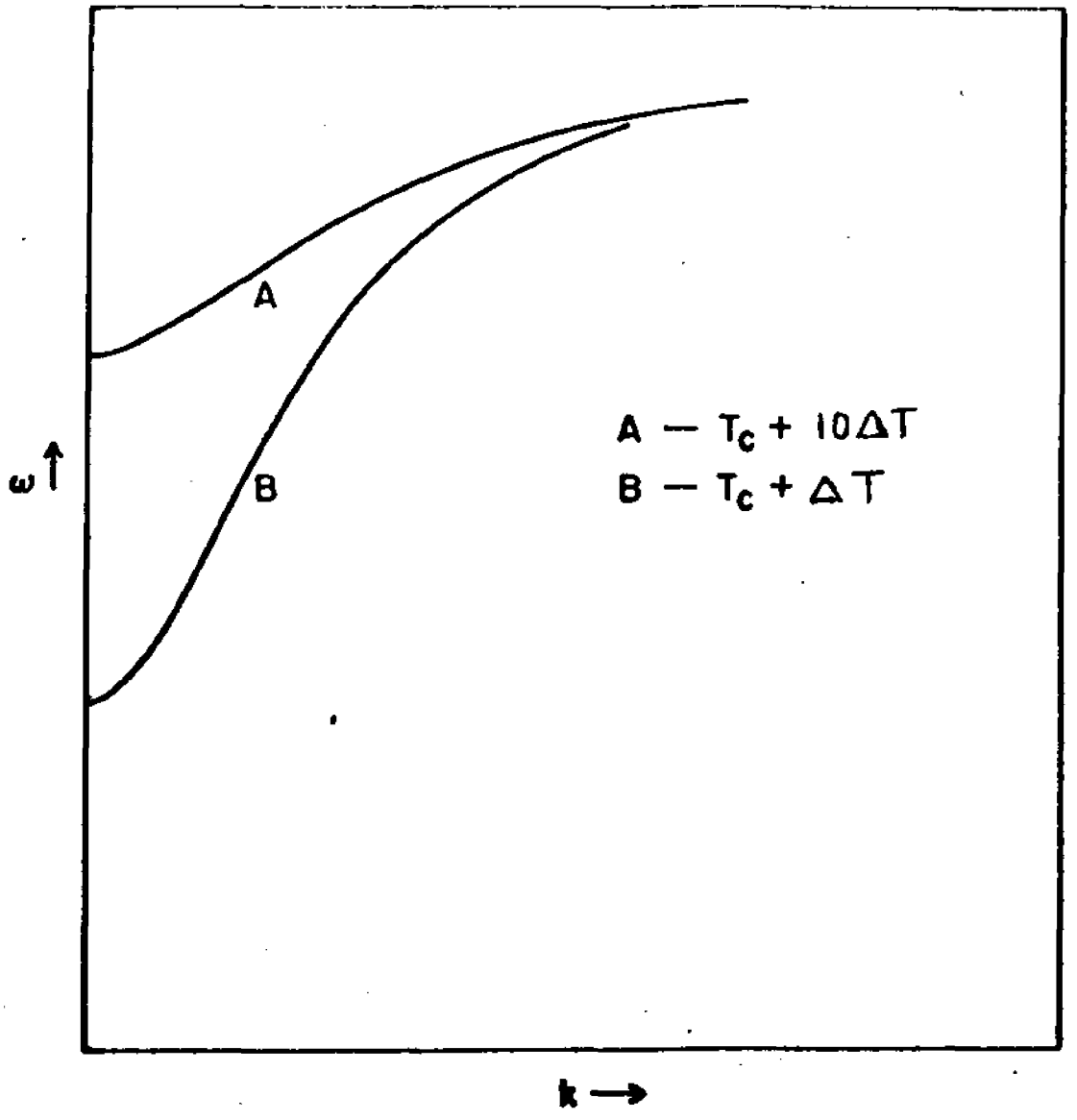

FIG. 3.3

The Behavior of the Low-Lying ($k \to 0$) End of a Hypothetical Dispersion Curve as the Temperature Approaches the Transition Region.

cold neutrons is roughly comparable to the interatomic spacing, allowing for easy detection of large momentum transfers. Finally, the energy of the neutrons is sufficiently low that one can easily measure the energies transferred between the neutrons and the phonons.

Neutrons probe a vibrational system on an energy scale of between 10^{-3} to 10^{-1} electron volts, on a wavelength scale of the order of 10^{-8} centimeters, and on a time scale of between 10^{-14} to 10^{-11} seconds. Comparing with different types of probes, x-rays for example have much higher energies and would be relatively unaffected by the hydrogens in phenanthrene. Optical scattering covers essentially the same frequency range, but the wavelength is roughly three or more orders of magnitude greater. In general the frequency range covered by cold neutron scattering (30-1000 cm^{-1}) contains some intramolecular and all intermolecular vibrations[19].

The two types of interactions that are possible between the neutrons and the phonons are elastic and inelastic scattering. If there is no change in energy between the incident and scattered neutron, the process is called elastic scattering. If the neutron and the lattice do exchange energy, the process is called inelastic scattering.

Because of the periodic structure of the lattice, coherent

interference among the scattered neutrons is possible. This coherent scattering can occur either elastically or inelastically. On the other hand, randomly distributed different isotopic states or spin states of nuclei act to destroy the coherent nature of scattering. This type of scattering is basically different from normal coherent scattering, which is analogous to the scattering of electromagnetic radiation. The scattering of a neutron wave from a system of identical nuclei having spin zero would be entirely coherent. In this situation, interference among the scattered waves is entirely probable. For a system of identical nuclei with nonzero spin, the interaction between the nuclei and the neutrons would be dependent on the relative orientation of the spins of the neutrons and the nuclei. The random orientations effectively destroys the coherence. The separate nuclei scatter independently and no interference is observed. For nuclei with zero spin, incoherence can still result if the scattering length can vary from nucleus to nucleus as would happen in an isotopic mixture.

Since the material being studied in this experiment contains an appreciable amount of amount of hydrogen, (the chemical formula for phenanthrene is $C_{14}H_{10}$) the scattering will be mostly incoherent, since the hydrogen nucleashas a nonzero spin.

The information that one can obtain from a neutron scattering experiment can be grouped into several categories. Firstly,

a measurement of the angular distribution of the scattered neutrons which have undergone coherent inelastic scattering, in which a single phonon is involved, yields directly the frequency versus wave number dispersion relation for the phonons. Unfortunately, this method for observing the low lying modes of vibration cannot be used due to the essential incoherent nature of the scattering spectrum of hydrogen.

Secondly, one-phonon coherent inelastic scattering provides a way for probing the phonon-phonon anharmonic interactions within a crystal. The neutron peaks corresponding to such scattering are broadened as a consequence of that interaction. Their widths may be measured as a function of temperature and of the wave number of the phonon under consideration. Again the incoherent nature of the scattering off phenanthrene militates against this method.

Elastic scattering provides information about diffusive motions in the scattering system. These diffusive processes manifest themselves as a broadening of the elastic peak in the scattered neutron spectrum.

Finally, incoherent, inelastic scattering can be used to obtain information about $\mathcal{A}(\omega)$, the spectral density of the lattice vibrations. Peaks in this spectrum indicate maxima in the density of vibrational states, $\mathcal{G}(\omega)$. These states are ordinarily populated, at high temperatures, according to a Boltzmann distribution.

For the purposes of this investigation, in which one is looking for ferroelectric-like behavior, an experiment which will provide information about $\mathcal{S}(\omega)$ is very useful, as was explained in Section 3.

A final consideration must be given to the problem of selection rules. The frequencies that appear in the infrared and Raman fundamental spectra are those which correspond to motion involving the fluctuations of the dipole moment or the polarizability. For crystals, this means the radiation couples only with the transverse optical modes. To obtain information about the entire spectrum, one must consider the overtones and combination bands where multiphonon and anharmonic effects cause a relaxation of the selection rules.[20] Inelastic neutron scattering has no analogous selection rules. However, since all frequencies are active, the spectrum takes the appearance of a continuous band. The conventional method of performing an analysis based on assigning energy levels is thus made considerably more difficult.

5. Description of the Experiment

In a conventional inelastic scattering experiment, one must insure that the following three functions are performed:[21] (1) neutrons in as small a velocity interval as possible, consistent with reasonable flux densities, must be obtained for the incident beam, (2) the energy of the scattered neutrons must be detected and analyzed to determine the energy change,

and (3) the angle of scattering with respect to the incident beam and with respect to the sample orientation must be measured to determine the momentum change.

Only the third of these will not be performed, since for incoherent scattering we assume the spectrum also to be isotropic.

The first function will be performed by using a beryllium filter. The second function will be performed using a standard time-of-flight analysis.

5a. The Neutron Beam

The experiment was performed at the Brookhaven Graphite Research Reactor. Fig.3.4 shows a diagram of the Slow Chopper Facility located on the top of the reactor. The neutron radiating surface is about three meters from the sample. Since the spectrum of neutrons from such a source possesses a broad range of energies, some method of "monochromating" the incident beam is required.

The technique employed to define the energy of the incident beam consists of the use of a beryllium filter. In this method a block of polycrystalline beryllium intercepts the reactor beam. Due to Bragg scattering, all the neutrons of energy greater than 5×10^{-3} electron volts, (corresponding to a wave-vector of about 3.96 Å), are eliminated from the beam. For neutrons of energy less than 5×10^{-3} electron volts, the

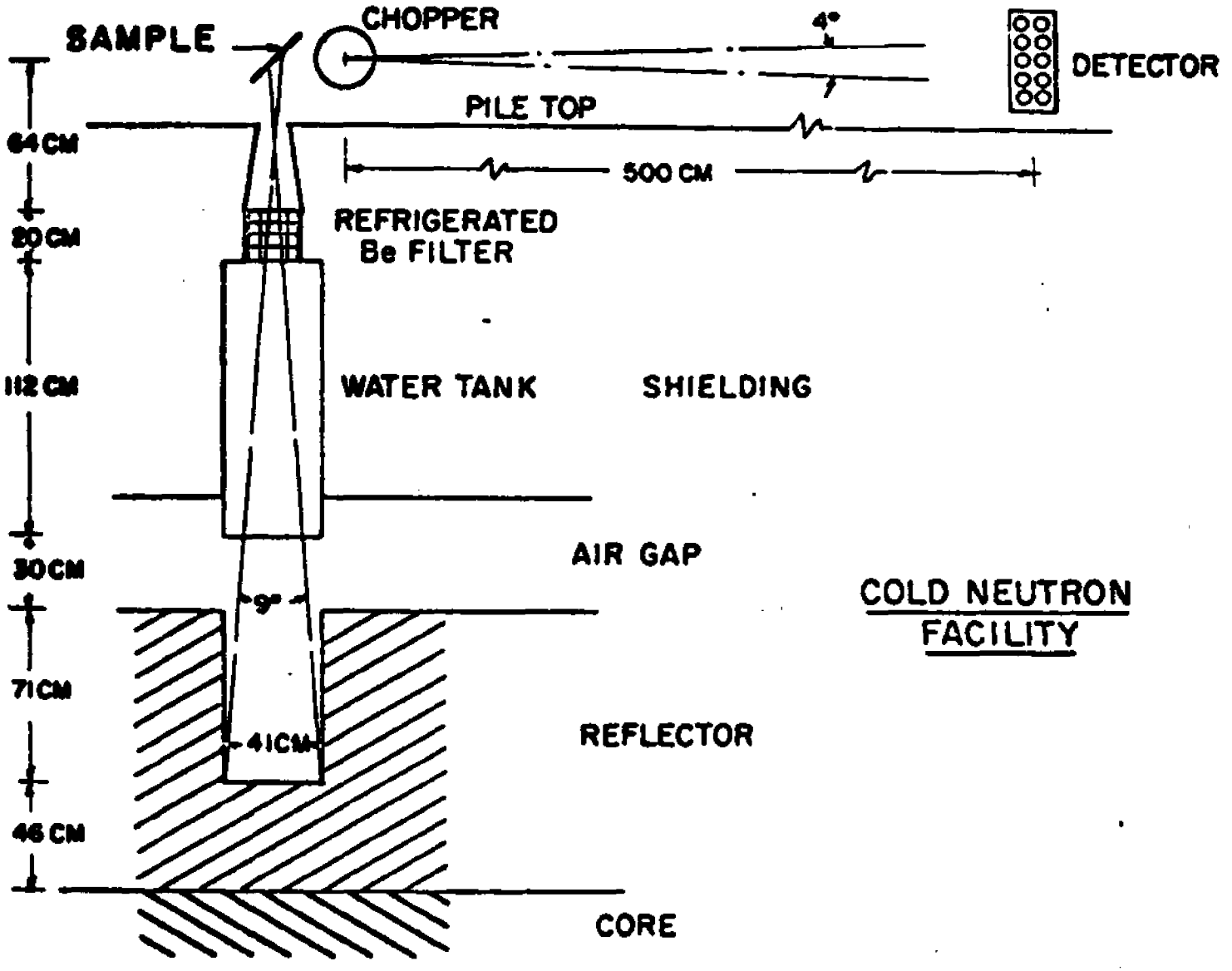

FIG. 3.4

Schematic Representation of the Brookhaven Graphite Research Reactor and Cold Neutron Facility.

beryllium filter is transparent, since the coherent scattering can only occur in the forward direction.[21] (See Fig.3.5.) The beryllium filter therefore acts as a good low pass filter for neutrons, allowing nearly 90% of the neutrons in the cold part of the reactor to be used, although it does not really monochromate the beam. The filter is also cooled to liquid nitrogen temperatures to minimize the attenuation of the low energy neutrons due to scattering from phonons.

The incident beam passes up through the pile top into a drum where the sample is located. An arm connected to the drum carries the chopper on one end and the BF_3 neutron detector bank on the other end.

5b. The Time-of-Flight Analysis[22]

Time-of-flight techniques are those where a burst of polychromatic neutrons is produced, and the time it takes for these neutrons to travel from the source of the burst (the chopper) to a detector is measured. The chopper thus acts as a neutron shutter.

Fig.3.6 shows a diagram of the chopper. It consistes of a stack of cadmium plated steel sheets, stacked in a four inch diameter shell. The rotor spins at about 7500 revolutions per minute, and transmits a burst of neutrons of about 30 microseconds.

Fig.3.7 illustrates the technique of time-of-flight analysis in which the slower neutrons take longer to travel to the detector, so that they are counted at a later time.

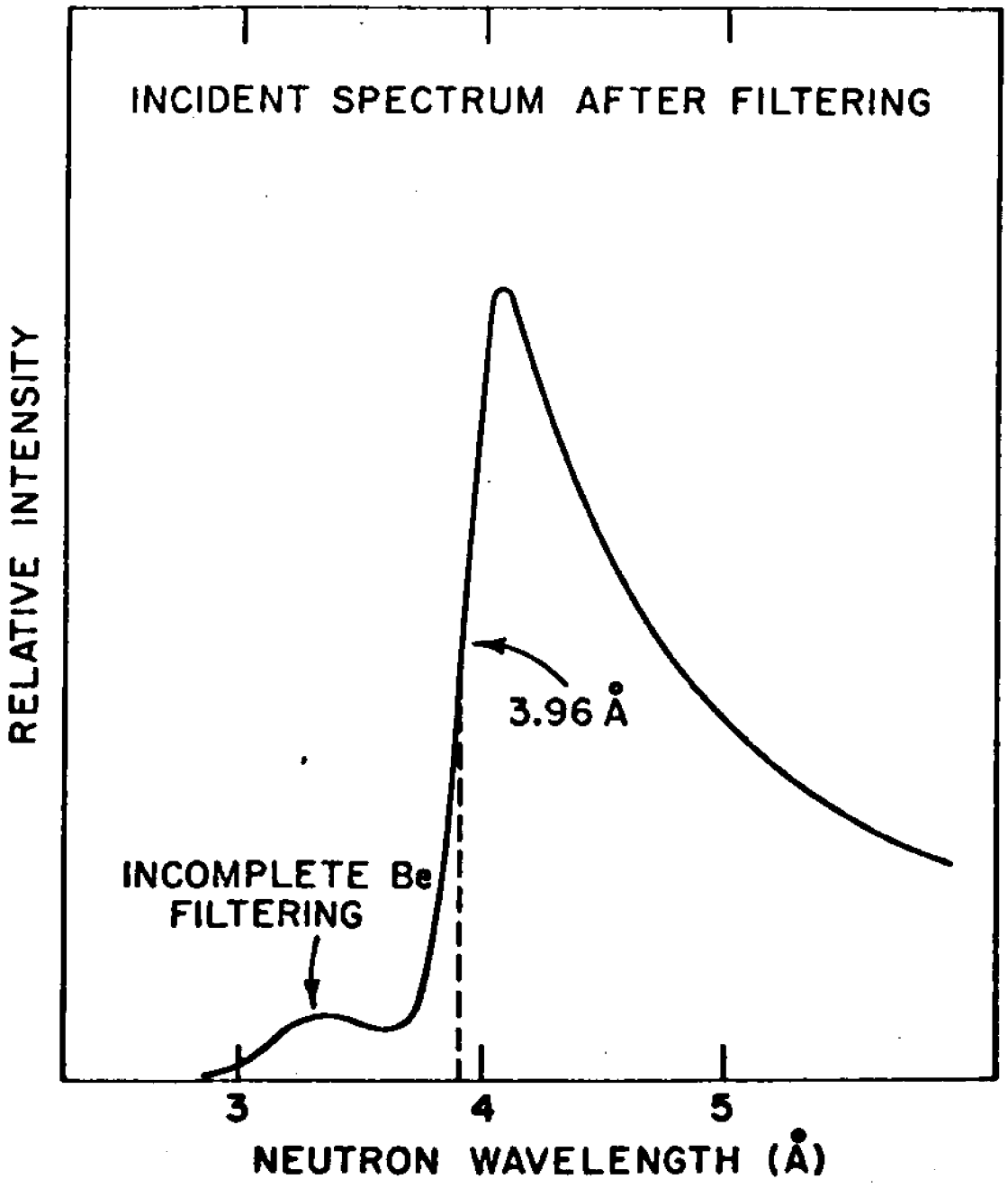

FIG. 3.5

The Wavelength Spectrum of the Filtered Cold Neutron Beam Incident on the Sample Material.

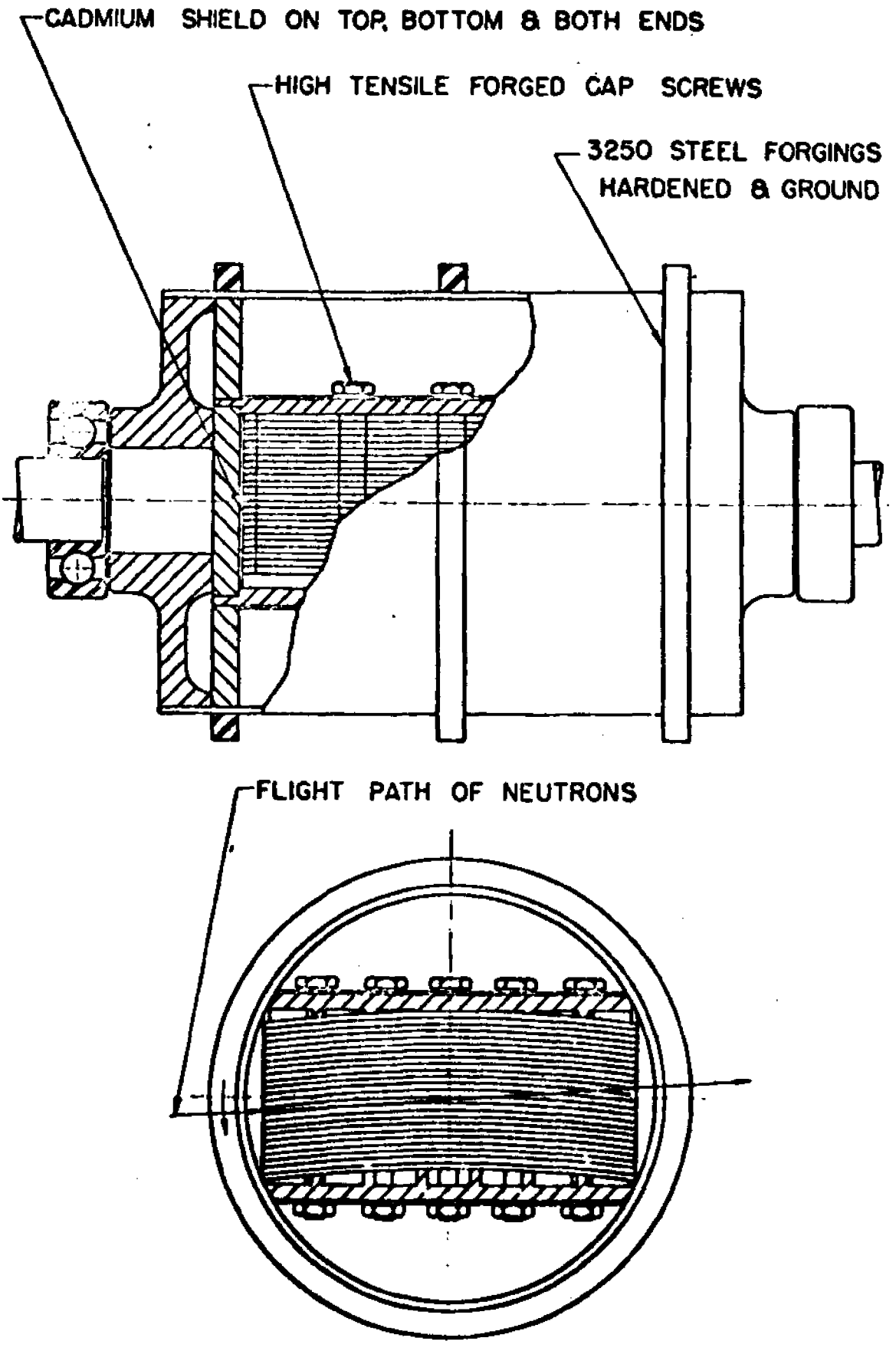

FIG. 3.6

The Slow Chopper Construction.

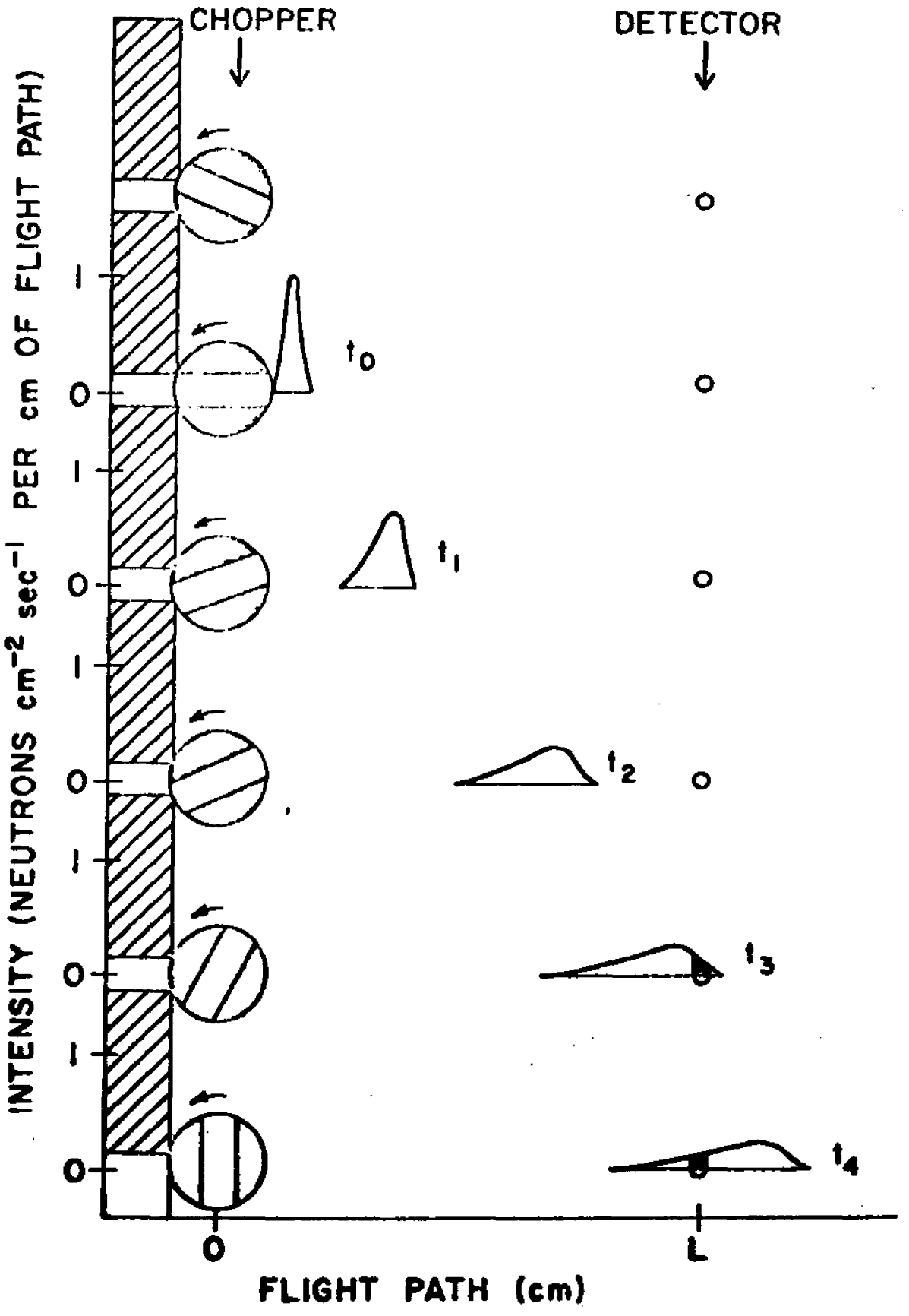

FIG. 3.7

Schematic Representation of a Time-of-Flight Analysis of a Maxwellian Energy Distribution of a Neutron Burst.

In Fig.3.7 the beam incident on the chopper is the neutron flux scattered from the sample. (In this experiment, the angle between the incident beam and the moveable arm with the detector bank was 90 degrees.) Assuming a Maxwellian distribution in energies, the chopper in the diagram opens at time t_0, successive subscripts indicate later times. It can be seen from the diagram that after a so-called dead time, the pulse reaches the detectors, which proceed to monitor the different energies at different times.

In this experiment, a RIDL 400 channel analyzer was used to record and store the pulses from the counter as a function of the channel number. The spectrum could be displayed on a cathode ray tube or put on punched paper tape. The channel separation was 25 microseconds, with only 200 of the 400 channels being used for each run.

In order to obtain a spectrum in terms of energy, it is necessary to determine the energy associated with each channel. To do this one must first determine the dead time, i.e., the time it takes for the neutron pulse to travel from the chopper to the detector. It will be shown how this may be determined using the elastic scattering peak, the energy of which is determined by the beryllium filtered incident beam and is known to be 5×10^{-3} electron volts.

The standard expression for the kinetic energy of the neutrons at the detector is:

$$E(ev) = \frac{m(gr)}{2}\left[\frac{L(m)}{T_0 + 2.5\times10^{-6}(sec)}\right]^2 \times (0.0625\times10^{12}) \qquad (3.59)$$

where T_D is the dead time, m is the mass of the neutron, 1.67×10^{-24} gr., L is the length of the flight path, 500 cm., N is the particular channel under consideration, and the constant factor converts from ergs to electron volts. If one uses N_e, the channel number for the elastic scattering peak, and $E = 5 \times 10^{-3}$ electron volts, Eqt.3.59 may be solved for the dead time T_D. Thereafter, Eqt.3.59 may be used to determine the energy of any desired channel in the spectrum by specifying N.

One may also determine the wavenumber of the neutrons, for any particular channel, using the equation

$$k(N) \equiv \frac{1}{\lambda(N)} = \frac{\sqrt{2mE(N)}}{h} \qquad (3.60)$$

where h is Planck's constant, 6.6×10^{-27} erg-sec, and E is the energy in ergs (Eqt.3.59 without the conversion factor.)

5c. The Sample Holder

The sample holder is made of 1100-type pure aluminum. This is unalloyed aluminum made especially for insertion into reactors. Because of its purity, the possibility of it becoming "hot" due to neutron irradiation is minimized. Because of aluminum's low cross section for cold neutrons, it makes a useful construction material, being relatively transparent to neutrons. Fig.3.8a shows a diagram of the sample holder with the open chamber visible. The sample chamber is a rectangular volume which was milled out of the solid sample block. It contains a volume of about 60 cubic centimeters.

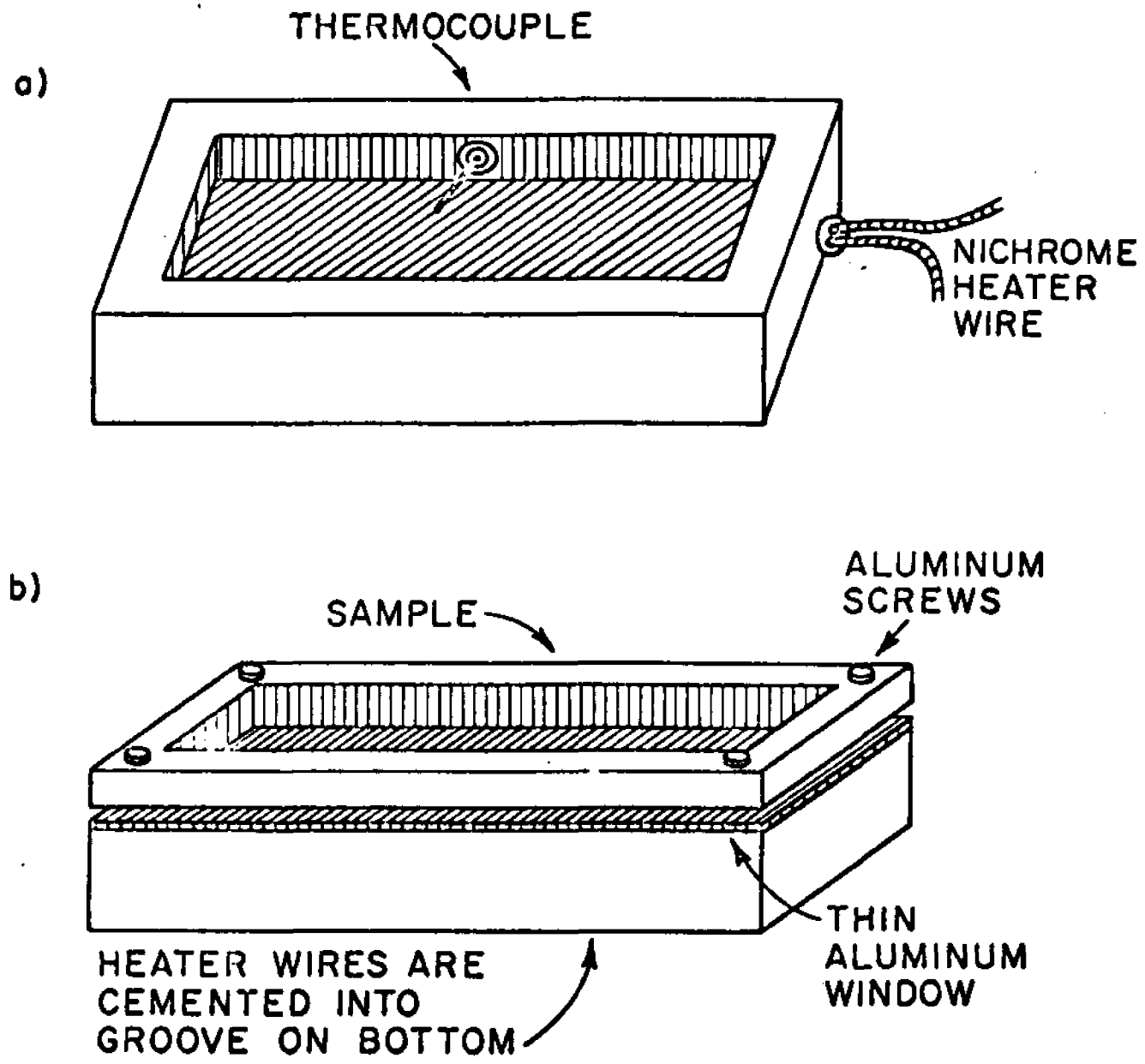

FIG. 3.8

The Neutron Scattering Sample Holder, Approximately 3/4 Actual Size. (a) The Sample Chamber. (b) The Sample Holder With the Frame and Window Attached. (c) Block Diagram of Circuitry.

A glass sealed feed through made by the Stupakoff Ceramics and Manufacturing Company provided the means of introducing an iron-constantan thermocouple into the sample chamber, through a side wall. This thermocouple was used with a West Instrument Corporation pyrometric proportional temperature controller, Gardsman Model JP.

On the underside of the sample holder, beneath the sample chamber, a winding groove was milled to accept an asbestos sheathed #24 nichrome heating wire. The heating wire was sealed into the groove using "Sauereisen", an insulating ceramic cement, manufactured by the Sauereisen Cements Company. A "Powerstat", type 20, manufactured by the Superior Electric Company, switched on and off by the temperature controller, supplied current to the heater wire. A block representation of the control of the heating system is shown in Fig.3.8c.

A thin (~ 0.0156 inches) 1100-type aluminum window was pasted over the open sample chamber after the sample material was introduced. RTV-102 white silicone rubber adhesive sealant, manufactured by the General Electric Company, was used to seal the window to the sample holder. Care was taken to insure that there were no openings through which the material might sublime out once the temperature was increased. To help insure a vaccuum tight seal, an 1100-type aluminum frame, with aluminum screws was used to press the aluminum window flush against the sample holder. (See Fig.3.8b.)

The entire sample holder was then placed in the drum over

the beryllium filter. To minimize air scattering of the beam, the drum was evacuated.

5d. The Phenanthrene Sample

The sample was purified in the same manner as was described in Chapter 2, Section 3a. Due to the fact that incoherent scattering was involved, a single crystal was not needed, so a powdered sample was used.

5e. Techniques and Results

The cold neutron inelastic scattering spectra for 90 degree incoherent scattering off phenanthrene were obtained for several different temperatures around the anomaly temperature of about 72°C. The ambiant temperature run was always performed first. The higher temperature runs were then performed. Finally, the room temperature run was repeated and compared with the first run to check for the possibility of the sample having melted. In this circumstance it is possible that all the material might flow into a corner, possibly out of the neutron beam. The results of each run were converted to punched paper tape, which in turn were converted to cards.

The analysis of the data was performed using the Control Data Corporation 6600 computer system available at Brookhaven

National Laboratory. The plotting of the data was done using the peripheral equipment at the Computer Center, in this case the Calcomp Model 565 Electro-Mechanical Plotter.

Using Eqt.3.60, the wave number of each channel was determined. In order to better observe the behavior at low energies, the log of the wave number was also determined for each channel. The displaced spectra are plotted as a function of the log of the wave number in Fig.3.9. The bars in the diagram represent the uncertainty in the points, and are the deviations of a Poisson distribution where only one total is taken. Also, since the width of the incident neutron beam is not insignificant compared to the energies examined in the scattered beam, a considerable loss of resolution results at the low energy end ($k \rightarrow 0$) of the spectrum.

Although there is no apparent shift in the peaks of the spectra, there is a discernable change in the relationship of the peaks to each other, from one spectrum to the next. For example, the peak at about 65 cm^{-1} becomes smaller in relation to the higher energy peaks as the temperature increases towards 72°C. Above the anomaly temperature, this peak seems to be regaining some of its relative strength.

In order to check for a possible loss of density of modes of vibration, a difference plot between the room temperature and the 75° C spectrum was obtained using the computer to perform the calculations. The results of this difference analysis

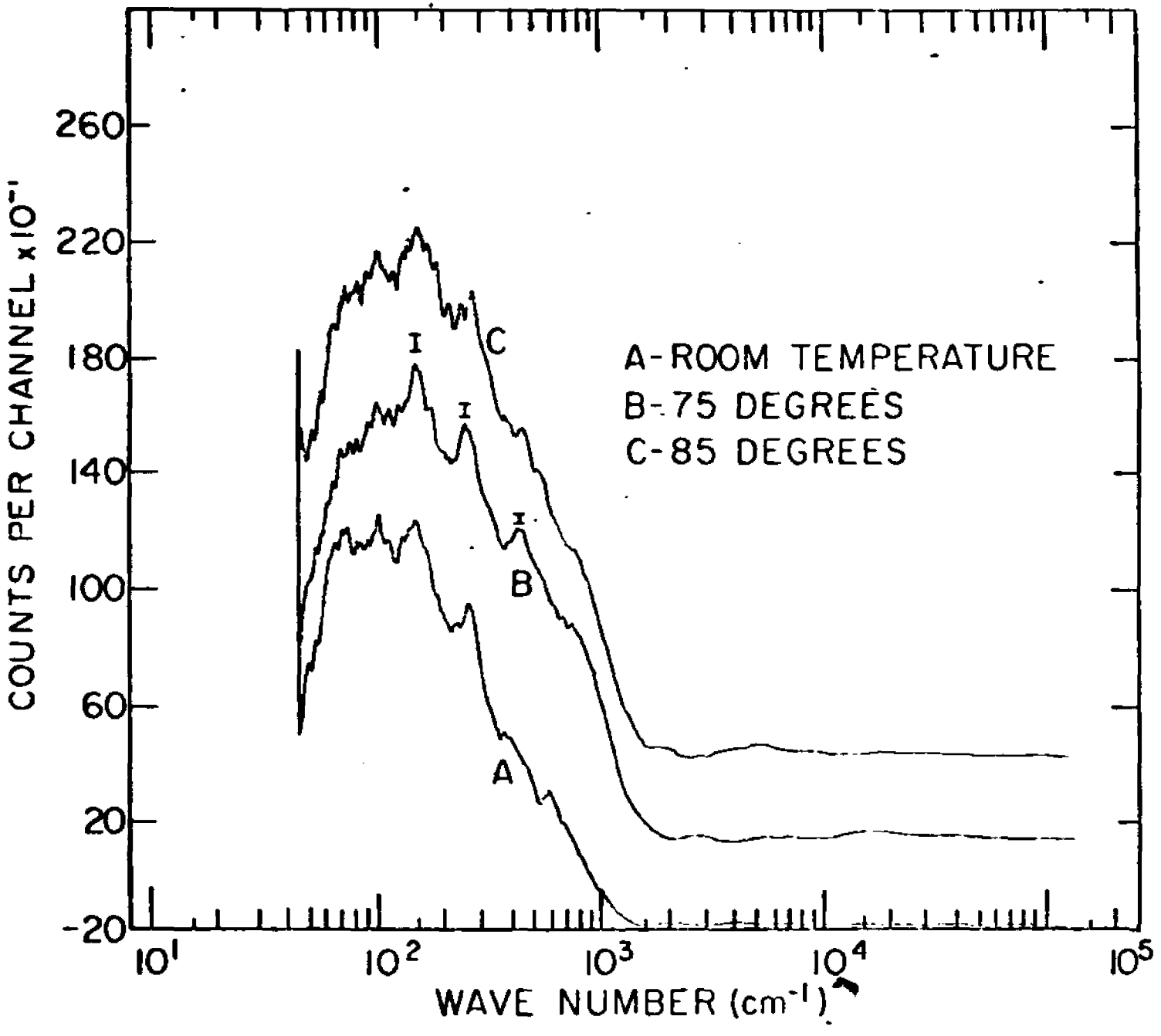

FIG.3.9. The Cold Neutron Inelastic Scattering Spectra Using the Brookhaven Graphite Research Reactor, at Room Temperature, at 75°C, and at 85°C. The Spectra are Displaced for Clarity 200 Counts Each Above Spectrum A.

are indicated in Fig.3.10. Directly in the region of the 65 cm^{-1} peak discussed above one can see a net loss in the number of low lying modes of vibration in going from room temperature to 75°C, in spite of the expected Boltzmann increase in the number of modes. In fact, when a Boltzmann correction is applied the loss in modes is even greater. Since only differences are of concern in this experiment, background runs with the sample material absent were not necessary.

The experiment was repeated using the High Flux Beam Reactor at Brookhaven National Laboratory when the Graphite Reactor was retired from service. (See Appendix C for a description of the High Flux Beam Reactor.) The results of this experiment are shown in Fig.3.11. On can see excellent agreement between the two difference spectra in Figs.3.10 and 3.11. Because the channel separation for the High Flux Beam Reactor was 8 microseconds, the energy resolution was better than that for the Graphite Reactor.

One must note at this point that the spectra indicated in Fig.3.9 are not the $\mathcal{G}(\omega)$ that was considered in Eqt.3.28, although they are related to the density of modes of vibration per frequency interval. However, since the channel counts in the analyzer are not arranged linearly with frequency, the size of the interval continually increases as one progresses to higher frequencies (energies). This, however, does not affect

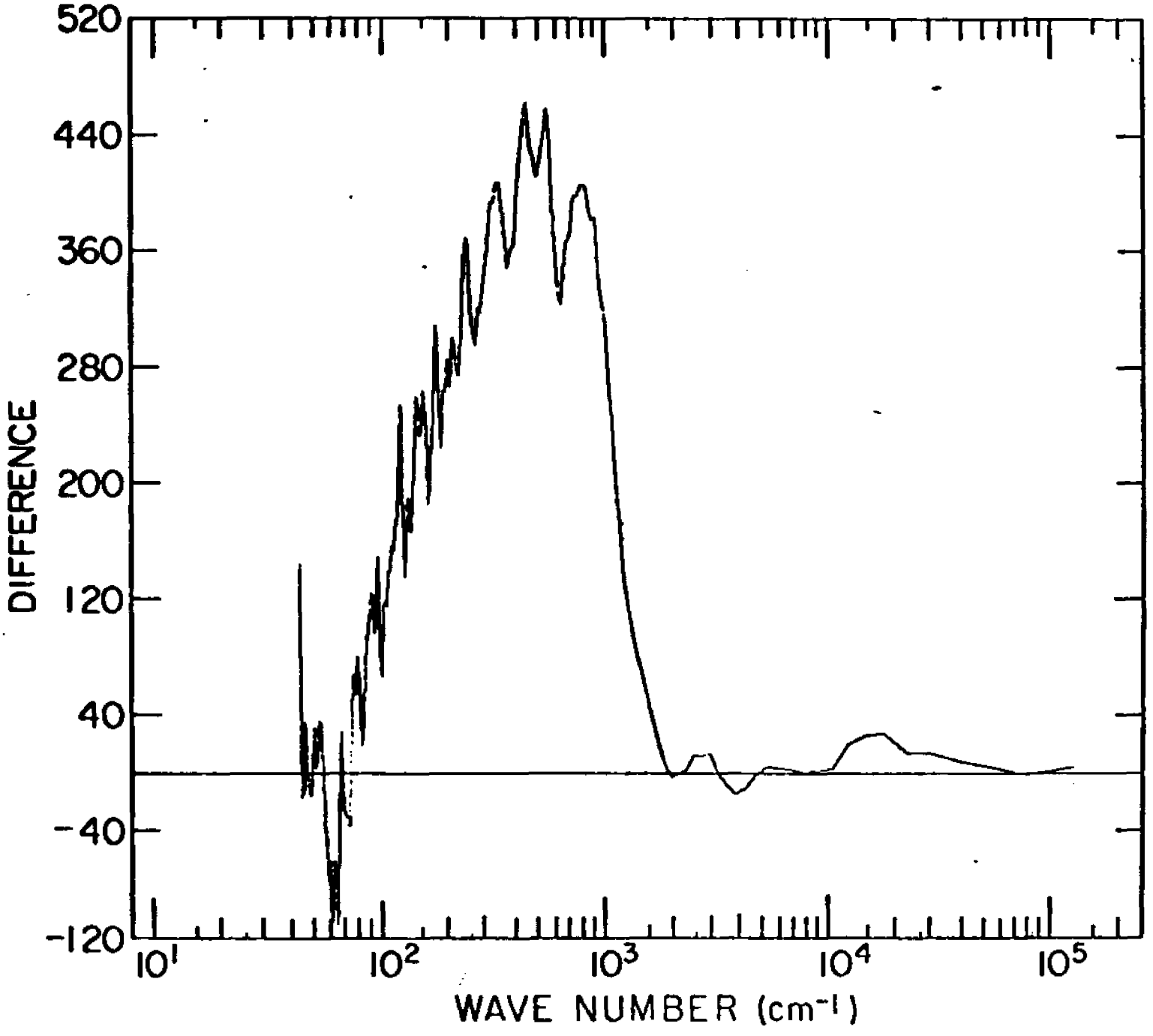

FIG.3.10. Difference Spectrum Determined Using the Room Temperature and 75°C Spectra Obtained at the BGRR.

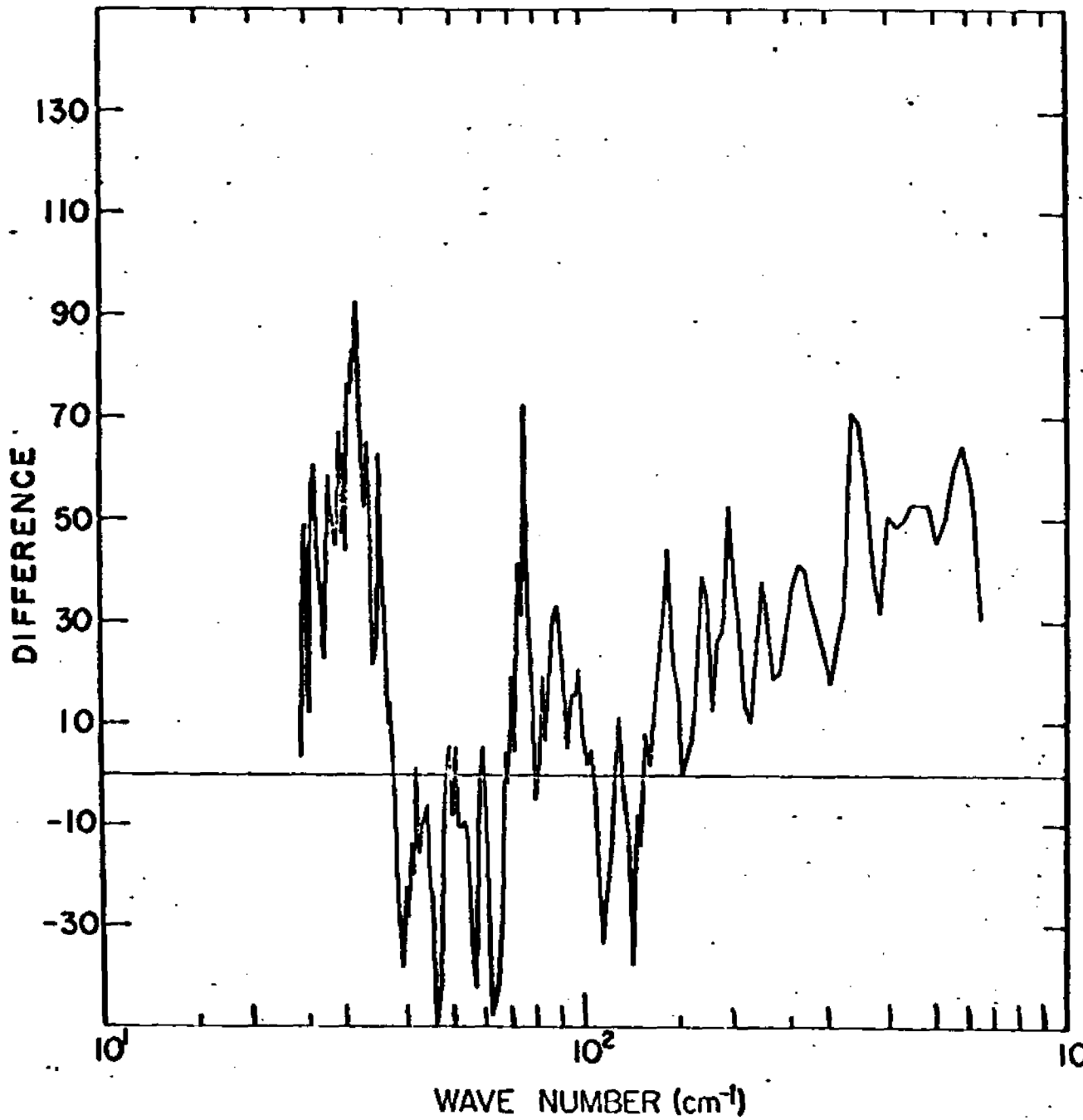

FIG.3.11. Difference Spectrum Using Data Obtained at the Brookhaven High Flux Beam Reactor, to Confirm the Results on the Graphite Reactor.

the qualitative analysis to be presented in the next section.

The resolution of the energies of the peaks is sufficient to allow for the establishing of their associated frequencies, for comparison with already published assignments for phenanthrene.[23] This comparison is made in Table 3.1, where it is observed that reasonable agreement is obtained.

6. Discussion

In order to attempt to draw conclusions from this experiment, it will help to summarize all relevant experimental facts so far available concerning phenanthrene in the temperature range between 25 and 85°C.[24]

i. There is a small (about 400 calories/mole) heat capacity anomaly,[25] manifesting itself as a heat absorption over a few degrees temperature range at about 72°C, which is present only in the solid, not in a solution of the molecules.[26]

ii. The is anomalous behavior in the electrical polarizability and dark conductivity of phenanthrene[27] around 72°C.

iii. There is a change in the temperature dependence of the dielectric constant and thermal expansion coefficients at about 72°C.[28]

iv. From the neutron data there is evidence for a loss in the density of low energy modes at about 72°C.

With these results in mind, some possible mechanisms to explain the anomalous behavior will be discussed.

TABLE 3.1

Comparison of Observed Structure with Reported[23] Infrared and Raman Spectra for Phenanthrene

Observed Peak (cm^{-1})	Infrared Data (cm^{-1})	Raman Data (cm^{-1})
70 100 150	123	
230	232 246	250
400	427	398 410
620	618	614

The anomalous absorption of heat at 72°C reported earlier[25] indicates that there must be a change in the dynamics of the system and in this thesis a dielectric anomaly at this temperature is found. Cochran and Cowley[29] have shown that the LST relation may be generalized to include the dynamics of molecular solids.

The difference curves shown in Figs.3.10 and 3.11 indicate that as predicted, the density of modes of vibration has decreased in the low-lying region of the spectrum. In accordance with Eqt.3.28 this can be related to an increase in the slope of the low-lying portion of the ω vs $\vec{k}$ dispersion curve. As indicated in Fig.3.3, this change in the slope may be related to a decrease in the frequency of the low-lying optic modes of vibration. Again, as indicated in Section 3, the LST relationship, applicable to the $k \to 0$ limit, predicts a relationship between ferroelectric-like behavior of the static dielectric constant and the value of the transverse optic frequencies at the $k \to 0$ limit. From the results presented in this chapter concerning the cold neutron scattering, one sees that the lattice dynamical point of view is consistent with the dielectric measurements discussed in Chapter 2. One can therefore conclude that phenanthrene exhibits behavior typical of a ferroelectric material.[24]

This does not mean to say that any other approach, such as a microscopic molecular theory, would not also provide consistent results. Other models have not thus far been ruled out

by the results of this experiment. Indeed there is no question that it is impossible to completely uncouple molecular effects from lattice effects. In future models, it may be possible only to describe the degree of coupling.

References - Chapter 3

1. W.Cochran, Phys. Rev. Letters 3, 412 (1959).
2. W.Cochran, Phil. Mag. Suppl. 9, 387 (1960).
3. R.H.Lydanne, R.G.Sachs,and E.Teller, Phys.Rev. 59,673 (1941).
4. R.A.Cowley, Phil.Mag. 11, 673 (1965).
5. R.A.Cowley, Phys. Rev. Letters 9, 159 (1962).
6. R.A.Cowley, Phys. Rev. 134, A981 (1964).
7. See for example,A.A.Maradudin, E.W.Montroll, and G.H.Weiss, "Theory of Lattice Dynamics in the Harmonic Approximation", in Solid State Physics, Supplement #3,(Academic Press, New York, 1963), and M.Born and K.Huang, Dynamical Theory of Crystal Lattices (Oxford University Press, London, 1954).
8. P.M.Morse and H.Feshbach, Methods Of Theoretical Physics (McGraw-Hill Book Company, New York, 1953),Vol.1,Ch.1.
9. A.J.Dekker,Solid State Physics (Prentice Hall Inc.,New Jersey,1965), p.240.
10. F.C.Brown, The Physics of Solids (W.A.Benjamin,Inc.,New York, 1967),p.186.
11. C.Kittel, Introduction to Solid State Physics (John Wiley & Sons,Inc., New York,1966),p.52.
12. C.Kittel, "General Introduction", in Phonons in Perfect Lattices, and in Lattices With Imperfections, R.W.H.Stevenson, ed., (Oliver & Boyd, London, 1966),p.40.
13. See Brown reference 10, p.156.
14. Ibid, p.241.
15. See for example,J.D.Jackson, Classical Electrodynamics (John Wiley & Sons, Inc., New York,1962),p.177.
16. See reference #3.
17. J.M.Ballantyne,Phys. Rev. 136, A429 (1964).
18. See for example, Thermal Neutron Scattering, P.A.Egelstaff,ed., (Academic Press,Inc., New York, 1965), and H.Boutin and S.Yip, Molecular Spectroscopy with Neutrons (M.I.T. Press, Cambridge,1968).
19. Boutin, p.93.

20. Ibid, p.5.

21. G.E.Bacon, Neutron Diffraction (Oxford University Press, Oxford, 1962), p.191.

22. R.M.Brugger, "Mechanical and Time-of-Flight Techniques", in P.A.Egelstaff, ed., Thermal Neutron Scattering (Academic Press, Inc., New York, 1968), p.54.

23. V.Schottino,K.Neto, and S.Califano,J.Chem.Phys. 4, 2725 (1966).

24. D.H.Spielberg, R.A.Arndt, A.C.Damask, and I.Lefkowitz, to be published.

25. R.A.Arndt and A.C.Damask,J.Chem.Phys. 45, 755 (1966).

26. H.Ringel, A.C.Damask, and R.A.Arndt,Mol.Cryst.3, 145 (1967).

27. R.A.Arndt and A.C.Damask, J.Chem.Phys. 45, 4627 (1966).

28. Preliminary work was performed at the Frankford Arsenal, using Arsenal equipment, and under the direction of I.Lefkowitz.

29. W.Cochran and R.A.Cowley, J.Phys.Chem.Solids 23, 447 (1962).

CHAPTER FOUR

1. Introduction

In order to obtain a simple model for charge transport in organic semiconductors, consider a set of molecules infinitely far apart. As the molecules are brought closer, the eigenfunctions of the electrons begin to overlap, allowing for the transfer of charges from place to place by tunneling. As the overlap increases, a coalescence occurs resulting in a solid, in which the electrons may become free to move throughout the material. One introduces perturbations on these free wave functions, due to impurities and phonon scattering. The energy levels occupied by the charge carriers (electrons or holes) are then broadened into bands by the overlap of the molecular orbitals. This model accounts for charge transport by a process which can be regarded as tunneling through a thin barrier. The hopping model will be considered shortly.

In agreement with experiment, it is easy to see how this model will give a negative temperature coefficient of mobility. The higher the temperature, the greater will be the phonon scattering, resulting in slower transport.

The band structure calculations based on this process may be carried out in two steps. The first step, the determination of the perfect lattice band structure, is performed by considering the electrons and holes as occupying states based, respectively, on the highest filled and lowest unfilled molecular orbitals of the parent molecules. Due to molecular overlap these orbitals broaden into bands. Knowing the crystal structure (see Fig. 4.1), and assuming reasonable molecular

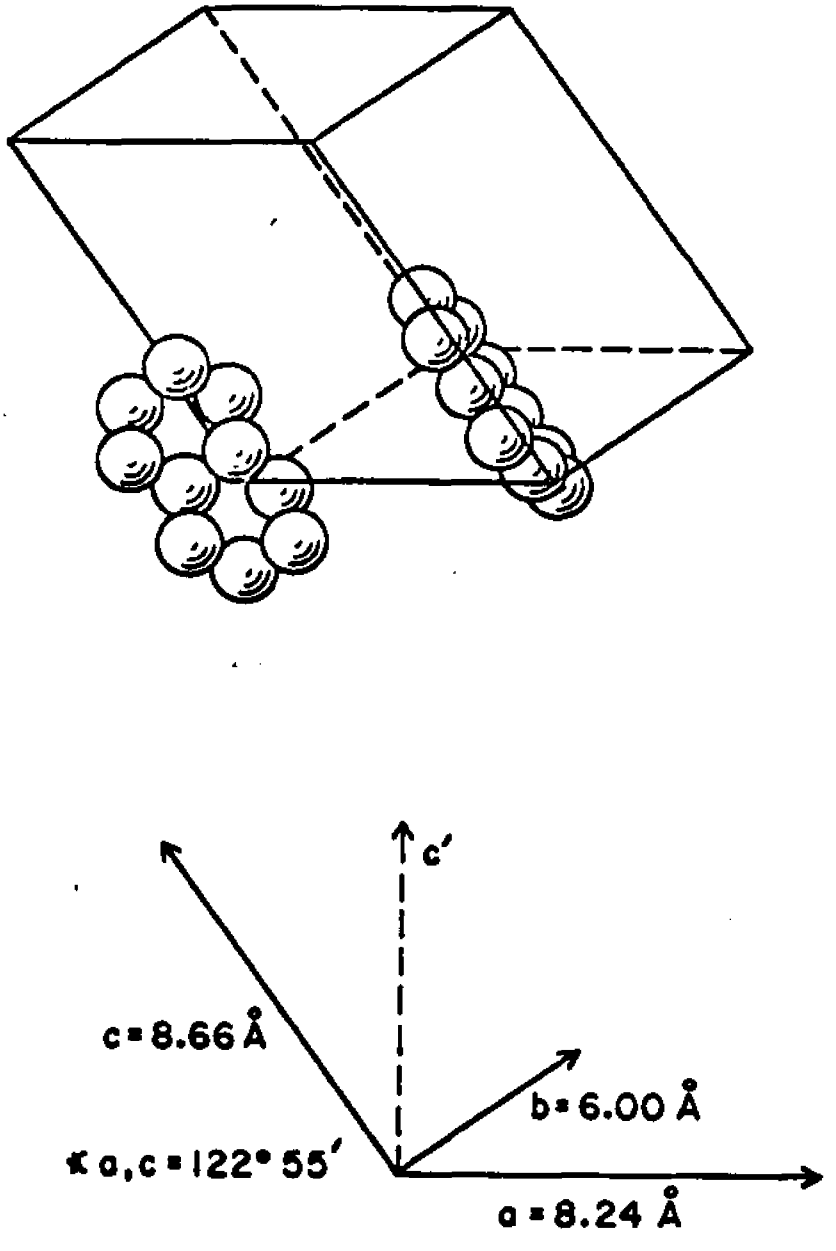

FIG. 4.1

(a) The Crystal Structure of Naphthalene.
(b) The Lattice Constants for Naphthalene and the Directions of the Lattice Vectors.

orbitals, one can calculate the band structure.

The second step, where the effects of phonon scattering are introduced, is more difficult to perform. The common procedure has been to assume all the effects of scattering can be described by one adjustable parameter, such as an isotropic mean free path. The drift mobility is calculated from the band structure up to this one parameter, which is then adjusted by comparison with experiment.[1] A test of this method is to correctly predict the anisotropy in the drift mobility. This should be independent of the adjustable scattering parameter.

Calculations for the energy band structure for naphthalene have been performed by LeBlanc,[2] Katz et al,[3] and Thaxton et al,[4] based more or less on the above recipe.

Friedman[5] has made an attempt at a first principles treatment of scattering with no adjustable parameters. He considered only the elastic, longitudinal acoustic mode phonon scattering, and for simplicity the phonon spectrum was approximated by the two dimensional Debye spectrum. Input parameters were various quantities derived from the energy band calculations of Thaxton[4]. Subsequent determination of the drift mobility gave the correct order of magnitude of 1 $cm^2/V\text{-}sec$ and the correct anisotropy.

Friedman extended his treatment of transport to a consideration of magnetic phenomena.[6] This introduces features of great interest. Since the allowed energy bands are narrow compared to kT, a carrier is likely to spend some time

near the top of the band, as well as near the bottom. However, a carrier near the top of a band has a negative effective mass. In the presence of a magnetic field, an electron in a negative effective mass state would deflect in the opposite sense from one in a positive mass state. Thus, depending on how the contributions from each state are weighted statistically, it may be possible for electrons to exhibit a Hall effect whose sign would be appropriate for holes. Similarly, holes may exhibit an anomalous Hall effect. This feature results directly from narrow band considerations.

One can consider the transport problem from another point of view. Returning to our original model of the coalescing molecules, if now the carriers are highly localized, such as generally is the case for organic semiconductors where the molecular overlap is quite small, the carriers do not move easily through the material. Thus the transport must be accomplished with tunneling through the potential barrier. This last process is referred to as the hopping model. Furthermore, if the interaction between the lattice and the electron is sufficiently strong the interaction results in a local deformation. The deformation must accompany the electron in any change in position. The electron and deformation combination are called a polaron, and the process is referred to as polaron motion. This amounts to a deep potential well for the electron since it is unable to move unless accompanied by its associated lattice deformation.

It is easy to see how the drift mobility increases with

increasing temperature, since it is a temperature activated process.

From uncertainty principle considerations, Glarum[7] concluded that the band model would be appropriate for drift mobilities greater than 1 $cm^2/V\text{-}sec$, and the hopping model would be appropriate for drift mobilities less than 1 $cm^2/V\text{-}sec$. Unfortunately, naphthalene, as well as anthracene, has a drift mobility of the order of 1 $cm^2/V\text{-}sec$, and thus appears to be an intermediate case.[8,9] Therefore, the magnitude of the drift mobility will not provide a criterion for the applicability of one model over another.

However, the signs and magnitudes of the Hall mobilities predicted by the energy band model and the hopping model may differ, depending on such things as carrier mean free path, band width and temperature.A determination of the signs and magnitudes of the Hall mobilities would therefore help determine the appropriateness of the different models.

2.Previous Hall Measurements

Most previous work.concerning Hall effect measurements suffered from either a lack of completeness in that all possible orientations of the electric and magnetic fields were not considered, or from an inability to unequivocally determine the sign of the charge carrier being observed. Also, the only work done in the organics concerns measurements on anthracene.

Dresner[11] made a surface photo-Hall effect measurement

in which he found two carrier effects to predominate. Therefore it was impossible for him to ascribe the Hall voltage to the Hall mobility of either carrier.

Delecote and Schott[12] measured the Hall mobility in anthracene using a pulsed light. However, they did not specify the direction of the magnetic field.

Pethig and Morgan[13] performed a Hall measuremont with the crystal unilluminated, and thus were unable to determine which injected carrier, or both, was responsible for their observations.

Toombs[14] measured the Hall effect with the magnetic field oriented along both the a or b directions. The charge carriers were photo-injected holes drifting along the c' direction. No anomalous results were observed.

Smith[15] made photo-Hall measurements using weakly absorbed light. He may have observed both types of charge carriers as a result.

Korn et al[16] measured the Hall mobility using strongly absorbed light. The measurements were performed in the six different possible orientations of the electric and magnetic field for hole carriers. Since the carriers were unambiguously known, the observed results could be analyzed for anomalous behavior. As predicted by LeBlanc[10] and Friedman[6] it was found that if an anthracene crystal was oriented with either its a or c' axis along the direction of an applied magnetic field, the Hall mobility had an anomalous sign. The effect for electrons was not investigated.

3. Elementary Theory of the Hall Effect

A simplified model for the Hall effect is first considered. One assumes we are dealing with a material having no thermal carriers. The carriers are all injected carriers of one sign. Also we assume the material to be the dielectric of a parallel plate capacitor, where the space charge of the carriers is negligible compared to the charge on the plates of the capacitor. This can be achieved by creating electron-hole pairs very near to one electrode, by photo-injection, for example. Thus the creation rate of the electrodes, not the space charge of the carriers, limits the photo-current. We also assume all charge carriers have the same drift velocity.

Referring to Fig. 4.2, we have the standard conditions for the Hall effect. Positive charge carriers are deflected in the negative y direction, while negative charge carriers are deflected in the positive y direction by the Lorentz force, $\vec{v} \times \vec{B}$. (MKS units will be used throughout.) In the case of positive charge carriers, an excess of holes builds up on the face V_2 until an electrostatic field E_H is established which just balances the Lorentz force giving

$$E_H = v_x B_z \tag{4.1}$$

where v_x is the average drift velocity of the charge carriers.

The current density is given by:

$$j_x = n e v_x \tag{4.2}$$

where n is the number of positive charge carriers per unit volume, and e is the charge. Thus Eqt.4.1 may be rewritten:

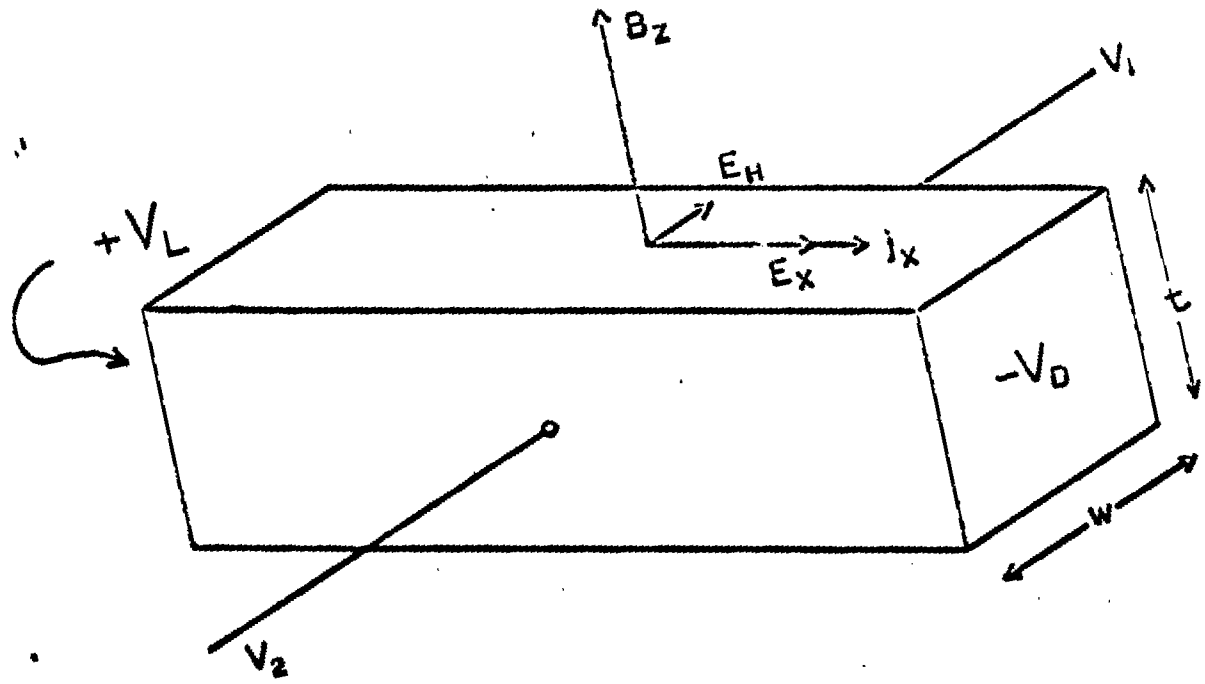

FIG. 4.2

The Normal Hall Effect for Positive Charge Carriers.

$$E_H = \left(\frac{1}{ne}\right) j_x B_z \tag{4.3}$$

One usually defines the Hall coefficient by:

$$E_H = R_H j_x B_z \,. \tag{4.4}$$

For the simple analysis of uniform drift velocity v_x, the Hall coefficient is inversely proportional to the concentration of charge carriers,

$$R_H = \frac{1}{ne} \,. \tag{4.5}$$

In order to relate conductivity to the Hall coefficient, we define the Hall mobility by:

$$\mu_H \equiv R_H \sigma \tag{4.6}$$

where σ is the electrical conductivity of the material. This in turn is defined as:

$$\sigma = n e \mu_D \tag{4.7}$$

where μ_D is the drift mobility. We see from Eqts.4.5 and 4.6 that:

$$\frac{\mu_H}{\mu_D} = 1 \,. \tag{4.8}$$

Also, $j_x = \sigma E_x$, so from Eqt. 4.4, $E_H = R_H \sigma E_x B_z$. But by Eqt. 4.6, $R_H \sigma = \mu_H$. Therefore, $E_H = \mu_H E_x B_z$. But by definition:

$$E_H \equiv \frac{V_H}{w} \tag{4.9}$$

where w is the sample width, and V_H is the measured Hall voltage, equal to $V_2 - V_1$, V_1 and V_2 being the Hall voltages relative to ground. Substituting Eqt.4.9 into the expression for the Hall field, we can solve for the Hall mobility as

$$\mu_H = \frac{V_H}{w E_x B_z} \,. \tag{4.10}$$

This now the definition of the Hall mobility.

4. General Transport Theory of the Hall Effect[17]

In thermal equilibrium, the distribution of electrons in energy in a crystal is given in terms of the density of states function N(E) and the Fermi-Dirac function $F[(E-E_F)/kT]$. The probability that a state with wavevector $\vec{k}$ is occupied, is the same as that of a state with wavevector $-\vec{k}$, so no transport takes place. To account for the transport of charges, the distribution function must be modified by electric and/or magnetic fields.

$f(\vec{k},\vec{r},t)$ is the probability at time t of occupation of the state corresponding to the wavevector $\vec{k}$ at a point in the crystal given by the position vector $\vec{r}$. When we consider the variation of f with respect to $\vec{r}$ we are concerned with a variation that is very small, of the order of a few lattice spacings, so that wave functions having a definite value of $\vec{k}$ may be specified locally in the crystal. The spatial variation is introduced to account for any inhomogeneity within the crystal.

If we have a force $\vec{F}$, acting on the electrons, the value of $\vec{k}$ will change at the rate given by the expression $\hbar\dot{\vec{k}} = \vec{F}$. That is, at time t+dt, $\vec{k}$ will be $\vec{k}+\hbar^{-1}\vec{F}dt$, while at time t + dt, $\vec{r}$ will be $\vec{r} + \vec{v}dt$. Thus the total rate of change of the probability function is:

$$\frac{Df}{Dt} = \frac{\partial f}{\partial t} + \frac{1}{\hbar}\left(F_x\frac{\partial f}{\partial k_x} + F_y\frac{\partial f}{\partial k_y} + F_z\frac{\partial f}{\partial k_z}\right) + v_x\frac{\partial f}{\partial x} + v_y\frac{\partial f}{\partial y} + v_z\frac{\partial f}{\partial z} \qquad (4.11)$$

or expressed vectorially:

$$\frac{Df}{Dt} = \frac{\partial f}{\partial t} + \frac{1}{\hbar}\vec{F}\cdot\nabla_k f + \vec{v}\cdot\nabla_r f \qquad (4.12)$$

If the total rate of change of f is due to collisions we may write:

$$\frac{Df}{Dt} = \left[\frac{\partial f}{\partial t}\right]_{Coll.} \tag{4.13}$$

and for the steady state df/dt=0. This gives

$$\left[\frac{\partial f}{\partial t}\right]_{Coll.} = \frac{1}{\hbar}\vec{F}\cdot\nabla_k f + \vec{v}\cdot\nabla_r f \tag{4.14}$$

It is usual to assume the rate of relaxation of f in the absence of external fields is proportional to the deviation of f from its equilibrium value, f_o, the constant of proportionality being the reciprocal of the relaxation time, or

$$\left[\frac{df}{dt}\right]_{Coll.} = -\frac{(f - f_o)}{\tau} \tag{4.15}$$

Therefore the Boltzmann Transport equation becomes

$$-\frac{(f - f_o)}{\tau} = +\frac{1}{\hbar}\vec{F}\cdot\nabla_k f + \nabla_r f\cdot\vec{v} \tag{4.16}$$

If the external force $\vec{F}$ is due to electric and magnetic fields, we have

$$-\frac{(f-f_o)}{\tau} = -\frac{e}{\hbar}(\vec{E} + \vec{v}\times\vec{B})\cdot\nabla_k f \tag{4.17}$$

where the spatial variation term is zero since we will deal only with a homogeneous crystal.

The Boltzmann Transport equation can now be solved using a method developed by Jones and Zener[18], where we make the substitution

$$f = f_o - \phi\left(\frac{\partial f_o}{\partial \mathcal{E}}\right) \tag{4.18}$$

where $\mathcal{E}$ is the energy of the state. Differentiating, we get

$$\nabla_k f = \nabla_k f_o - (\nabla_k \phi)\frac{\partial f_o}{\partial \mathcal{E}} - \phi\,\nabla_k\left(\frac{\partial f_o}{\partial \mathcal{E}}\right) \tag{4.19}$$

If we remember that

$$\nabla_k \mathcal{E} = \hbar\vec{v} \quad \text{and} \quad \nabla_k f_o = \hbar\vec{v}\frac{\partial f_o}{\partial \mathcal{E}} \tag{4.20}$$

we can substitute back into Eqt.4.19 to get

$$\nabla_k f = \hbar\vec{v}\frac{\partial f_o}{\partial \mathcal{E}} - \phi\frac{\partial}{\partial \mathcal{E}}\left[\hbar\vec{v}\frac{\partial f_o}{\partial \mathcal{E}}\right] - (\nabla_k\phi)\frac{\partial f_o}{\partial \mathcal{E}}$$

or

$$\nabla_k f = \hbar\vec{v}\left[\frac{\partial f_o}{\partial \mathcal{E}} - \phi\frac{\partial^2 f_o}{\partial \mathcal{E}}\right] - (\nabla_k\phi)\frac{\partial f_o}{\partial \mathcal{E}} \tag{4.21}$$

Therefore, remembering that $\vec{v} \times \vec{v} = 0$, we get for Eqt.4.17

$$-\frac{e}{\hbar}(\vec{v}\times\vec{B})\cdot\nabla_k f = -\frac{e}{\hbar}\vec{B}\cdot(\nabla_k f \times \vec{v})$$

or

$$-\frac{e}{\hbar}(\vec{v}\times\vec{B})\cdot\nabla_k f = -\frac{e}{\hbar^2}\vec{B}\cdot\left(\frac{\partial f_0}{\partial \varepsilon}(\nabla_k \varepsilon \times \nabla_k \phi)\right) \quad (4.22)$$

If we choose the magnetic field along the z axis, Eqt.4.22 becomes

$$-\frac{e}{\hbar}(\vec{v}\times\vec{B})\cdot\nabla_k f = -\frac{e}{\hbar^2} B_z \frac{\partial f_0}{\partial \varepsilon} \Omega_z \phi \quad (4.23)$$

where

$$\vec{\Omega} = \nabla_k \varepsilon \times \nabla_k \quad (4.24)$$

Now Eqts.4.18 and 4.23 are substituted into Eqt.4.17, in order to obtain an equation for the unknown function $\phi = \phi(\vec{k})$. This gives the linear first order equation

$$\frac{\phi}{\tau} + \frac{e}{\hbar}\vec{E}\cdot\nabla_k \varepsilon + \frac{e}{\hbar^2} B_z \Omega_z \phi = 0 \quad (4.25)$$

The solution of this equation, first obtained by Jones and Zener,[18] is

$$\phi = -\frac{e}{\hbar}\left[\tau\vec{E}\cdot\nabla_k\varepsilon - \left(\frac{e}{\hbar^2}\right)\tau\vec{B}\cdot\vec{\Omega}(\tau\vec{E}\cdot\nabla_k\varepsilon) + \left(\frac{e^2}{\hbar^4}\right)\tau\vec{B}\cdot\vec{\Omega}\left[\tau\vec{B}\cdot\vec{\Omega}(\tau\vec{E}\cdot\nabla_k\varepsilon)\right] + \ldots\right] \quad (4.26)$$

The current density is given by

$$\vec{J} = -\frac{e}{4\pi^3}\int (f - f_0)\vec{v}\, d\vec{k} = \frac{e}{4\pi^3}\int \phi \frac{\partial f_0}{\partial \varepsilon}\vec{v}\, d\vec{k} \quad (4.27)$$

Since f_0 is the Fermi-Dirac distribution function, it follows that

$$-\left(\frac{\partial f_0}{\partial \varepsilon}\right) = f_0(1 - f_0)/kT \quad (4.27)$$

Furthermore, in the non-degenerate case, with a small density of electrons in the conduction band, $f_0 \ll 1$. Therefore

$$-\left(\frac{\partial f_0}{\partial \varepsilon}\right) \approx \frac{f_0}{kT} \quad (4.28)$$

This makes Eqt.4.27 become

$$\vec{J} = -\left(\frac{e}{4\pi^3}\right) \frac{1}{kT} \int \vec{v}\, \phi\, f_0\, d\vec{k} \tag{4.29}$$

In order to calculate the drift mobility, we assume $\vec{B}=0$, and $\vec{E}=E_x \hat{i}$. Then Eqt.4.26 reduces to

$$\phi = -\frac{e}{\hbar} \tau E_x \frac{\partial \varepsilon}{\partial k_x} = -e \tau E_x v_x \tag{4.30}$$

Substituting this into Eqt. 4.27 for the current density we get:

$$J_x = \frac{e^2}{4\pi^3} \frac{E_x}{kT} \int v_x^2 f_0 \tau\, d\vec{k} \tag{4.31}$$

This may be rewritten as

$$J_x = \frac{ne^2}{kT} E_x \langle \tau v_x^2 \rangle \tag{4.32}$$

where n is the charge density, given by

$$n = \frac{1}{4\pi^3} \int f_0\, d\vec{k} \tag{4.33}$$

The brackets indicate the usual statistical average

$$\langle A \rangle = \frac{\int A f_0\, d\vec{k}}{\int f_0\, d\vec{k}}$$

Since the current density is given by

$$J_x = -n e \mu_x E_x$$

where μ_x is the drift mobility in the x direction, we write for the drift moblity

$$\mu_x = -\left(\frac{e}{kT}\right) \langle \tau v_x^2 \rangle \tag{4.34}$$

with similar equations for the other directions.

Thus we nolonger are dealing with the uniform drift mobility of the elementary theory, but have averaged the values over k space.

To calculate the Hall mobility, external fields are introduced, where the electric field is given by $\vec{E} = E_x \hat{x} + E_H \hat{y}$, and the magnetic field by B_z. Substituting into Eqt.4.26 we get

$$\phi = -\left(\frac{e}{\hbar}\right) \tau \left[E_x \left(\frac{\partial \varepsilon}{\partial k_x}\right) + E_H \left(\frac{\partial \varepsilon}{\partial k_y}\right)\right] + \tag{4.35}$$
$$+ \left(\frac{e^2}{\hbar^2}\right) \tau B_z \Omega_z \left\{\tau \left[E_x \left(\frac{\partial \varepsilon}{\partial k_x}\right) + E_H \left(\frac{\partial \varepsilon}{\partial k_y}\right)\right]\right\}$$

Substituting this equation into Eqt.4.29 for the current, gives

$$J_y = \frac{e^2}{4\pi^3}\left(\frac{1}{kT}\right)\int \tau v_y (E_x v_x + E_H v_y) f_o \, d\vec{k}$$

$$- \frac{e^3}{4\pi^3 \hbar^2}\frac{B_z}{kT}\int \tau v_y \Omega_z [\tau (E_x v_x + E_H v_y)]\, d\vec{k} \qquad (4.36)$$

Since E_x and E_H are constant

$$J_y = \frac{ne^2}{kT} E_x \langle \tau v_y v_x \rangle + \frac{ne^2}{kT} E_H \langle \tau v_y^2 \rangle$$
$$- \frac{ne^3}{\hbar^2}\frac{B_z}{kT} E_x \langle \tau v_y \Omega_z (\tau v_x) \rangle \qquad (4.37)$$
$$- \frac{ne^3}{\hbar^2}\frac{B_z}{kT} E_H \langle \tau v_y \Omega_z (\tau v_y) \rangle$$

But in the steady state, $j_y = 0$. Also, the last term in Eqt.4.37 represents the magneto-resistance term, and is not significant for naphthalene. Finally, $\langle \tau v_y v_x \rangle$ is small since $j_y \approx 0$ in the absence of a magnetic field. Therefore Eqt.4.37 becomes

$$E_H \langle \tau v_y^2 \rangle = \frac{e}{\hbar^2} B_z E_x \langle \tau v_y \Omega_z (\tau v_x) \rangle \qquad (4.38)$$

Since from Eqt.4.9 and 4.10

$$\mu_H = \frac{E_H}{E_x B_z} \qquad (4.39)$$

we get for the Hall mobility

$$\mu_H = \frac{E_H}{E_x B_z} = \frac{e}{\hbar^2}\frac{\langle \tau v_y \Omega_z (\tau v_x) \rangle}{\langle \tau v_y^2 \rangle} \qquad (4.40)$$

If we expand the operator Ω_z in the numerator of Eqt.4.40, we get

$$\langle \tau v_y \Omega_z (\tau v_x) \rangle = \hbar^2 \langle \tau^2 (v_y v_x M_{yx}^{-1} - v_y^2 M_{xx}^{-1}) \rangle + \langle \tau v_y v_x \Omega_z \tau \rangle \qquad (4.41)$$

where M_{ij}^{-1} is the symmetric effective mass tensor, defined by

$$M_{ij}^{-1} \equiv \frac{1}{\hbar^2}\left(\frac{\partial^2 \varepsilon}{\partial k_i \partial k_j}\right) \qquad (4.42)$$

The two situations usually considered are:

1) Constant mean free path ($\tau = f(\vec{k})$)
2) Constant relaxation time, τ.

The second case, where τ is a constant is simpler, since the last torm of Eqt.4.41 drops out, leaving for μ_H

$$\mu_H = \frac{e\tau \langle v_y v_x M^{-1}_{yx} - v_y^2 M^{-1}_{xx} \rangle}{\langle v_y^2 \rangle} \tag{4.43}$$

Combining Eqts.4.43 and 4.34, we get for the ratio of the Hall to the drift mobility:

$$\frac{\mu_H}{\mu_0} = \frac{kT \langle v_y^2 M^{-1}_{xx} - v_y v_x M^{-1}_{yx} \rangle}{\langle v_x^2 \rangle \langle v_y^2 \rangle} \tag{4.45}$$

Case 1) results in the same expression.

5. Theoretical Band Energy Calculation of the Hall Mobility

Naphthalene crystallizes in a monoclinic lattice with two molecules per unit cell, located at (0,0,0) and (a/2,b/2,0) as in Fig. 4.1. The lattice constants are[19]:

$$\vec{a} = 8.24\text{Å}\hat{a}$$
$$\vec{b} = 6.00\text{Å}\hat{b}$$
$$\vec{c} = 8.66\text{Å}(\cos\beta\hat{a} + \sin\beta\hat{c}')$$
$$\beta = 122^\circ 55'$$

The reciprocal lattice vectors are defined by:

$$2\pi\vec{a}^{-1} = \frac{2\pi(\vec{b} \times \vec{c})}{\vec{a}\cdot(\vec{b} \times \vec{c})}, \quad \text{etc.}$$

The unit vectors $\hat{a}$, $\hat{b}$, and $\hat{c}'$ form a right handed coordinate system as shown in Fig.4.1. One obtains therefore:

$$2\pi\vec{a}^{-1} = .955\text{Å}^{-1}(-\cos\beta\hat{a} + \sin\beta\hat{c}')$$
$$2\pi\vec{b}^{-1} = 1.05\text{Å}^{-1}\hat{b} \tag{4.46}$$
$$2\pi\vec{c}^{-1} = .912\text{Å}^{-1}\hat{c}'$$

In order to calculate μ_H/μ_0 one integrates Eqt.4.45 in $\vec{k}$ space over the first Brilluoin zone. The first Brillouin zone is constructed from a reciprocal lattice formed by the vectors of

Eqt.4.46. Planes are drawn which are the perpendicular bisectors of these lattice vectors. The smallest volume enclosed by these planes is the first Brillouin zone[20], as is shown in Fig.4.3.

For the theoretical calculation, using a tight binding approximation, the band structure used was[3]

$$\begin{aligned}\mathcal{E}(\vec{k})_{\pm} = {} & 2\mathcal{E}_2 \cos(\vec{k}\cdot\vec{c}) + 2\mathcal{E}_3 \cos(\vec{k}\cdot\vec{b}) + 2\mathcal{E}_4 \cos[\vec{k}\cdot(\vec{b}+\vec{c})] \\ & + 2\mathcal{E}_5 \cos(\vec{k}\cdot\vec{a}) + 2\mathcal{E}_6 \cos[\vec{k}\cdot(\vec{a}+\vec{c})] \\ & \pm 4\mathcal{E}_9 \cos(\tfrac{1}{2}\vec{k}\cdot\vec{a})\cos(\tfrac{1}{2}\vec{k}\cdot\vec{b}) \\ & \pm 4\mathcal{E}_{10} \cos(\tfrac{1}{2}\vec{k}\cdot\vec{b})\cos[\vec{k}\cdot(\tfrac{1}{2}\vec{a}+\vec{c})]\end{aligned}$$

where $\mathcal{E}_7, \mathcal{E}_8, \mathcal{E}_{11}, \mathcal{E}_{12}, \mathcal{E}_{13}$, and $\mathcal{E}_{14}$ have been omitted since they are in general smaller than the other intermolecular resonance integrals. The subscripts label the resonance integrals according to the scheme of Fig.4.4. For example, $\mathcal{E}_2$ is the intermolecular resonance integral between the molecule at the origin (molecule 1) and molecule 2. Both Katz et al[3] and Thaxton et al[4] have determined values for the resonance integrals. Both sets of values are used separately to determine the ratio expressed in Eqt.4.45

The procedure for calculating the ratio of the Hall mobility to the drift mobility is to employ a computer to pick a point in the first Brillouin zone and then to compute $\vec{v}$ $(=\nabla_k \mathcal{E})$ and M^{-1} $(=\nabla_k \nabla_k \mathcal{E})$ for the point. The proper combinations of these values, according to Eqt.4.45, were formed, weighted by the Boltzmann factor, $\exp(-\mathcal{E}(\vec{k})/kt)$, and then added to the results

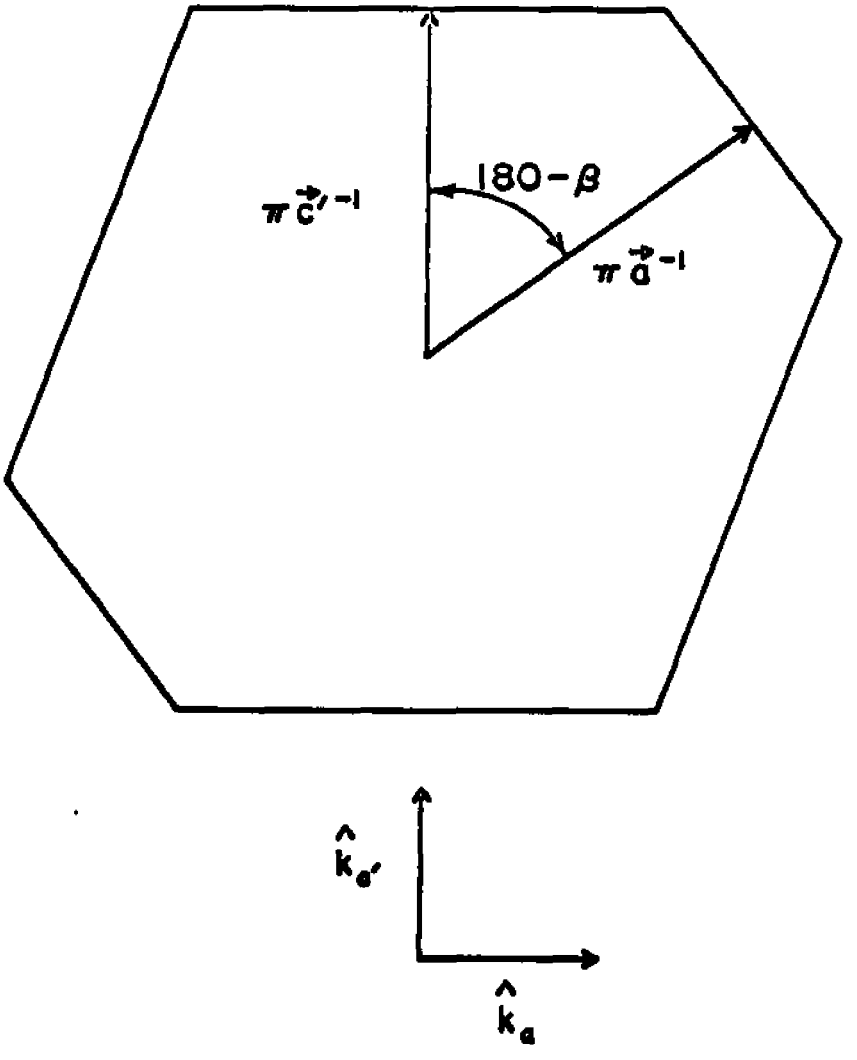

FIG. 4.3

Cross Section of the First Brillouin Zone of Naphthalene in the a^{-1},b^{-1} Plane of the Reciprocal Lattice.

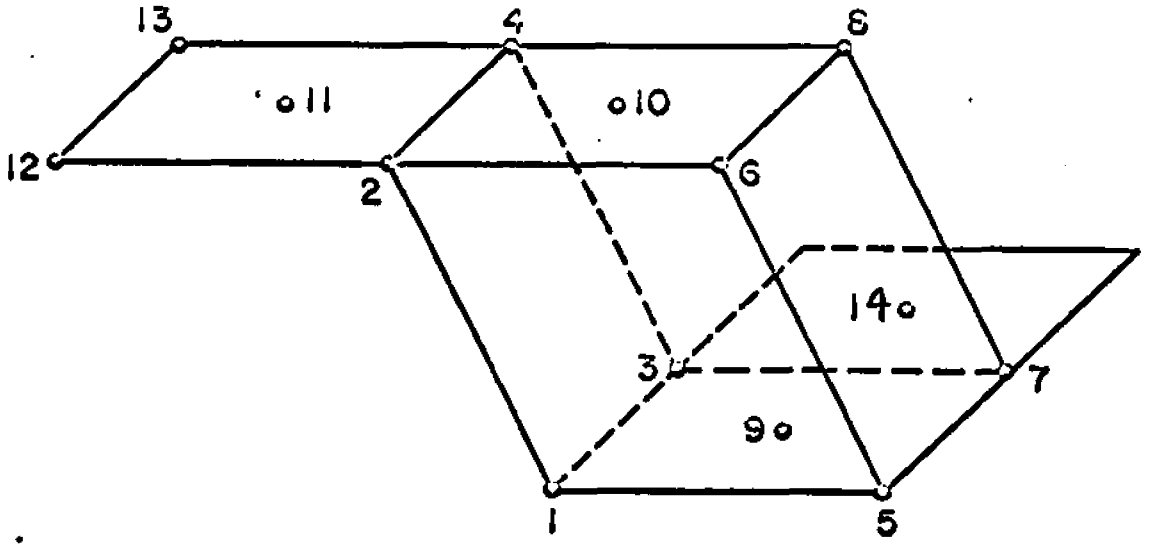

FIG. 4.4

Naphthalene Unit Cell. Molecular Centers in the Unit Cell and at Sites Adjacent to the Unit Cell, Showing the Numbering Scheme Used by Katz et al.[3]

for the previous points, until the whole zone has been covered. The density of points chosen for the computation is determined by trial and error until the value for the summation converged. In this manner μ_H/μ_D were calculated for naphthalene in all six possible orientations of the electric and magnetic fields. The program used was developed by Korn[21] for calculations on anthracene. The results of the theoretical calculations are given in Table 4.1a. The minus signs indicate anomalous Hall mobilities. One can see that the values obtained using Thornton's resonance integrals[4] predict anomalous behavior for holes with the magnetic field in the a or c' directions, and similarly for electrons. The values obtained using the resonance integrals determined by Katz[3] also predict anomalous behavior for holes with the magnetic field in the a or c' directions. However, for electrons the prediction calls for anomalous behavior with the magnetic field in the c' direction only.

Table 4.1. (a) Theoretical Calculation of μ_H/μ_D Using the Resonance Integrals Obtained by Katz and Thaxton. (b) μ_H/μ_D Calculated Using the Experimental Data.

a)

		Katz			Thaxton			
I// \ B//		a	b	c'	a	b	c'	
Holes	a		+.08	-1.3		+1.0	-16	
	b	-1.3		-1.3	-16		-16	
	c'	-1.3	+.08		-16	+1.0		
Electrons	a		+1.3	-1.8		+1.5	-11	
	b	+.7		-1.8	-10		-11	
	c'	+.7	+1.3		-10	+1.5		

b)

		a	b	c'	
I// \ B//					
Holes	a		+.57	-3.6	
	b	-3.9		-3.7	
	c'	-2.7	+.37		
Electrons	a		+2.8	-3.0	
	b	+1.1		-2.9	
	c'	+0.9	+2.2		

6. Computation of the Hall Mobility From the Measured Voltage

The computations follow the analysis due to Mott and Gurney[22] and adapted by Korn et al[16] for his investigations on anthracene. With the exception of using a conventional magnet in place of Korn's superconducting magnet.

The geometry of the crystal sample is shown in Fig.4.2 and the signs of the voltages correspond to hole conduction. For electron conduction, the signs are reversed. The directions of the various fields are also indicated in the diagram. The photo-injecting electrode (V_L) is located at $x = -\frac{1}{2}l$, while the dark electrode (V_D) is located at $x = +\frac{1}{2}l$, where l is the sample length.

In the elementary theory of the Hall effect V_H would equal $2V_m$ where V_m is the measured voltage with respect to ground potential of one of the Hall probes (corresponding to V_1 or V_2.) However, the real problem must include the effects of the finite dimensions of the sample as well as the fact that the photo-injecting electrode forms an ohmic contact leading to a space charge limited current showing quadratic dependence on the voltage. Therefore, the internal field E_x is not equal to E_0, where

$$E_0 = \frac{V_L + V_D}{l}$$

The primary electric field will now be determined.

6a. Determining the Primary Electric Field, E_x

For convenience we choose a coordinate system x', y, and z where

$$x' = x + \ell$$

so that the illuminated electrode is at x'= 0 and the dark electrode is at x'= +1. For a homogeneous material $E_x(x)=E_{x'}(x')$.

Assuming we are dealing with steady state space charge limited currents with no trapping, we have the boundary conditions $n(0) = \infty$, and $E_{x'}(0) = 0$, where n is the carrier charge density. From the continuity equation

$$J_{x'} = e n(x') \mu E_{x'}(x') \tag{4.47}$$

and is independent of x.

The Poisson equation gives $$e n(x') = \frac{dE_{x'}(x')}{dx'} \tag{4.48}$$

Finally, if one integrates the field strength, one obtains

$$\int_0^{\ell} E_{x'}(x')dx' = V_L + V_D \tag{4.49}$$

Taking en(x'0 from Eqt.4.48 and substituting it into Eqt.4.47, one gets

$$J_{x'} = \mu E_{x'}(x') \frac{dE_{x'}(x')}{dx'} = \frac{\mu}{2} \frac{d[E_{x'}(x')]^2}{dx'} \tag{4.50}$$

Integrating this equation and solving for $E_{x'}(x')$ gives

$$E_{x'}(x') = \sqrt{\frac{2}{\mu} J_{x'} x'} \tag{4.51}$$

Inserting this result into Eqt.4.49 and integrating gives

$$\sqrt{\frac{2 J_{x'}}{\mu}} \frac{2}{3} \ell^{3/2} = V_L + V_D \tag{4.52}$$

Solving this equation for j and substituting into Eqt.4.51 gives

$$E_{x'}(x') = \frac{3}{2} \frac{(V_L + V_D)}{\ell} \left(\frac{x'}{\ell}\right)^{1/2} = E_x(x) \tag{4.53}$$

The potential distribution is obtained by integrating

Eqt.4.53 from zero to x', remembering that $V(x'=0)=V_L$ and $V(x'=+1)=-V_D$. This gives

$$V_{x'}(x') = V_L - \left(\frac{V_L + V_D}{1}\right)\left(\frac{x'}{l}\right)^{3/2} \tag{4.54}$$

Adding V_D to both sides gives

$$V_{x'}(x') + V_D = (V_L + V_D)\left(1 - \left(\frac{x'}{l}\right)^{3/2}\right) \tag{4.55}$$

One can adjust V_L and V_D to make the Hall probe potential $V(x_o') = 0$. From Eqt.4.55 one can then obtain the value of $(x_o'/1)$ at the Hall probes. The result for $V(x_o')=0$ is

$$\left(\frac{x_o'}{l}\right)^{3/2} = \frac{V_L}{V_L + V_D} = \left[\frac{(x_o + \pm\ell)}{l}\right]^{3/2} \tag{4.56}$$

where we also used the fact that $x' = x + \frac{1}{2}l$ to return to the original coordinate system.

From Eqt.4.56 one can obtain the value of $(x_o/1)$ for the Hall probes, giving

$$\frac{x_o}{l} = \left(\frac{V_L}{V_L + V_D}\right)^{2/3} - \frac{1}{2} \tag{4.57}$$

Substituting Eqt.4.57 into 4.53 gives

$$E_x(x_o) = \frac{3}{2}\frac{(V_L)^{1/3}(V_L + V_D)^{2/3}}{l} \tag{4.58}$$

which is the electric field strength at the Hall probes.

6b. Calculating the Hall Voltage From the Measured Voltage

In order to account for the effect of finite sample dimensions and space charge effects, we introduce the parameters G and S in the following expression

$$V_H = \frac{2 V_m}{G S} \tag{4.59}$$

where G is the geometrical factor due to the finite dimensions and S is the space charge factor.

6c. Evaluating G

The case where space charge effects are neglected can be defined by setting S = 1.

Because of the finite dimensions $E_y \neq E_H$ where E_H is the standard homogeneous field for an infinite parallel plate capacitor, given by

$$E_H = \frac{V_H}{\omega}$$

Now it is assumed that E_y is independent of z. It is also assumed that the field E_y results from a charge distribution located at $y = \pm\frac{1}{2}w$, $-\frac{1}{2}l \leq x \leq +\frac{1}{2}l$. Therefore $\nabla \cdot \vec{E}_y = 0$ for the interior of the sample. Similarly $\nabla \times \vec{E}_y = 0$ for the interior. Thus

$$\vec{E}_y(x,y) = -\nabla V_y(x,y) \tag{4.60}$$

and

$$\nabla^2 V_y = 0 \tag{4.61}$$

V_y satisfies the following boundary conditions

$$V_y(x, \pm \tfrac{1}{2}w) = \pm V_m \qquad (-\tfrac{1}{2}l \leq x \leq +\tfrac{1}{2}l)$$

and

$$V_y(\pm l, y) = 0$$

A solution to Eqt.4.61 obeying the above boundary conditions

has been obtained by Isenberg, Russell, and Green[23]

$$V_y(x,y) = \frac{4\ell V_H}{\pi^2 w} \sum_{n=0}^{\infty} \frac{(-1)^n \sinh[(2n+1)\pi y/\ell] \cos[(2n+1)\pi x/\ell]}{(2n+1)^2 \cosh[(2n+1)\pi w/2\ell]} \tag{4.62}$$

Since $2V_m = V_y(x,+w) - V_y(x,-w)$ and $\sinh(a) = -\sinh(-a)$

we have $$2V_m = V_H\left[\frac{8\ell}{\pi^2 w} \sum_{n=0}^{\infty} \frac{(-1)^n \tanh[(2n+1)\pi w/2\ell] \cos[(2n+1)\pi x/\ell]}{(2n+1)^2}\right] \tag{4.63}$$

But comparing this with Eqt.4.59, we obtain

$$G = \frac{8\ell}{\pi^2 w} \sum_{n=0}^{\infty} \frac{(-1)^n \tanh[(2n+1)\pi w/2\ell] \cos[(2n+1)\pi x/\ell]}{(2n+1)^2} \tag{4.64}$$

We will of course be concerned with the value of G for $x/l = x_o/l$, where by Eqt. 4.57

$$\frac{x_o}{\ell} = \left(\frac{V_H}{V_H + V_D}\right)^{2/3} - \frac{1}{2} \tag{4.57}$$

This series rapidly converges.

6d. Evaluating S

If we consider the y,z plane defined by Eqt.4.57, where the Hall probe potential is zero, and assume that the density of charge carriers in this plane is only a function of y, we get for the steady state continuity equation

$$J_y = e n \mu_y E_y + e n \mu_y \mu_H E_x B_z - e D\left(\frac{dn}{dy}\right) = 0 \tag{4.65}$$

where μ_y is the drift mobility in the y direction, μ_H is the Hall mobility given in Eqt.4.10, and D is the diffusion constant for the charge carrier. Solving for dn/dy, and letting $E_y = -dV_y/dy$ we get

$$\frac{dn}{dy} = \left(\frac{\mu_y n}{D}\right)\left[\mu_H E_x B_z - \frac{dV_y}{dy}\right] \tag{4.66}$$

This may be integrated to give

$$\ln\left(\frac{n}{n_o}\right) = -\left(\frac{\mu_y}{D}\right)V_y + \left(\frac{\mu_y \mu_H E_x B_z}{D}\right)y \tag{4.67}$$

where n_o is the carrier concentration for zero magnetic field.

Within the dielectric material we have

$$\frac{dE_y}{dy} = \frac{e}{\varepsilon_y \varepsilon_o}(n - n_o) \tag{4.68}$$

where ε_y is the dielectric constant in the y direction, and ε_o is the permitivity.

From Eqts.4.67 and 4.68 one obtains

$$-\frac{d^2V_y}{dy^2} = \frac{e}{\varepsilon_y \varepsilon_o} n_o\left[\exp\left[-\left(\frac{\mu_y}{D}V_y\right) + \left(\frac{\mu_y \mu_H E_x B_z}{D}\right)y\right] - 1\right] \tag{4.69}$$

The boundary conditions for Eqt.4.69 are

$$V_y(0) = 0 \tag{4.70}$$

and

$$\left(\frac{dV_y}{dy}\right)_{y = \pm \frac{1}{2}w} = 0 \tag{4.71}$$

Eqt.4.70 follows from symmetry considerations, while Eqt.4.71 follows from neglecting the edge effects of the finite sample.

Banbury, Henisch, and Many[24] obtained as the solution to Eqt.4.69

$$V_y = V_H\left[\left(\frac{y}{w}\right) - \left(\frac{L}{w}\right)\frac{\sinh(y/L)}{\cosh(w/2L)}\right] \tag{4.72}$$

But, since $2V_m = V_y(+\frac{1}{2}w) - V_y(-\frac{1}{2}w)$ one obtains the relation

$$2V_m = V_H S = V_H\left[1 - \left(\frac{2L}{w}\right)\tanh\left(\frac{w}{2L}\right)\right] \tag{4.73}$$

This gives for S

$$S = 1 - \left(\frac{2L}{w}\right)\tanh\left(\frac{w}{2L}\right) \tag{4.74}$$

where L is

$$L = \left[\varepsilon_y \varepsilon_o \left(\frac{kT}{e}\right)\left(\frac{at}{\pi}\right)\left(\frac{\mu_x}{I_x}\right)\right]^{1/2} \tag{4.75}$$

I_x is the photo-current of the photo-injecting electrode, and using Eqt.4.58 for E_x

$$\eta = \frac{2}{wE_x} = \left(\frac{4}{3}\right)\left(\frac{L}{w}\right)\frac{1}{(V_L)^{1/3}(V_L + V_0)^{2/3}} \tag{4.76}$$

6c. Calculation of the Hall Mobility

From $$\mu_H = \frac{V_H}{w E_x B_z} \tag{4.10}$$

and $$V_H = \frac{2 V_m}{G S} \tag{4.59}$$

and Eqt.4.76, one obtains $$\mu_H = \left(\frac{\eta}{\sigma S}\right)\left(\frac{V_m}{B_z}\right) \tag{4.77}$$

If μ_H is to be expressed in terms of $cm^2/V\text{-sec}$, V_m in millivolts, B_z in kilogauss, and η in V^{-1}, Eqt.4.77 must be written as

$$\mu_H = \left(\frac{100\eta}{\sigma S}\right)\left(\frac{V_m}{B_z}\right) \tag{4.78}$$

7. Description of Experimental Apparatus

The equipment involved using a conventional electromagnet and a more powerful light source than the one used by Korn[16] for his measurements on hole conduction in anthracene. Since Korn used a superconducting magnet he required a heater to keep the sample at room temperature. Using the conventional magnet eliminated this. The sensitivity increase over Korn's equipment was about a factor of 30.

7a. The Crystal Holder

The crystal holder is shown in Fig.4.5. It is essentially two Teflon discs held together by four 0-80 brass screws. The illuminated electrode made of tin-oxide coated quartz fits into a depression cut into one of the Teflon discs. The dark electrode consists of a spring-loaded copper platform. Five Teflon insulated copper wires provide the necessary electrical connections and pass through a Teflon pressure seal. There is also a #30 copper-constantan thermocouple introduced to monitor the sample temperature.

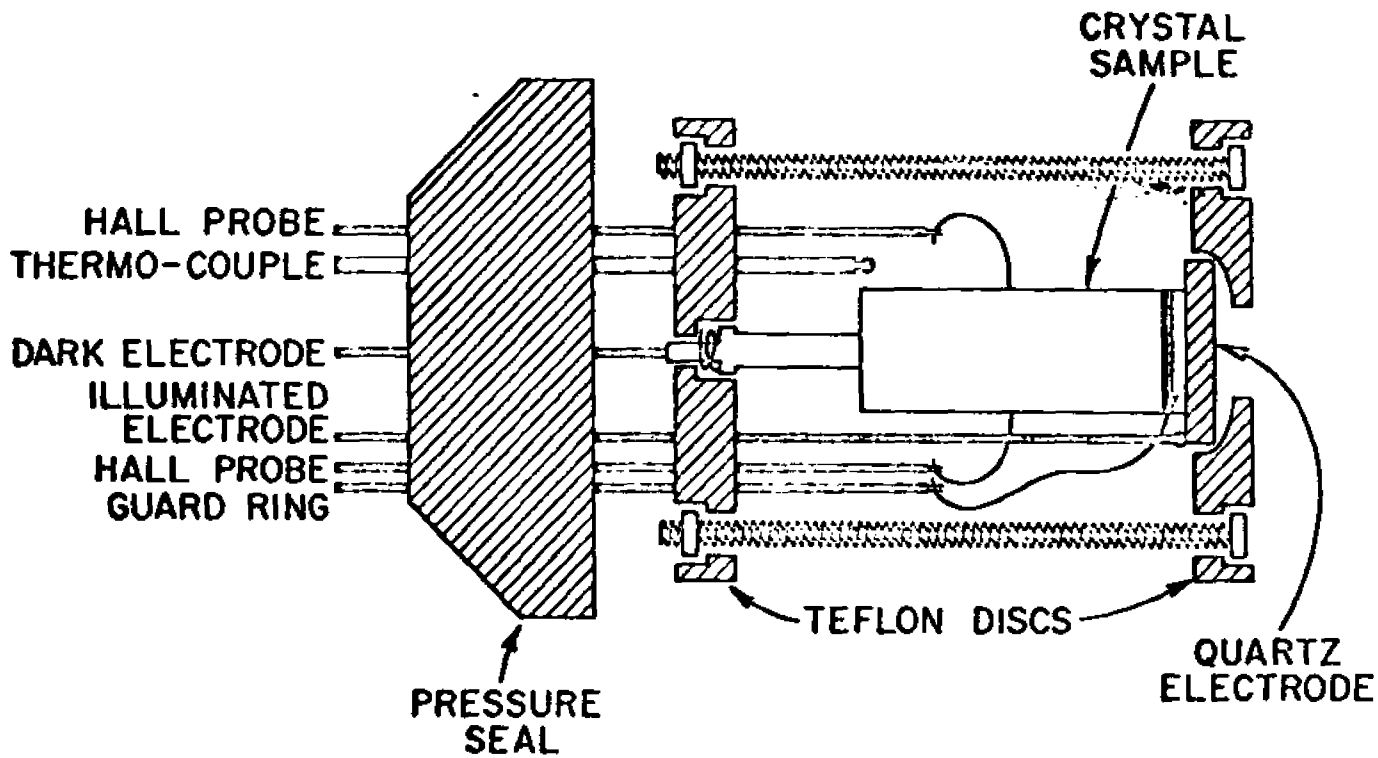

FIG. 4.5

Crystal Holder. Approximately 3X Actual Size.

The crystal was prepared by polishing in ethanol on a "Kleenex".A guard ring was painted on the crystal as near to the illuminated electrode as possible using "Eccobond 57c" silver conducting paint thinned with toluene. The dark side of the crystal was first coated with a thin coat of"Dupont #4817" silver paint to insure as uniform a field as possible, and then pasted to the spring loaded copper electrode using the "Eccobond 57c" paste, to insure good eletrical contact.

After the crystal was placed in the holder, between the spring loaded copper electrode and the tin-oxide coated quartz electrode, the four brass screws of the holder were carefully tightened to insure that the crystal did not shift its position. The two Hall probes were then connected by using springy brass wires etched in hydrochloric acid. The brass wires were soldered at one end to the #24 Teflon insulated copper wires for support and electrical contact with the electrometers. The free ends were bent to press against the surface of the crystal, one on each side.

For the guard ring connection, a #40 copper wire was soldered at one end to another supporting #24 Teflon insulated copper wire, while the free end was pasted to the painted guard ring with the quick drying "Dupont #4817" silver conducting paint.

Electrical contact to the tin-oxide coated quartz electrode was accomplished by pasting a #24 Teflon insulated copper wire to the edge of the coated surface using the "Dupont #4817" paint which had not been thinned with the butyl acetate.

A layer of epoxy glue was then spread over the connection. The epoxy was allowed to dry over night with an infrared lamp heating the connection to aid in curing.

A mask of black "Apiezon" wax was placed on the quartz electrode to shield the sides of the crystal from being illuminated. This insured against the generation of carriers by the guard ring.

The brass spring for the copper electrode and for the Hall probes were made from 0.020 inch diameter brass wire that had been drawn down to a diameter of 0.010 inches to increase its stiffness. The copper electrode was soldered to one end of the brass spring. The free end of the wire was soldered to another #24 Teflon insulated wire. All five Teflon insulated wires were passed through separate holes in the Teflon pressure seal. The sample holder is then placed in the sample chamber.

7b. The Sample Chamber

The sample chamber consists essentially of a square copper block, hollowed out to receive the sample holder. It also has a copper finger with cooling coils wound it. This provides the necessary cooling for the sample holder. See Fig.4.6.

The quartz window, sandwiched between two o-rings, is connected to the illuminated side of the sample chamber by a brass flange. A gas inlet pipe provides the means of maintaining a dry, inert atmosphere over the crystal sample. Another brass flange at the dark side of the sample chamber is shaped to conform the the Teflon pressure seal. Tightening down on this flange secures the sample holder within the sample chamber.

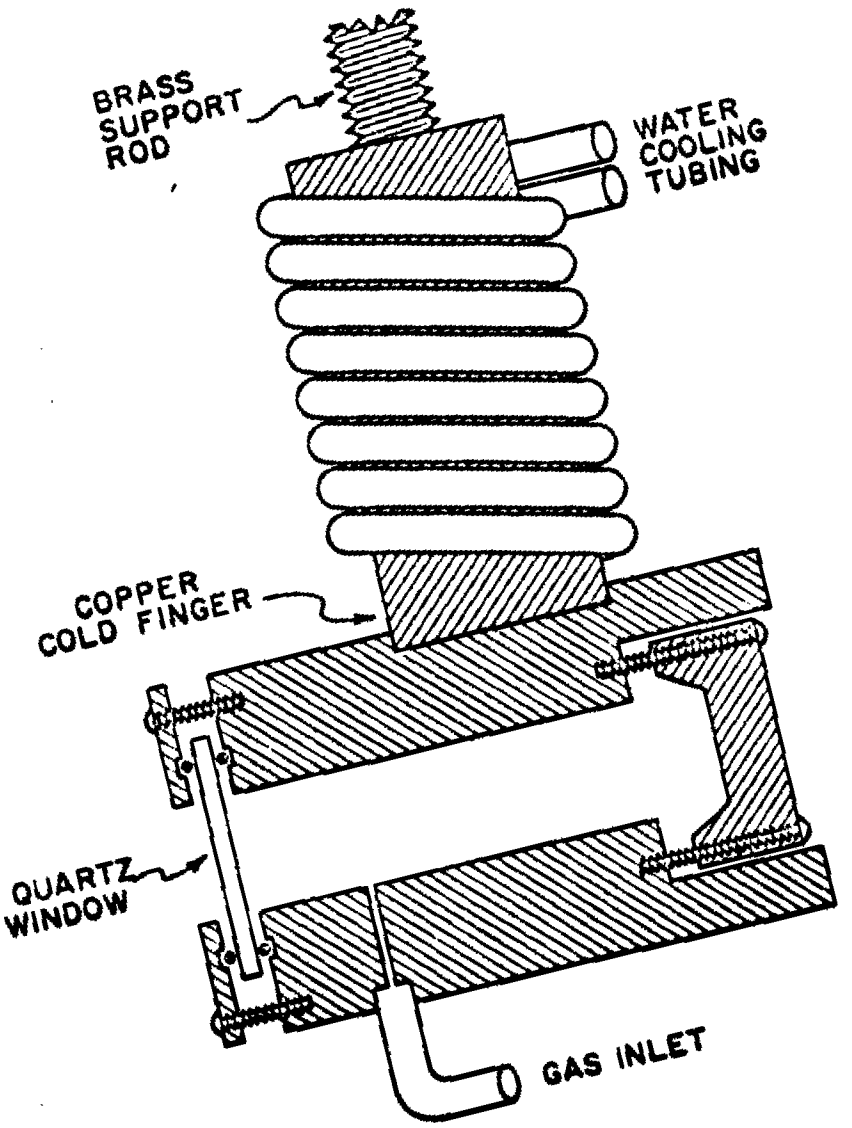

FIG. 4.6

The Sample Chamber.

The cold finger consists of a solid copper cylinder, soft soldered to the copper block, with copper tubing soft soldered to the finger. Cold water is pumped through the tubing to provide a constant heat sink. This is necessary because naphthalene easily sublimes at temperatures only slightly above room temperature. The cooling provided by the cold water proved to be adequate to significantly reduce this sublimation. Putting some flakes of naphthalene in the sample chamber also helped reduce the sublimation by providing a partial naphthalene atmosphere above the crystal.

Finally, a brass rod was screwed into the top of the copper cold finger in order to provide a handle to mount the sample chamber between the poles of the magnet.

The Teflon insulated wires were directed out the back of the chamber to a copper pipe fitted with Teflon separators. These discs have five separate holes drilled into them to insure maximum separation of the wires to prevent any leakage currents.

At the top of the copper pipe was an aluminum box, fitted with five MHV, high voltage connectors. As can be seen in Fig.4.7, we have thus insured that all the wires are completely enclosed in metal for effective insulation from stray fields.

It was also necessary to make everything as rigid as possible to prevent motion of the leadswhen the magnetic field is on.

There is a small aluminum mounting bracket used to attach the sample chamber to the shielded feed-through, and another mounting bracket connecting the brass rod to the copper pipe, to provide additional strength.

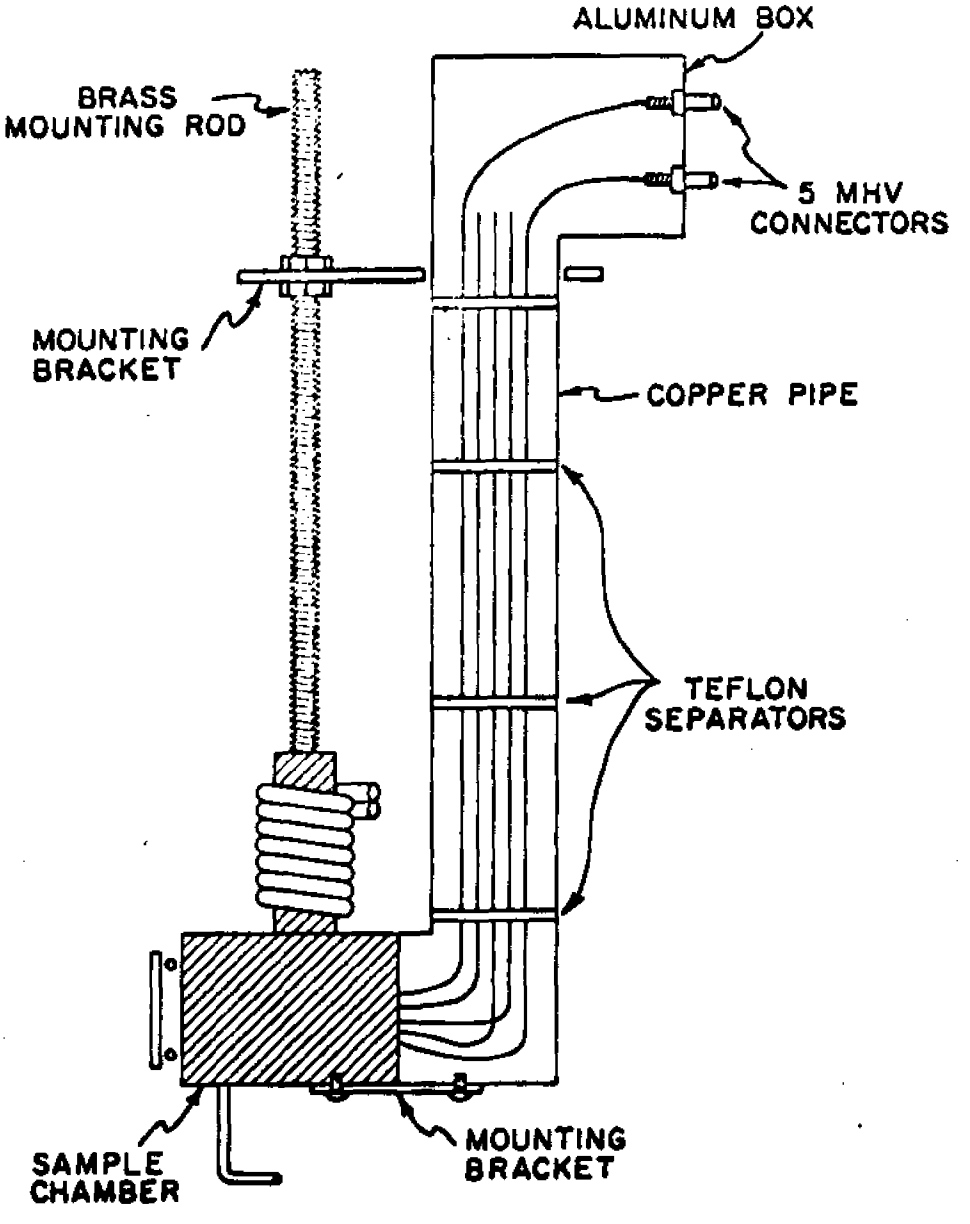

FIG. 4.7

The Sample Chamber Mounted on the Shielded Connector Housing.

7c. Optical System

A 1000 watt, mercury-xenon lamp, Hanovia 977b-1, Model C-47-35-5S, from Oriel Optics Corporation was used to illuminate the crystal. In a crystal of high purity, charge carriers must be injected, since the conduction is not intrinsic. The lamp is used to photo-inject charge carriers into the naphthalene. A heat filter was placed in the beam to reduce the amount of heat getting to the crystal. This was another precaution against the sublimation problem. The heat filter was a quartz container filled with a solution of copper sulphate in distilled water. It is prepared by taking a saturated solution of copper sulphate and diluted it one part to four with distilled water. A Corning Glass 7-59 glass filter was also used to remove most light with a wavelength above 4000 Å to insure against bulk generation of carriers. A fan was used to cool the heat filter to prevent it from cracking. A block diagram of the optics is found in Fig.4.8.

7d. The Electrical System

A block diagram of the circuit used for the Hall effect measurement is shown in Fig.4.9.

In practice, it was not possible to align the Hall probes on the crystal so that they would be on any given equipotential surface. Therefore, by adjusting the applied voltage one could not avoid a slight misalignment voltage for the two

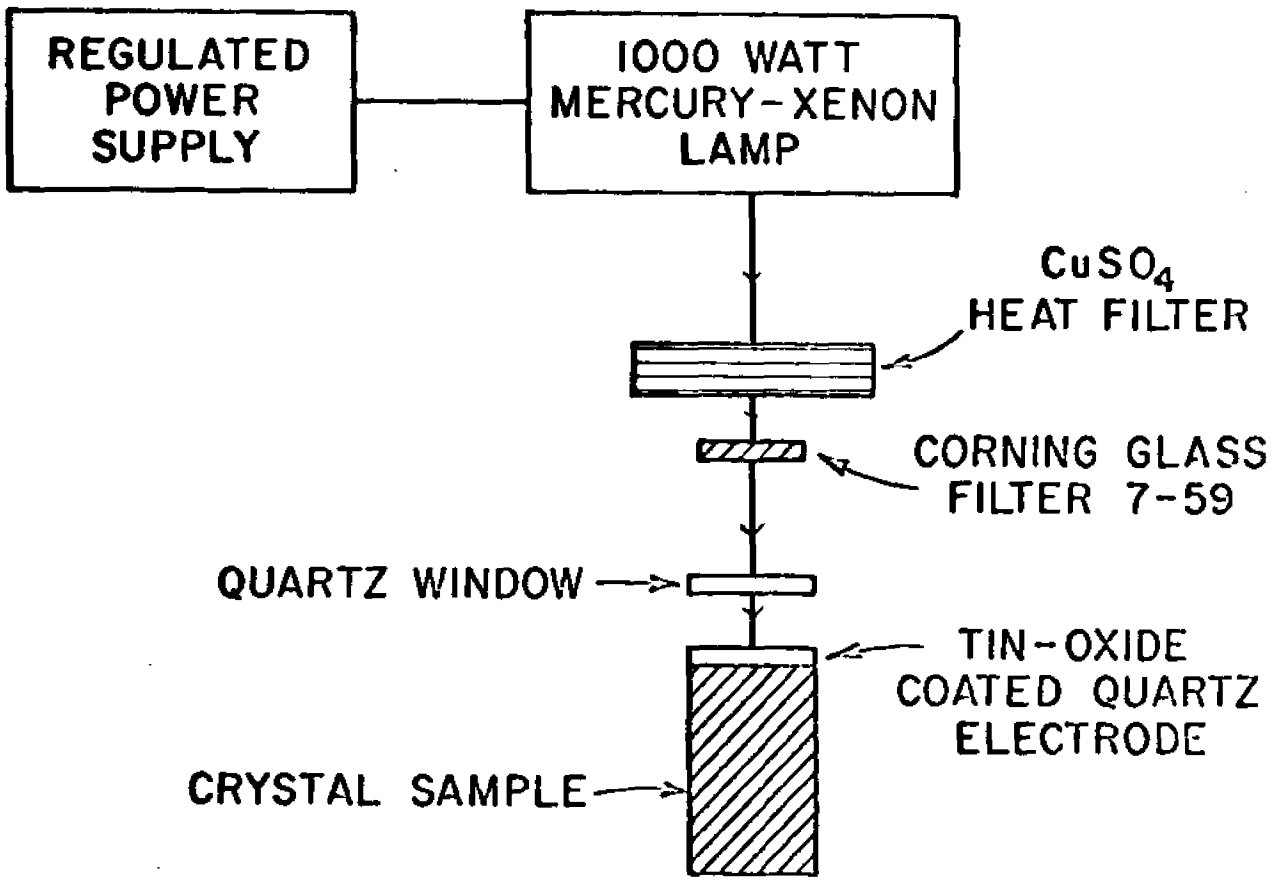

FIG. 4.8

Block Diagram of the Optical System Used to Illuminate the Crystal Sample.

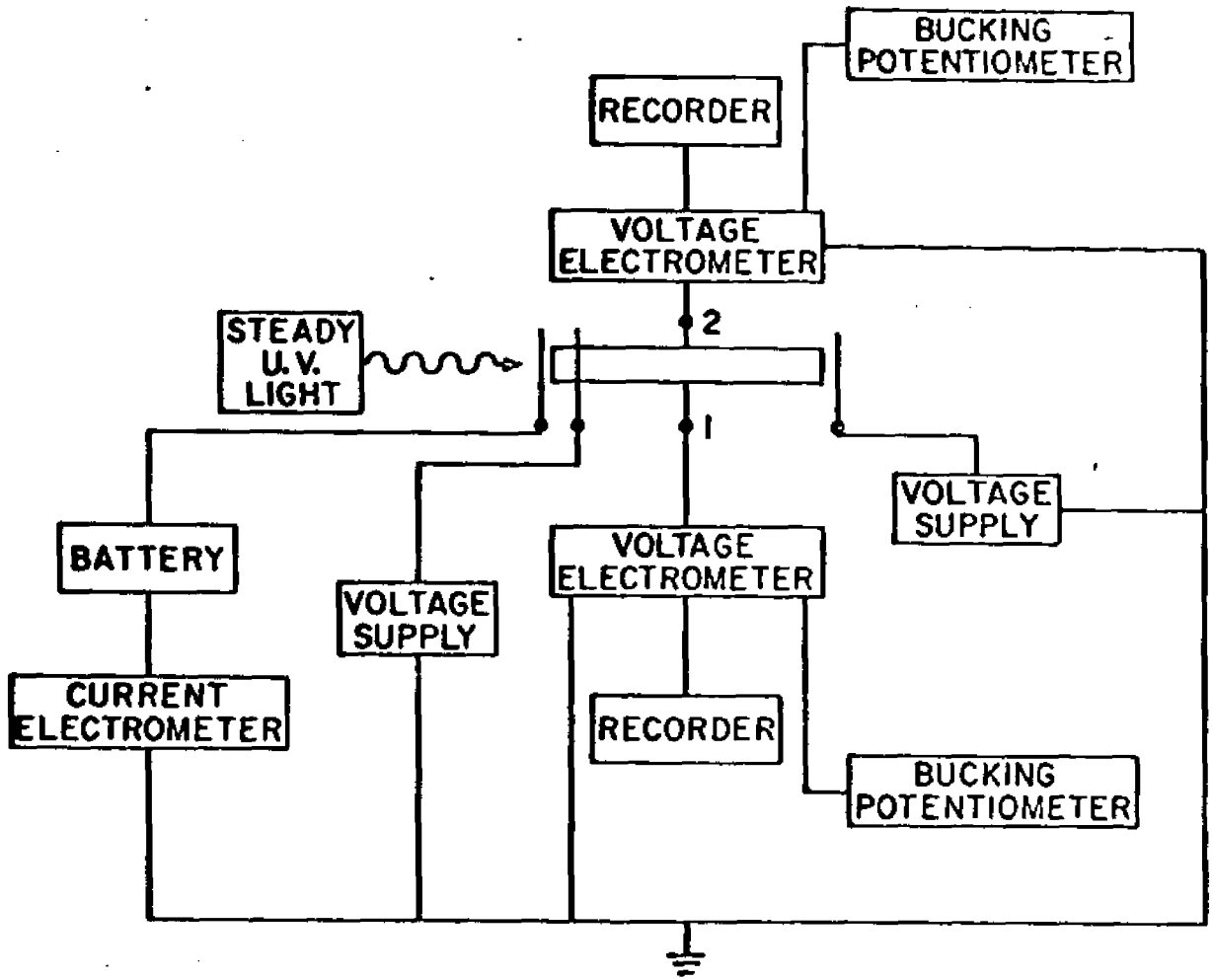

1 AND 2 ARE THE HALL PROBES

FIG. 4.9

Block Diagram for the Measurement of the Hall Voltage and the Photoconductivity of Naphthalene.

probes. This voltage had to be balanced out by using a bucking potentiometer. See Fig.4.10.

7e. The Vibrating Reed Electrometers

Separate Cary Vibrating Reed Electrometers were used to measure the potential difference of each Hall probe because it was necessary to ground input terminals of one electrometer when using it to measure voltages. The symmetry of the circuit also made it easier to match the impedances for the two Hall probe circuits.

A vibrating reed electrometer, with a 10^8 ohm resistor across its input was used as an ammeter to measure the photoconductivity.

Because of the very high circuit resistances and the low currents involved, leakage currents were a major source of concern. Great care was taken to keep all insulators as clean as possible to prevent currents from leaking across the insulation.

7f. The Magnet

The magnet used was a conventional electromagnet, model V-3400 made by Varian Associates. The power supply was model V-FR2500 Fieldial Magnetic Field Regulator, also by Varian Associates, with a continuously variable field from 0-20 kilogauss. The magnet had a two inch pole gap. It was found that the field could be changed at a rate of about 20 kilogauss/minute.

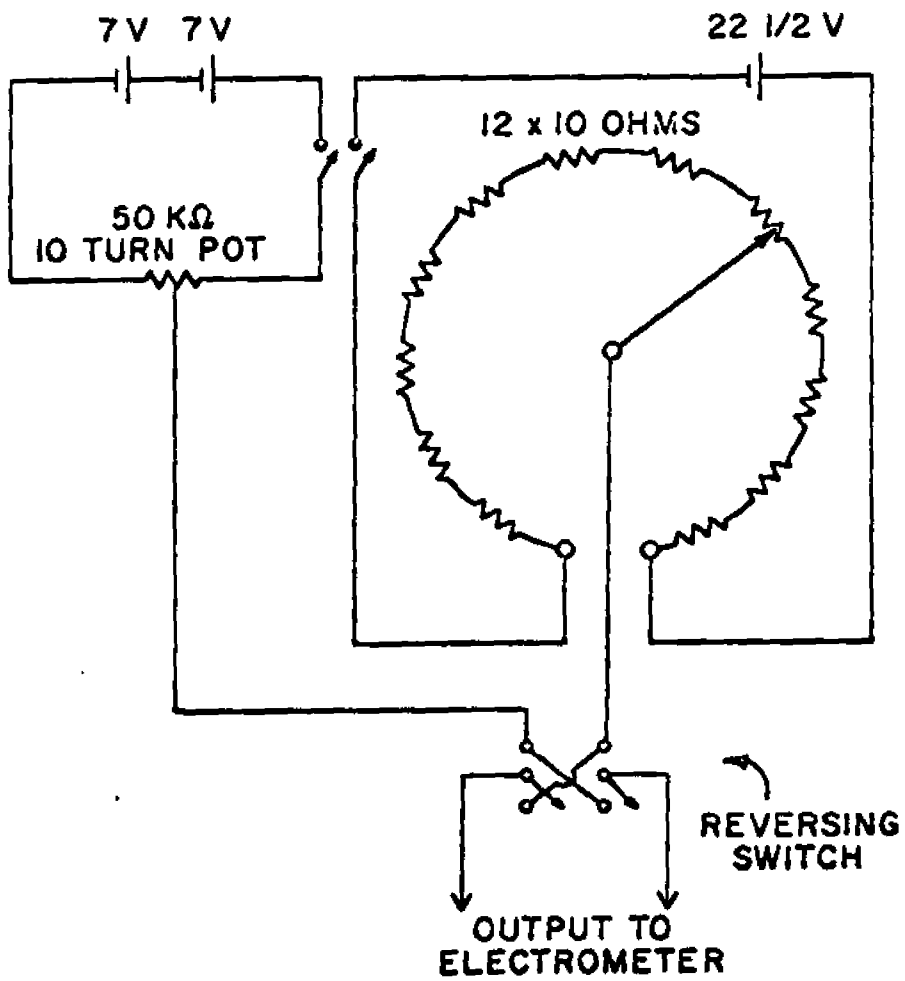

FIG. 4.10

Circuit Diagram for the Bucking Potentiometer.

8. Techniques and Results

After the sample chamber was placed in the pole gap, all the electronics connected, and the meters turned on, the first thing to do is check the dark current. This was usually of the order of 10^{-15} to 10^{-14} amperes, and provided a check on the integrity of the insulation and isolation of the electrical contacts. Larger values for the current indicated shorting out somewhere.

The guard ring was effective in eliminating surface currents. With the guard ring absent, the photo-current was typically an order of magnitude greater.

The potential at the dark electrode was then adjusted so that one of the Hall probe potentials was zero with respect to ground potential, using the bucking potentiometers to eliminate the unbalance of the Hall probes. After a sufficiently slow rate of drift was achieved in the probes, by adjustment of the dark electrode potential, the recorder trace would indicate a zero magnetic field baseline. The magnetic field was then turned on and as quickly as possible brought up to a full strength of either 10 kilogauss or 15 kilogauss. The time involved to achieve full field was typically 15 to 30 seconds. The recorder would monitor the build-up in the Hall potential until saturation occurred, usually after about 8 to 10 minutes, due to the time constant of the circuit. After saturation, the probes would resume drifting with the slope of the initial drift for zero magnetic field. The voltage

difference between the two baselines was the measured Hall voltage and could be read directly off the recorder trace.

Usually, only one of the two probes could be adjusted to have a small enough drift to make a measurement possible. The probe which was not being used had its electrometer kept on a less sensitive scale.

The field was then turned off to allow the Hall voltage to return to zero, at which time we would again observe the zero magnetic field baseline. After this baseline was again established, the magnetic field was turned on in the opposite direction, and the Hall potential again would increase. However, the deflection of the Hall probe potential would be in the opposite direction from the first case.

A typical data set is shown in Fig.4.11, including drift.

To perform the experiment for the second charge carrier, the sign of the potentials for the dark and illuminated electrodes, and for the guard ring, were simply reversed, the remainder of the procedure remaining the same.

Knowing the direction of the magnetic field, of the current, and of the deflection of the probe voltages, it was a simple matter to determine whether the observed effects were anomalous or not.

The results in all six possible orientations for both holes and electrons are given in Tables 4.2 through 4.7. The Hall mobilities were calculated from Eqt.4.78, where η is calculated from Eqt.4.76, S from Eqt.4.74, and G from Eqt.4.64. For the evaluation of L in the expression for S, the anisotropic

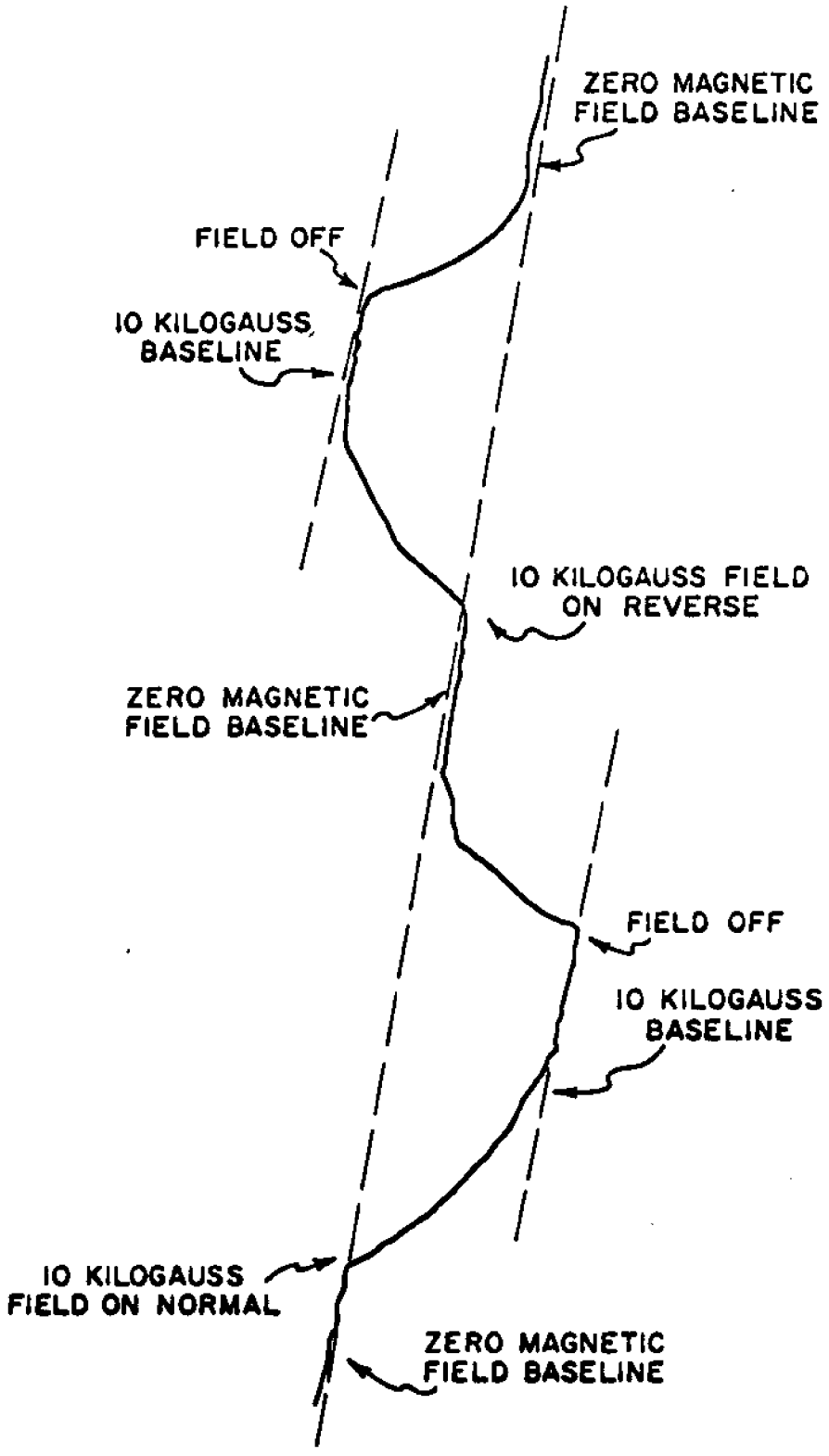

FIG. 4.11

Hall Probe Potential Recording, V_m as a Function of Time, Showing Symmetry With Reversal of the Magnetic Field.

TABLE 4.2. Experimental Data and Hall Mobility at Room Temperature.

B//c'

Crystal Orientation and Dimension l x w x t (mm^3)	V_L (V)	V_D	Photo-current (10^{-11}amp)	$\frac{V_m}{B_z}$ (mv/kG)	S	G	μ_H (cm^2/V-sec)
5x2.5x2.5	70	42	.4	.2	.24	.84	-2.7
I//a holes	70	42	.2	.13	.14	.84	-3.0
I//a electrons	70	44	.35	.15	.27	.85	-3.0

V_L is the magnitude of the voltage applied to illuminated electrode.

V_D is the magnitude of the voltage applied to the collecting electrode.

V_m is the voltage measured at the Hall probe.

B_z is the magnetic field intensity.

S is the factor due to space charge effects.

G is the geometrical factor due to the finite dimensions of the crystal sample.

TABLE 4.3. Experimental Data and Hall Mobility at Room Temperature.

B//c'

Crystal Orientation and Dimonsion l x w x t (mm^3)	V_L (V)	V_D	Photo-current (10^{-11}amp)	$\frac{V_m}{B_z}$ (mv/kG)	S	G	μ_H (cm^2/V-sec)
5x1.5x3	140	290	.42	.084	.02	.99	-5.3
I//b holes	140	41	1.9	.184	.16	.85	-3.6
I//b electrons	140	37	.12	.36	.58	.60	-1.4
	140	125	.12	.12	.08	.84	-1.8
	140	125	.16	.10	.08	.84	-1.5
	140	125	.12	.13	.11	.84	-1.5
	140	125	.70	.09	.08	.84	-1.3

V_L is the magnitude of the voltage applied to the illuminated electrode.

V_D is the magnitude of the voltage applied to the collecting electrode.

V_m is the voltage measured at the Hall probe.

B_z is the magnetic field intensity.

S is the factor due to space charge effects.

G is the geometrical factor due to the finite dimensions of the sample.

TABLE 4.4. Experimental Data and Hall Mobility at Room Temperature.

B//b

Crystal Orientation and Dimonsion l x w x t (mm^3)	V_L (V)	V_D	Photo-current (10^{-11}amp)	$\frac{V_m}{B_z}$ (mv/kG)	S	G	μ_H (cm^2/V-sec)
5.5x3x3	70	137	4.0	.12	.49	.91	+.46
I//a holes	70	137	4.6	.14	.52	.91	+.50
I//a electrons	70	149	.86	.24	.237	.91	+1.9
	70	137	.86	.20	.233	.91	+1.5

V_L is the magnitude of the voltage applied to the illuminated electrode.

V_D is the magnitude of the voltage applied to the collecting electrode.

V_m is the voltage measured at the Hall probe.

B_z is the magnetic field intensity.

β is the factor due to space charge effects.

G is the geometrical factor due to the finite dimensions of the crystal sample.

TABLE 4.5. Experimental Data and Hall Mobility at Room Temperature.

B//b

Crystal Orientation and Dimonsion l x w x t (mm^3)	V_L (V)	V_D (V)	Photo-current (10^{-11} amp)	$\frac{V_m}{B_z}$ (mv/kG)	S	G	μ_H (cm^2/V-sec)
5x3x1.5	140	206	.19	.018	.11	.88	+.16
I//c' holes	140	206	.20	.021	.11	.88	+.18
I//c' electrons	140	176	.17	.110	.09	.87	+1.3
	140	176	.15	.096	.08	.87	+1.3

V_L is the magnitude of the voltage applied to the illuminated electrode.

V_D is the magnitude of the voltage applied to the collecting electrode.

V_m is the voltage measured at the Hall probe.

B_z is the magnetic field intensity.

S is the factor due to space charge effects.

G is the geometrical factor due to the finite dimensions of the crystal sample.

TABLE 4.6. Experimental Data and Hall Mobility at Room Temperature.

B//a

Crystal Orientation and Dimension l x w x t (mm^3)	V_L V_D (V)	Photo-current (10^{-11}amp)	$\frac{V_m}{B_z}$ (mv/kG)	S	G	μ_H (cm^2/V-sec)
4.5x2x2 I//b holes	140 140	.28	.090	.03	.93	-4.7
5x3x1.5 I//b electrons	140 125	.12	.031	.06	.84	+.6

V_L is the magnitude of the voltage applied to the illuminated electrode.

V_D is the magnitude of the voltage applied to the collecting electrode.

V_m is the voltage measured at the Hall probe.

B_z is the magnetic field intensity.

S is the factor due to the space charge effects.

G is the geometrical factor due to the finite dimensions of the crystal sample.

TABLE 4. 7. Experimental Data and Hall Mobility at Room Temperature.

B//a

Crystal Orientation and Dimonsion l x w x t (mm^3)	V_L (V)	V_D	Photo-current (10^{-11}amp)	$\frac{V_m}{B_z}$ (mv/kG)	S	G	μ_H (cm^2/V-sec)
5.5x2.5x2.5	70	100	.10	.060	.10	.94	-1.5
I//c' holes	70	105	.10	.054	.10	.95	-1.3
I//c' electrons	70	80	.13	.024	.116	.94	+.55
	70	80	.18	.028	.153	.94	+.49
	70	80	.24	.036	.192	.94	+.50

V_L is the magnitude of the voltage applied to the illuminated electrode.

V_D is the magnitude of the voltage applied to the collecting electrode.

V_m is the voltage measured at the Hall probe.

B_z is the magnetic field strength.

S is the factor due to space charge effects.

G is the geometrical factor due to the finite dimensions of the crystal sample.

dielectric constants of naphthalene are needed. These values were obtained in a manner identical with that for obtaining the dielectric constants for phenanthrene.(See Appendix B.)

The drift mobility values were determined using the flash technique developed by Kepler[25], as described in Appendix C.

The results of the calculation of the Hall mobility to the drift mobility ratio from the experimental data is given in Table 4.1b. According Onsager[17] the matrix formed by the values of the ratios of the mobilities should be reciprocal. That the data in Table 4.1b agrees with this provides a good test for the consistency of the results of the experiment. There is an error of about 30% due to the deviations from the average values for the experimentally determined drift and Hall mobilities. The minus signs indicate anomalous Hall mobilities.

9.Discussion

The results given in Tables 4.2 to 4.7 for naphthalene show that for the magnetic field aligned along the a or c' crystal directions anomalous Hall mobilities result for holes in naphthalene. The holes were deflected in the opposite direction from what one would expect from a Lorentz force. This result was predicted by the band theory when the resonance integrals obtained from Katz[3] and Thaxton[4] were used. (See Table 4.1) However, for electrons, anomalous Hall mobilities were observed with the magnetic field aligned only in the c' direction. This agrees well with the results predicted using Katz's resonance integrals. Although the results using Thaxton's resonance integrals predict anomalous signs, they predicts, for electrons, anomalous Hall

mobilities with the magnetic field aligned in either the a or c' directions, as in the case for holes. The magnitudes of the ratios are also closer to the theoretical values predicted by Katz. This indicates that the amount of overlap between the wavefunctions for the various resonance integrals used by Thaxton was not in good agreement with the actual situation.

A test for the validity of the method used was a run on anthracene, to compare the results with those obtained by Korn[16]. These results agreed within the experimental error. The validity of the space charge could not be checked, unfortunately. The method for checking this dependence is to realize that the measured Hall voltage is a function of the photocurrent, as can be seen from Eqts. 4.72 and 4.75. After explicitly determining this dependence, one can vary the measured Hall voltage by varying the photocurrent. The results should agree with the predicted functional dependence. It was impossible to employ this test for naphthalene, however, since it was impractical to vary the photocurrent. If the photocurrent was made any less than the best obtainable, the Hall probe voltages became marginal. Fortunately, this test was employed on anthracene measurements, and the agreement with the predicted functional dependence is observed.[21] The agreement of the results with the Onsager relation is evidence, however, that the values for S (see Tables 4.2 to 4.7) are at least of the correct order of magnitude.

In an attempt to determine the influence of the magnetic field strength results were spot checked at either 10 kilogauss

or 15 kilogauss. The results were found to be independent of the field strength under these conditions.

A value for the band width could not be determined from the experimental data since the details of the energy band structure are not yet known.

References - Chapter 4

1. O.H.LeBlanc, Conductivity in D.Fox, M.M.Labes, and A. Weisberger, eds., Physics and Chemistry of the Organic Solid State (Interscience Publishers, New York, 1967), Vol.III, p.155.

2. O.H.LeBlanc, J. Chem. Phys. 35, 1275 (1961).

3. J.I.Katz, S.A.Rice, S.Choi, and J.Jortner, J. Chem. Phys. 39, 1683 (1963).

4. G.D.Thaxton, R.C.Jarnagin, and M.Silver, J. Phys. Chem. 66, 2461 (1962).

5. L. Friedman, Phys. Rev. 140, A1649 (1965).

6. L. Friedman, Phys. Rev. 133, A1668 (1964).

7. S.H.Glarum, J. Phys. Chem. Solids 24, 1577 (1963).

8. R.G.Kepler, Phonons and Phonon Interactions, T.A.Bak ed., Benjamin Press, New York, 1963), p.578.

9. M.Silver, J.Rho, D.Olness, and R.C.Jarnagin, J. Chem. Phys. 38, 3030 (1963).

10. O.H.LeBlanc, J.Chem. Phys. 39, 2395 (1963).

11. J.Dresner, Phys. Rev. 143, 558 (1966).

12. G.Delacote, and M.Schott, Solid State Comm. 4, 177 (1966).

13. R.Pethig and K. Morgan, Nature 214, 266 (1967)

14. T.Toombs, Ph.D. Thesis, Princeton University (Unpublished, 1968).

15. G.C.Smith, Bull. Am. Phys. Soc. 14, 370 (1969).

16. A.Korn, R.A.Arndt, and A.C.Damask, Phys. Rev., in press.

17. J.M.Ziman, Electrons and Phonons, (Oxford Press, Oxford), Ch.7.

18. H. Jones and C. Zener, Proc. Roy. Soc. 145A, 268 (1934).

19. J. Trotter, Acta Cryst. 16, 605 (1963).

20. A.J.Dekker, Solid State Physics, (Prentice Hall, Inc., New Jersey, 1965), p.278.

21. A.Korn, Private communication.

22. N.F.Mott and R.W.Gurney, Electronic Processes in Ionic Crystals, (Oxford Press, Oxford, 1947).

23. I.Isenberg, B.R.Russell, and R.F.Green, Rev. Sci. Inst. 19, 685 (1948).

24. P.C.Banbury, H.K.Henisch, and A.many, Proc. Phys. Soc. 66A, 753 (1953).

25. R.G.Kepler, Charge Carrier Mobility and Production in Anthracene in J.J.Brophy and J.W.Buttrey,eds., Organic Semiconductors, (MacMillan, New York, 1962), p.1.

CHAPTER FIVE

1. Introduction

Hexamethylbenzene (HMB) consists of a benzene ring with a methyl group substituted for each of the six hydrogen atoms, as shown in Fig.5.1. In the pure state HMB is colorless and has a melting point of 166°C.[1]

HMB has been found to undergo a λ-point transition (a higher-order phase transition) in the specific heat[2] at about 110°K. The crystal structure above and below the λ-transition has been determined to be triclinic, with one molecule per unit cell.[3] A second phase transition[4] occurs at about 383°K involving a change in the crystal structure from triclinic to orthorhombic.

The molecular motion and vibrational spectra of HMB have been studied by a variety of techniques. Andrew[5] investigated the variation of the nuclear magnetic resonance absorption line widths as a function of temperature. In this way he was able to attribute the low temperature transition to the onset of rotation of the methyl groups.

Leech et al[6] presented infrared evidence for internal rotation of the CH_3 groups above 110°K.

Rush and Taylor[7] performed a neutron inelastic scattering investigation of HMB above and below the 110°K transition, much like that performed on phenanthrene in Chapter 3 of this work. Changes in the density of modes of vibration were discussed in terms of changes in the energy of the barrier to the internal rotation of the methyl groups.

One sees, therefore, that by a variety of methods the low temperature transition of HMB is generally attributed to the onset of a new degree of freedom, characterized by a rotation

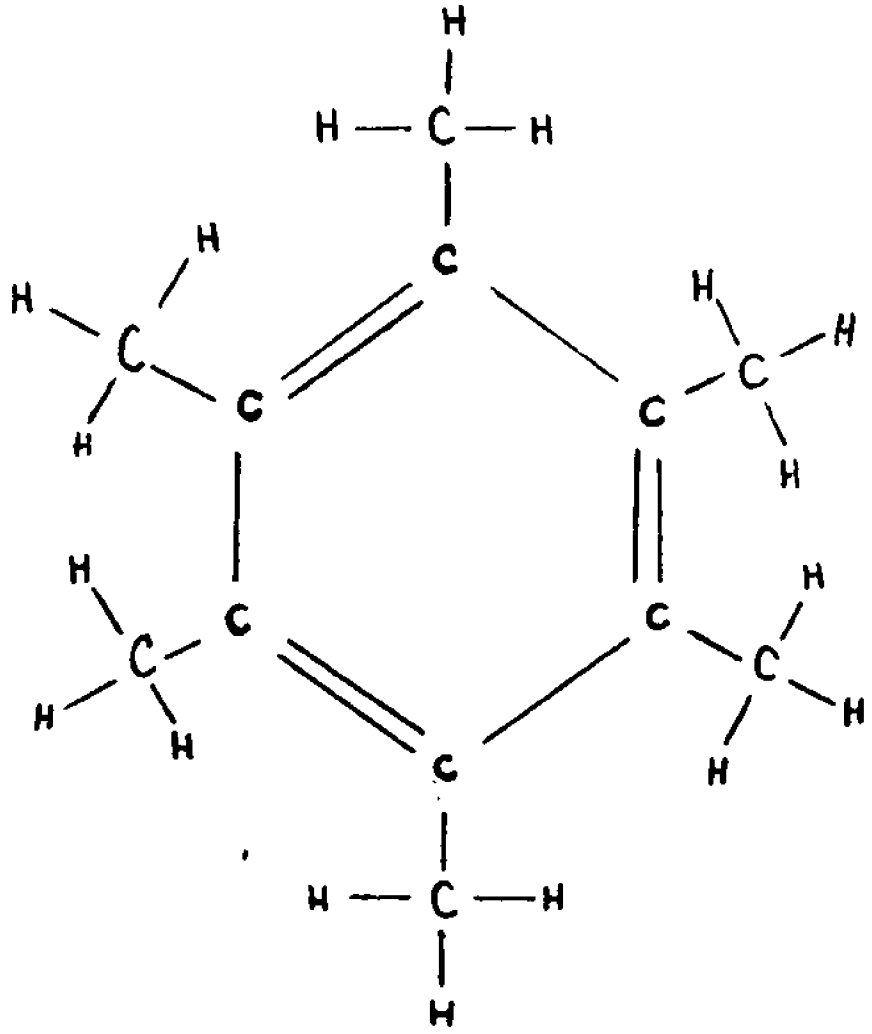

FIG.5.1. The Hexamethylbenzene Molecule.

of the CH_3 methyl groups.

In an effort to explore potentially new phonon assisted properties it was decided that it would be of interest to do a phosphorescence study of HMB through the transition temperature to see if there is a measurable effect of change in the phonon distribution on triplet exciton lifetime. It will be shown that phosphorescence (a radiative process) is in competition with vibrational (and presumably phonon assisted) processes of energy deactivation.

The existance of phosphorescence was established by Sponer and Kanda[8] when they reported phosphorescence in crystalline HMB at 4°K and at 77°K.

Olness and Sponer[9] reported phosphorescence half-lives in HMB crystals of about 8 seconds at 4.5°K.

With the existance of phosphorescence firmly established, it was decided to examine the decay times in the region of the low temperature transition.

2. Theory of Monomolecular Triplet Exciton Decay

An electron in an atom or molecule behaves as if it generates two types of angular momenta, one associated with its motion about the nucleus, the other pictorially visualized as originating in an inherent "spin" with an angular momentum of $\frac{1}{2}\hbar$.

According to molecular orbital theory, the ground state of a molecule may be derived by adding electrons one at a time to the molecular orbitals, beginning with the lowest, each orbital containing two electrons of opposing spin. If the total spin S of the electrons cancel in pairs, then the number of ways (2S+1) in which the total spin angular momentum can combine with the

total orbital orbital momentum is one. The multiplicity of the state is said to be one, and the state is called singlet. An excited state is derived by removing one of the electrons from the uppermost filled orbital of the ground state to a vacant orbital of higher energy. If the spin of the excited electron is conserved in the process, the total spin of the excited state is still zero. The multiplicity is still one and the state is still referred to as singlet. If, however, the spin of the excited electron is not conserved and consequently no longer cancels the spin of the odd electron left in the lower orbital, then the total spin is unity. The multiplicity (2S+1) is three, and the state is referred to as triplet.

Excited molecules may be produced in a variety of ways. For example, one may excite a molecule by optical absorption, by thermal excitation, or by bombardment with fast particles. By choosing light of known frequency, one can excite molecules from a well-defined initial state to a well-defined final state.

Using Fig.5.2[10], one can describe the different processes for energy transfer possible in a molecule in a condensed state. By optical absorption, the molecule may be excited to a high vibrational level of S_1 (denoted by S_1^*). Through a process called internal conversion, states of like multiplicity may undergo a radiationless vibrational deactivation to a lower energy level. When the nonradiative transition occurs between states of different multiplicity but equal energy, for example $S_1 \rightarrow T_1^*$, the process is called "intersystem crossing"[11]. As can be seen in Fig.5.2, intersystem crossing is responsible for both the formation of the triplet state ($S_1 \rightarrow T_1^*$) and its subsequent decay ($T_1 \rightarrow S_0^*$) and occurs as a result of the increased inter-

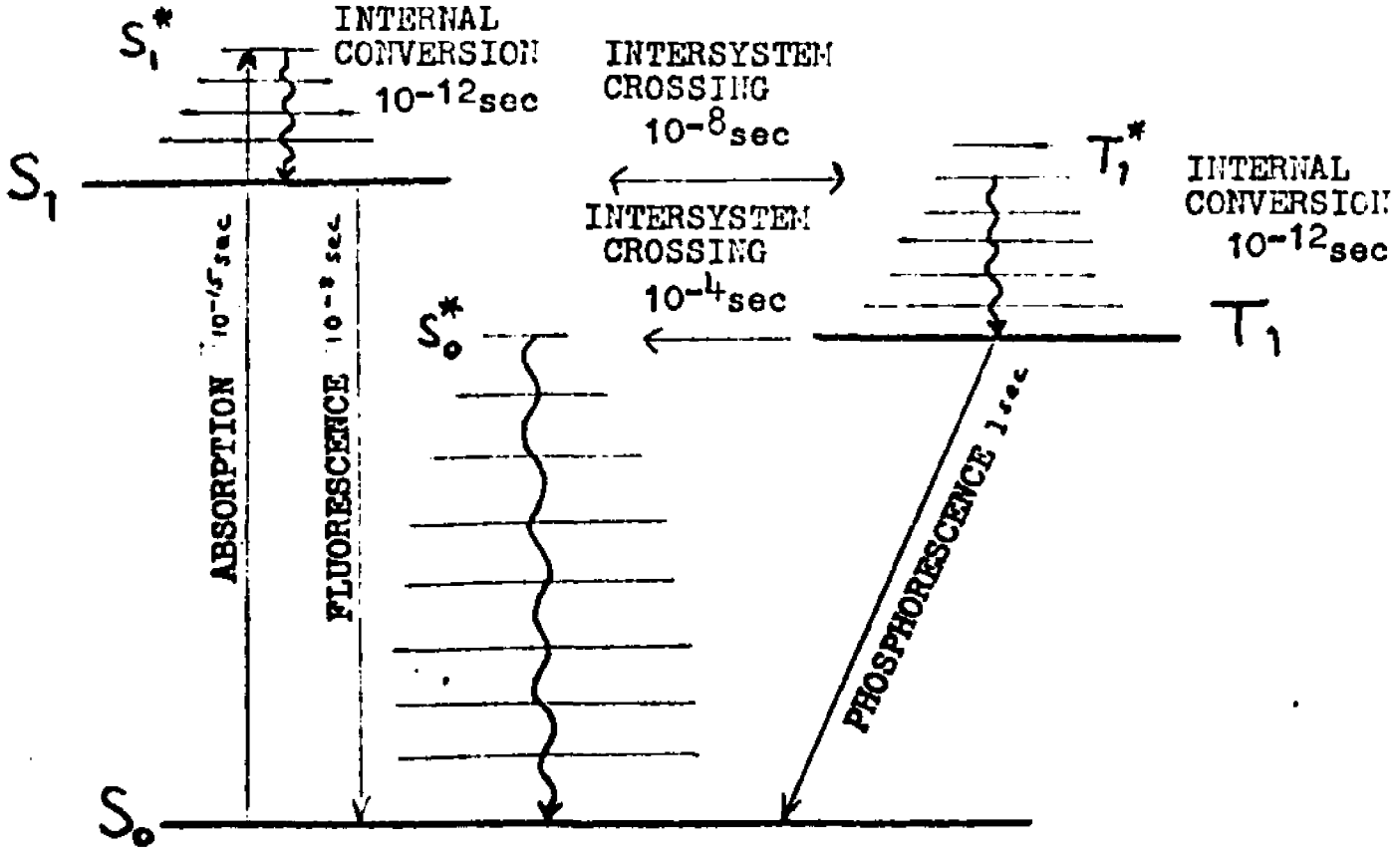

FIG.5.2. Energy Levels and Energy Transfer in a Complex Molecule.

molecular coupling in the condensed phase.

As a general rule, radiative deactivation becomes more efficient as the motion of the molecules is restricted. This is due to the fact that radiationless energy transfer requires coupling between the excited molecule and its neighbors. This coupling becomes less as the amplitude of the molecular motions decrease. Therefore, lowering the temperature increases the probability of radiative deactivation.

3.Kinetics of Triplet Exciton Decay

In weakly coupled systems,such as occur in molecular crystals, the lattice has time to distort around the excited molecules. The excited state is thus not confined to isolated molecules, but may affect several hundred or even thousand molecules. Such a delocalized excited state is called an exciton[12]. Through a diffusion type of process excitons may transport energy rapidly along a chain of molecules to a site which may be far removed from the original absorption site.

Singlet excitons are generated by ultraviolet light, while triplet excitons are generated by intersystem crossing with a rate constant K_{ST}. Due to the high purity of the sample, the kinetic analysis of exciton decay will ignore trapping.On removal of the exciting radiation, the singlet and triplet exciton densities, n_S and n_T respectively, can be described by the expressions[13]

$$\frac{dn_S}{dt} = -K_{ST} n_S + \phi\gamma n_T^2 \qquad (5.1)$$

and

$$\frac{dn_T}{dt} = K_{ST} n_S - \beta n_T - \gamma n_T^2 \qquad (5.2)$$

where K_{ST} is the rate constant for monomolecular singlet

decay, β for monomolecular triplet decay, and δ for triplet-triplet annihilation. The triplet-triplet annihilation is possible because the greater lifetime of the triplets allows for their interaction. This greater lifetime is due to the "prohibited" nature of their deactivation. ϕ is an efficiency factor equal to the ratio of the singlet excitons produced to the triplet excitons destroyed, and is therefore less than or equal to $\frac{1}{2}$.

For the long times involved in phosphorescence measurements (of the order of a second) one can set $K_{ST}n_S = 0$ since there will nolonger be any intersystem crossing of the type $S_1 \rightarrow T_1^*$. This is due to the decreased population of singlets due to their rapid ($\sim 10^{-8}$sec) deactivation. Eqt.5.2 therefore reduces to

$$\frac{dn_T}{dt} = -\beta n_T - \delta n_T^2 \tag{5.3}$$

For low intensities, where monomolecular triplet decay predominates over triplet-triplet annihilation, one has

$$\beta n_T \gg \delta n_T^2 \tag{5.4}$$

giving for Eqt.5.3

$$\frac{dn_T}{dt} = -\beta n_T \tag{5.5}$$

or

$$n_T = \text{const}_1 \times e^{-\beta t} \tag{5.6}$$

The phoshorescence intensity, due to the radiative decay of the triplet is given by

$$I_{PH} = K_p n_T \tag{5.7}$$

where K_p is the rate constant for radiative triplet decay. Therefore at times long compared to singlet decay, the phosphorescence decay has, using Eqt.5.6, the form

$$I_{PH} = \text{const}_2 \times e^{-\beta t} \tag{5.8}$$

One concludes that for the case where trapping effects can

be ignored, and the time involved is long compared to singlet exciton decay, that the phosphorescence decay follows an exponential law.

4. Description of the Experiment

One can observe the phosphorescence intensity as a function of time, after the exciting radiation has been removed, to determine the monomolecular triplet decay constant β. This was done over the temperature range from about 90°K to 120°K. The assumption was made that the phosphorescence was due only to triplet decay and not to singlet decay from impurities.

4a. The Apparatus

In accordance with Eqt.5.8 one should observe an exponential decay of the phosphorescence intensity. Therefore, one may illuminate the crystal sample with ultraviolet light, remove the light and monitor the decay in intensity of the phosphorescence. Plotting the decay on semilogarithmic paper will enable one to obtain the value of β, at the given temperature, by evaluating the slope of the resulting straight line. Doing this at regular temperature intervals allows one to determine the temperature dependence of the monomolecular decay constant, β.

The instrument used to observe the phosphorescence was the Aminco-Bowman Spectrophotofluorometer made by the American Instrument Company. This instrument consists essentially of a xenon lamp for the light source, two monochromators, one for the emission spectrum and one for the excitation spectrum, and a photomultiplier connected to an amplifier and a galvanometer. See Fig.5.3. The output of the galvanometer is fed into a

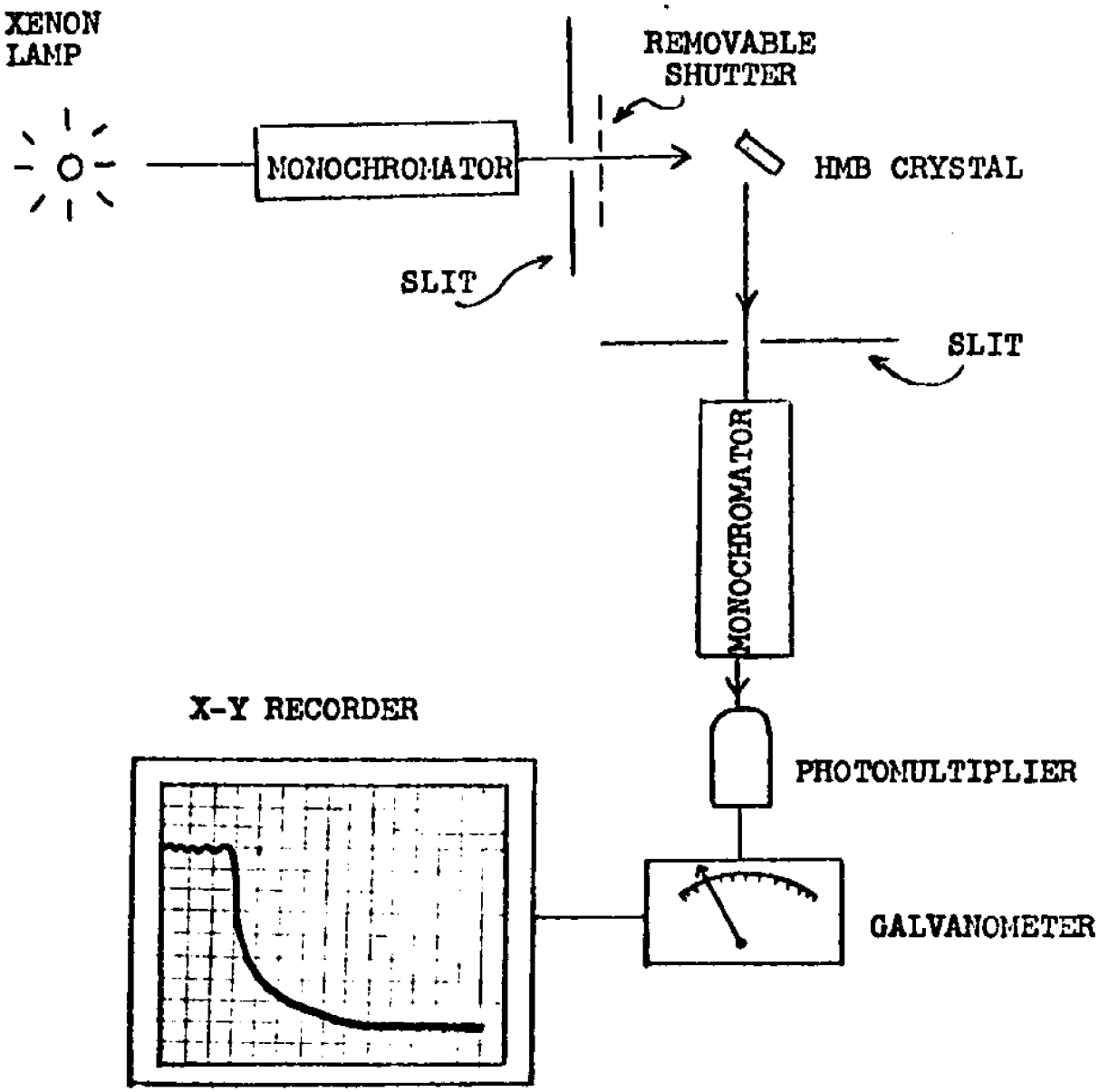

FIG.5.3. Block Diagram of the Experimental Set-Up.

Hewlett-Packard Model 7004A X-Y Recorder. Using the time base of the recorder set at 1 inch per second, the decay of the phosphorescence was recorded. A typical recording of this decay is shown in Fig.5.4a. Fig.5.4b shows the decay plotted on semilogarithmic scales.

A copper cold finger, one end of which was immersed in a liquid nitrogen bath, was used to cool the crystal sample, which was placed on the other end of the cold finger. The sample temperature was monitored using a copper-constantan thermocouple imbedded in the cold finger near the sample. The voltage developed by the thermocouple was measured by using a Honeywell Model 2745 Potentiometer.

4b.The Hexamethylbenzene Crystal

For phosphorescence delayed fluorescence measurements where long triplet lifetimes are involved, the purity of the sample is essential. This is because an exciton trapped in an impurity momlecule wil decay, exhibiting the phosphorescence spectrum of the the impurity rather than the host material.

High purity was obtained using the standard techniques of vacuum sublimation and zone refining. When the purified HMB was examined for impurities using a Varian "Aerograph" Analytical Gas Chromatograph, several impurities were detected. Additional zone refining failed to remove these impurities. However, the Varian "Aerograph Model 700" Preparatory Gas Chromatograph can be used to separate the components of the sample material, although this is a tedious and time-consuming technique. By observing the different times at which the various components of the sample material exit from the chromatograph column, one

a)

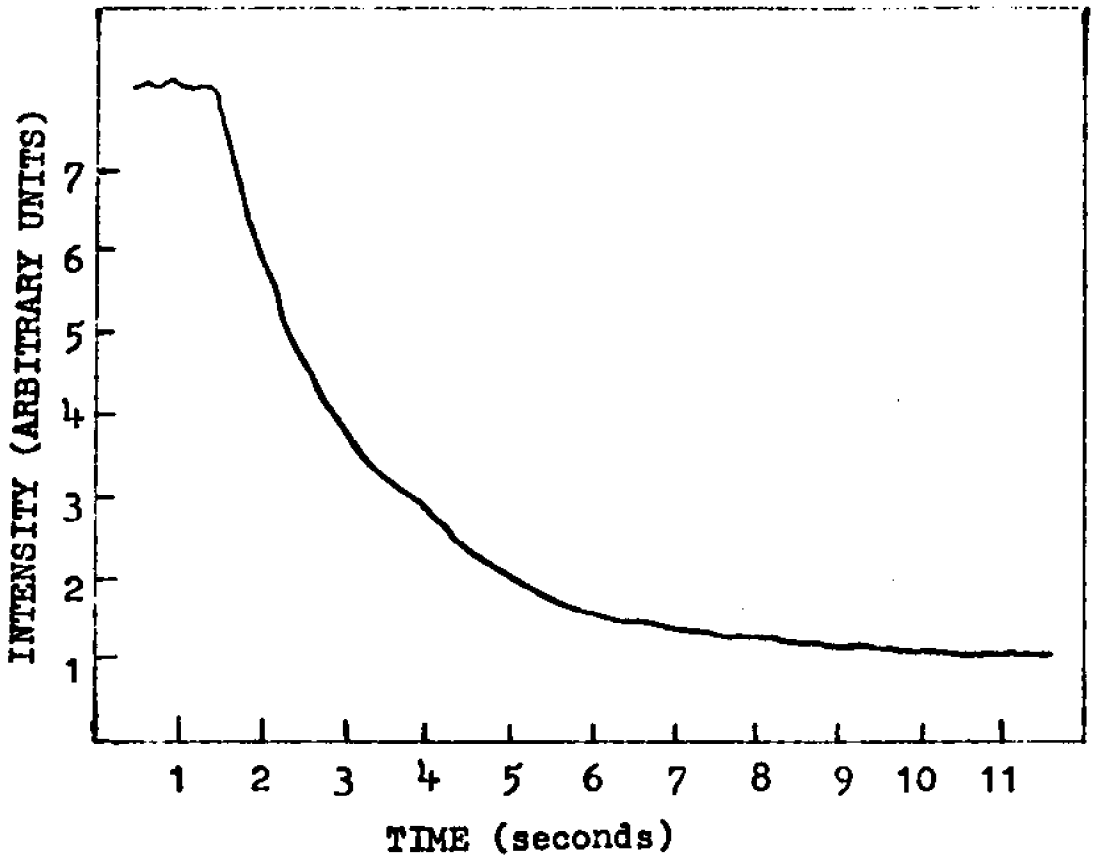

b)

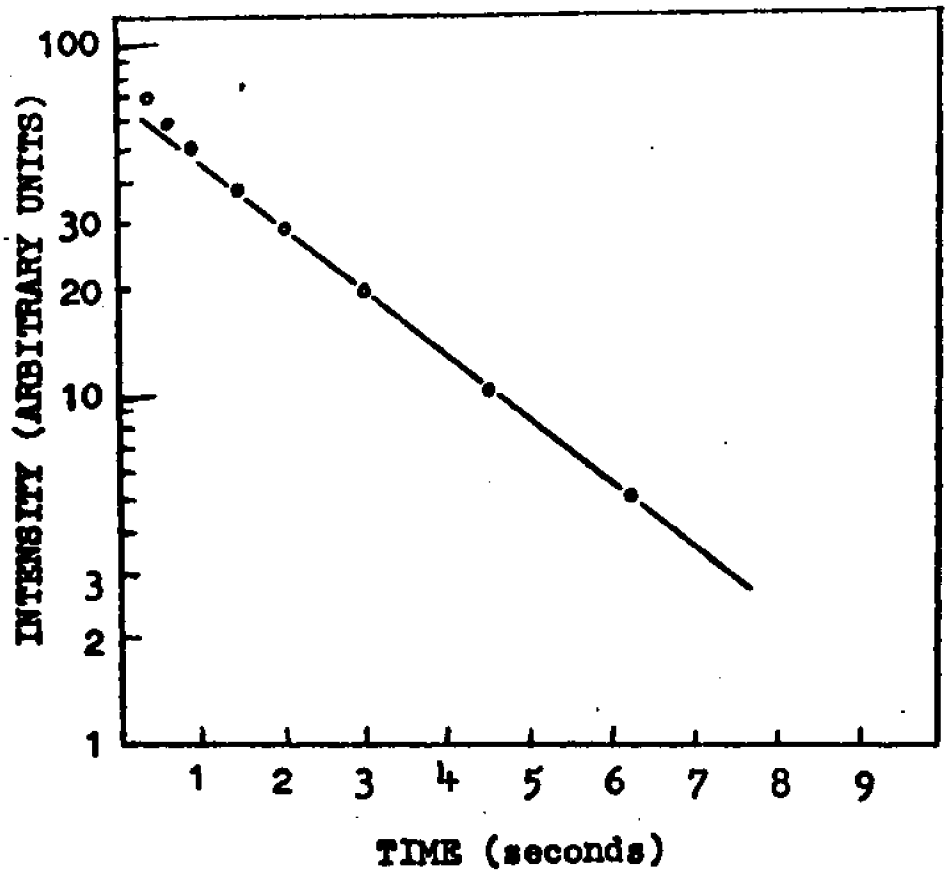

FIG.5.4. (a) Phosphorescence Decay. (b) Semi-Logarithmic Plot of the Decay Intensity.

can isolate pure HMB and collect it in a bottle as it exits from the gas column. Since samples of only ½ gram could be processed in this way at each operation, the procedure was repeated about 60 times in order to obtain 30 grams of pure HMB. Checking this material for impurities using the analytical chromatograph resulted in no impurities being detected. Spectrophotometric analysis also failed to uncover the presence of impurities. This would indicate an impurity concentration of less than one part per million, which is the sensitivity of the spectrophotometer.

When some of this ultra-pure material was melted and analyzed for impurities an unknown thermal decomposition product appeared. This necessitated keeping the temperature of the column of the preparatory chromatograph as low as possible (about 170°C) to prevent thermal decomposition. It also made it undesirable to grow the crystal from the melt. The crystal was therefore grown from the vapor. By reducing the pressure to about 500 microns the temperature of the furnace can be kept at only 90°C and sublimation will occur quite readily under these conditions. The crystal grows against a flat portion of the glass container which is cooled below the surrounding temperatures using a copper cold finger. The resulting crystal was approximately 1 centimeter in diameter, and, although not single had several large clear sections.

5. Techniques and Results

With the crystal in place, liquid nitrogen was pumped into the cold bath and the temperature of the sample was monitored. The temperature was lowered as far as possible (about 90°K) and maintained at that temperature for 15 minutes to allow for

thermal equilibrium to be established between the cold finger and the crystal sample. The phosphorescence decay curves were then taken while the system was allowed to warm up at its own rate of about of about 3 degrees centigrade per minute. Each measurement took about 15 seconds, of which only the first 10 seconds or so are significant for determining the exponential decay constant. Therefore the temperature did not vary by more than ½ of a degree centigrade during any particular measurement. To prevent the crystal from fogging over at low temperatures, dry nitrogen was blown through the sample compartment.

A plot of the monomolecular triplet decay constant β as a function of temperature in the region of the low temperature transition in HMB is shown in Fig.5.5. The solid line represents a least squares fit to the data points. The data points contain a vertical uncertainty of about 3% due to the uncertainty in determining the slope of the semilogarithmic plot in Fig.5.4b, and a horizontal uncertainty of about ½ degree centigrade. These are indicated in the Figure by error bars. It is seen that there is no evidence for any anomalous change in the decay constant at 110°K, the temperature of the phase transition.

6. Discussion

It is well established that the low-temperature transition exhibited by hexamethylbenzene is due to the onset of a new degree of freedom, characterized by the hindered rotation of the CH_3 methyl groups. It has been shown in this experiment that this new degree of freedom does not detectably affect the monomolecular triplet decay constant β. One may compare this result with the results obtained by Whitten et al[13] where no

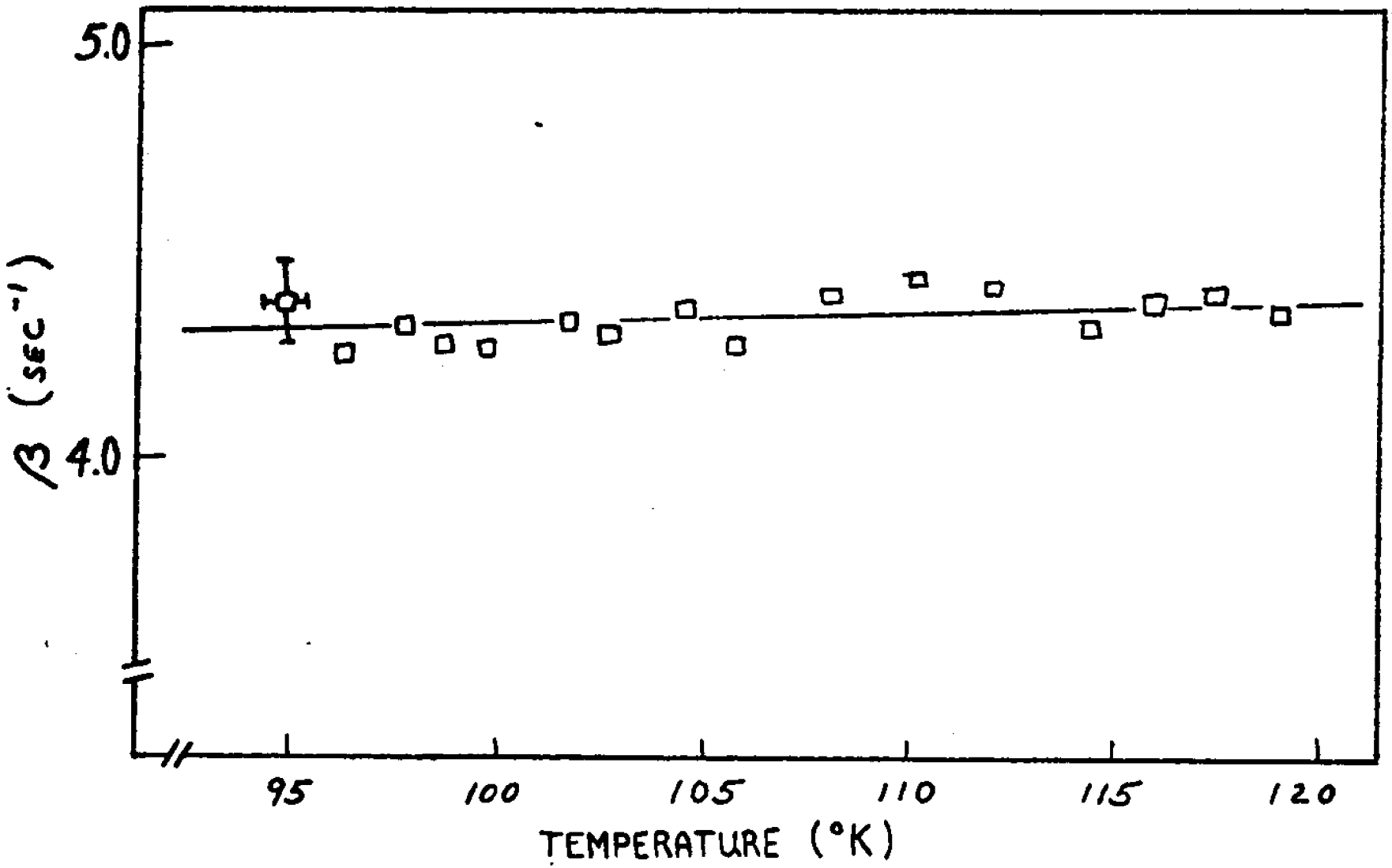

FIG.5.5. Monomolecular Triplet Decay Constant as a Function of Temperature Near the Low Temperature Anomaly in HMB.

anomalous effects were observed for β in phenanthrene on going through the temperature at which phenanthrene exhibits a second-order phase change.

It is of some interest that no effect was observed for the temperature dependence of β, since it is generally assumed to be representative of a phonon assisted process. One must conclude as a result of this experiment that vibrational changes associated with second or higher order phase changes are not strongly coupled to the process of radiative triplet decay.

References - Chapter 5

1. L.F.Fieser and M.Fieser, Organic Chemistry (D.C.Heath and Company,Boston, 1944), p.531.

2. H.M.Huffman, G.S.Parks, and A.C.Daniels, J.Am.Chem. Soc. 52, 1547 (1930).

3. L.O.Brockway and J.M.Robertson, J.Chem.Soc. 1939,1324.

4. S.Seki and H.Chihara, Sci.Papers Osaka Univ. 1, 1 (1949).

5. E.R.Andrew, J.Chem.Phys. 18, 607 (1950).

6. R.C.Leech, D.B.Powell and N.Sheppard, Spectrochimica Acta 22, 1 (1966).

7. J.J.Rush and J.I.Taylor, J.Chem.Phys. 44,2749 (1966).

8. H.Sponer and Y.Kanda, J.Chem.Phys. 40, 778 (1964).

9. D.Olness and H.Sponer, J.Chem.Phys. 38, 1779 (1963).

10. M.W.Windsor,"Luminescence and Energy Transfer" in D.Fox, M.M.Labes, and A.Weisberger,eds.,Physics and Chemistry of the Organic Solid State (Interscience Publishers, New York, 1965), Chapter 4.

11. M.Kasha, Discussions Faraday Society. 9, 14 (1950).

12. R.S.Knox,"Theory of Excitons," Solid State Physics, Supplement 5, 1913

13. W.Whitten, R.A.Arndt, and A.C.Damask, Mol.Cryst. 9,239 (1969).

Appendix A. The Linear Coefficient of Thermal Expansion

In Chapter 2, the capacitance of a parallel plate capacitor is described, which has a single crystal of phenanthrene as the dielectric material. Neglecting edge effects, since they represent errors smaller than the other uncertainties already present in the system, the standard equation for the parallel plate capacitor is:

$$C = \frac{A\varepsilon}{\ell}(0.08842) \qquad (A.1)$$

where C is the capacitance in picofarads, A is the surface area of the electrodes in cm^2, ℓ is the separation of the electrodes in cm, and ε is the static dielectric constant.

In examining this equation, it is noted that ε is not the only temperature dependent term. Since the electrodes are painted surfaces, on opposite sides of the crystal, if the crystal size increases, so will the separation of the electrodes. Phenanthrene, as with most other materials, expands or contracts in accordance with changes in the environmental temperature.

It becomes necessary, if we wish to investigate the effects of temperature on the static dielectric constant, to eliminate the effects of temperature on the separation of the electrodes.

A.1 The Calculation of the Thermal Coefficient of Expansion

The geometry of the sample holder used for this measurement is shown in Fig.A.1, where l_s is the distance between the inner surfaces of the upper and lower glass slides, l_c is the height of the single crystal of phenanthrene, l_g is the width

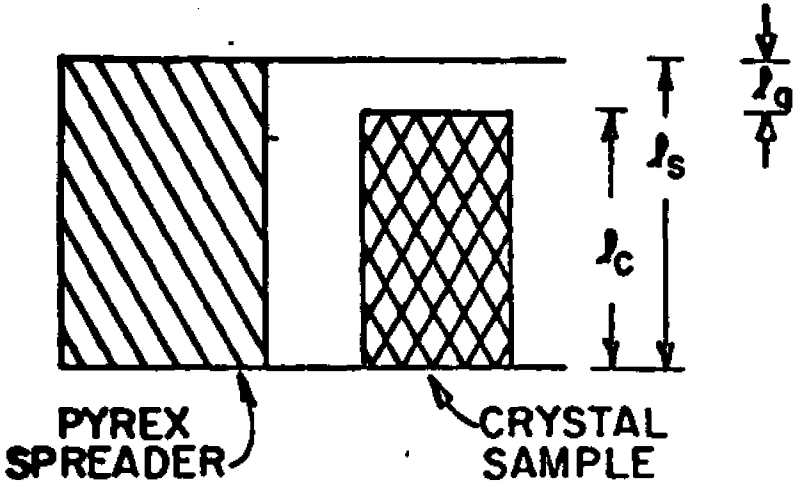

FIG. A.1

Geometry of the Phenanthrene Thermal Expansion Experiment Crystal Holder.

of the air gap capacitor.

For different temperatures, we have:

$$\ell_g(T_1) = \ell_s(T_1) - \ell_c(T_1)$$

and (A.2)

$$\ell_g(T_2) = \ell_s(T_2) - \ell_c(T_2)$$

where the T's represent different temperatures.

Using the first order approximation, the equations become:

$$\ell_g(T_1) = \ell_s(T_0)[1+\alpha_g(T_1-T_0)] - \ell_c(T_0)[1+\alpha_c(T_1-T_0)]$$

and (A.3)

$$\ell_g(T_2) = \ell_s(T_0)[1+\alpha_g(T_2-T_0)] - \ell_c(T_0)[1+\alpha_c(T_2-T_0)]$$

where α_g is the linear coefficient of thermal expansion of the pyrex spreader, and α_c is the linear coefficient of thermal expansion of the crystal sample.

Subtracting the width of the air gap at these two temperatures, to obtain the change in the air gap size, we get:

$$\ell_g(T_2) - \ell_g(T_1) = \ell_s(T_0)\alpha_g[T_2-T_1] - \ell_c(T_0)\alpha_c[T_2-T_1] \qquad (A.4)$$

Solving this equation for α_c, we get:

$$\alpha_c = -\left[\frac{\ell_g(T_2)-\ell_g(T_1)}{(T_2-T_1)\,\ell_c(T_0)} - \alpha_g\frac{\ell_s(T_0)}{\ell_c(T_0)}\right] \qquad (A.5)$$

In performing the experiment, the air gap is made as small as possible to maximize the values obtained for the capacitance of the air gap capacitor. It is, after all, the capacitance of this air dielectric capacitor that we are measuring. This makes the ratio of $\ell_s(T_0)$ to $\ell_c(T_0)$ in Eqt.A.5 approximately equal to unity. Furthermore, the value of the linear coefficient of thermal expansion of the pyrex separator is small compared to that for the crystal. This makes it small compared to the first term in the right hand side of Eqt.A.5. So, we may simplify Eqt.A.5 to

read:

$$\alpha_c = -\left[\frac{l_g(T_2) - l_g(T_1)}{(T_2 - T_1)\, l_c(T_0)}\right] \qquad (A.6)$$

The values for $l_g(T)$ were obtained using Eqt.A.1 solved for l:

$$l_g(T) = \frac{(0.08842)\,A}{C(T)} \qquad (A.7)$$

where for the air dielectric, the dielectric constant is equal to unity, and C(T) are the values for the capacitance of the air dielectric capacitor resulting from the experiment.

A.2 The Sample Holder

The sample holder is shown in Fig.A.2. Flint glass slides were used as the basic structural body of the sample holder. Pyrex spreaders of various sizes were made by sawing a pyrex tube into sections of assorted lengths. The spreaders were held between the two glass slides with a nylon bolt. The bolt had a soft rubber washer at either end to prevent cracking the slides in the event of inadvertently tightening down too hard on the bolt.

The crystal sample was glued to the the lower slide using "Duco"cement around the sides only. Care was taken to insure that no glue got under the crystal, since this would effect the expansion properties of the air gap.

The top electrode was made by gluing a piece of brass shim, cut in the shape of the top surface of the crystal, to the under side of the top slide, using the "Duco" cement. A #40 copper wire was glued at one end to the brass electrode, using "Dupont #817" silver conducting paint. The wire was then glued

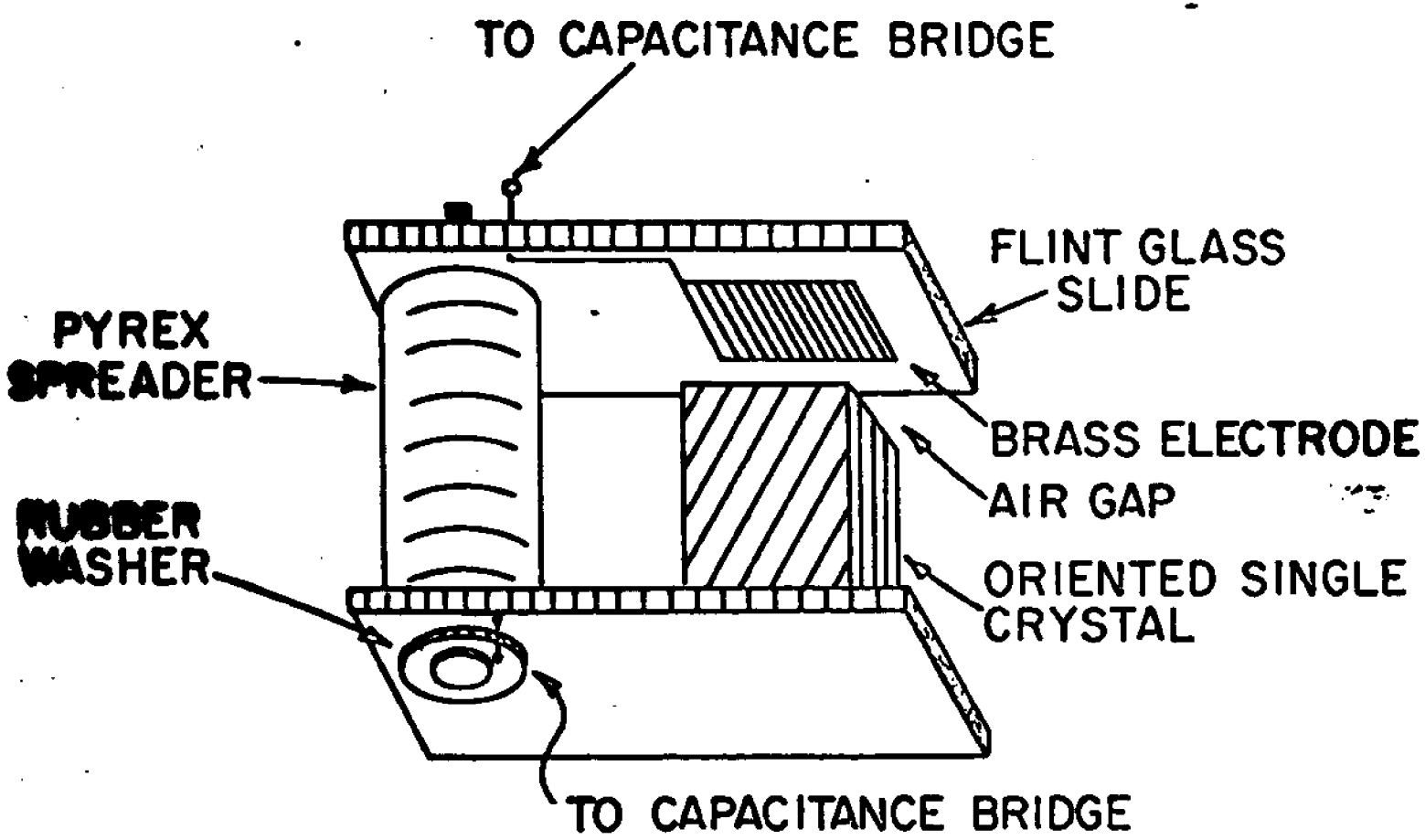

FIG. A.2

Crystal Holder for Measuring the Linear Coefficient of Thermal Expansion. Approximately 2X Actual Size.

to the glass slide, using "Duco" cement, and run back to the spreader, where a hole was drilled in the upper slide. The wire was fed through this hole to a #24 Teflon insulated wire that was secured to the holder using epoxy cement. (See Fig.A.3)

The lower electrode was the top surface of the phenanthrene crystal, painted with the"Dupont #4817" paint. A short piece of #30 copper wire was glued tothis electrode using the "Dupont #4817" paint. The wire was then run down the crystal, glued to the lower slide using the "Duco"cement, and out through a hole drilled in the bottom slide, near the spreader. It was ben attached to another #24 Teflon insulated wire, as in Fig.A.3. These two #24 wires were then attached to the capacitance bridge, described in Chapter 2. The sample holder was then placed in the temperature bath, also described in Chapter 2.

The capacitance of the resulting air dielectric capacitor was then monitored as a function of temperature. The separation of the plates of this capacitor was determined by the expansion properties of the crystal, which was supporting the lower electrode, and to a lesser extent by the expansion properties of the pyrex spreader. This however, had a linear coefficient of thermal expansion of only about $0.03\times10^{-4}/°C$.

A.3 Techniques and Results

The experiment is performed in exactly the same way as the experiment described in Chapter 2.

Eqt.A.7 is used to convert the measured capacitances into values for the gap width. Fig.A.4 shows the functional dependence

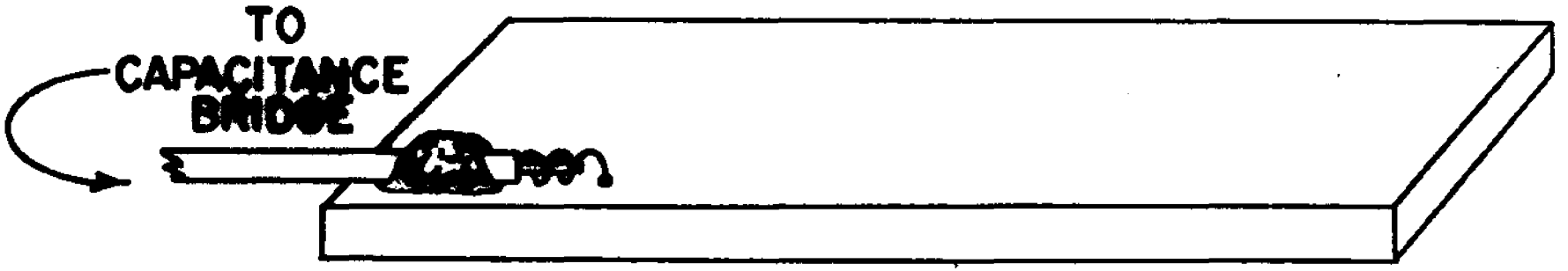

FIG. A.3

Epoxy Cement Used to Secure Electrical Lead
to Crystal Holder Plate.

of the gap width on temperature.

From the slopes of the lines in Fig.A.4, and the fact that the crystal length is approximately constant, we may use Eqt.A.6 to calculate the linear coefficients of thermal expansion. The results in the three crystallographic directions are given in Table A.1.

A.4 Discussion

The results shown in Table A.1, for the values of the thermal expansion coefficients, agree with those obtained by Matsumoto[1]. Matsumoto 's work, unfortunately was done on fused samples, and therefore only an average value was obtained in his work. This investigation overcomes this difficulty by using single crystals oriented in the a, the b, and the c' directions.

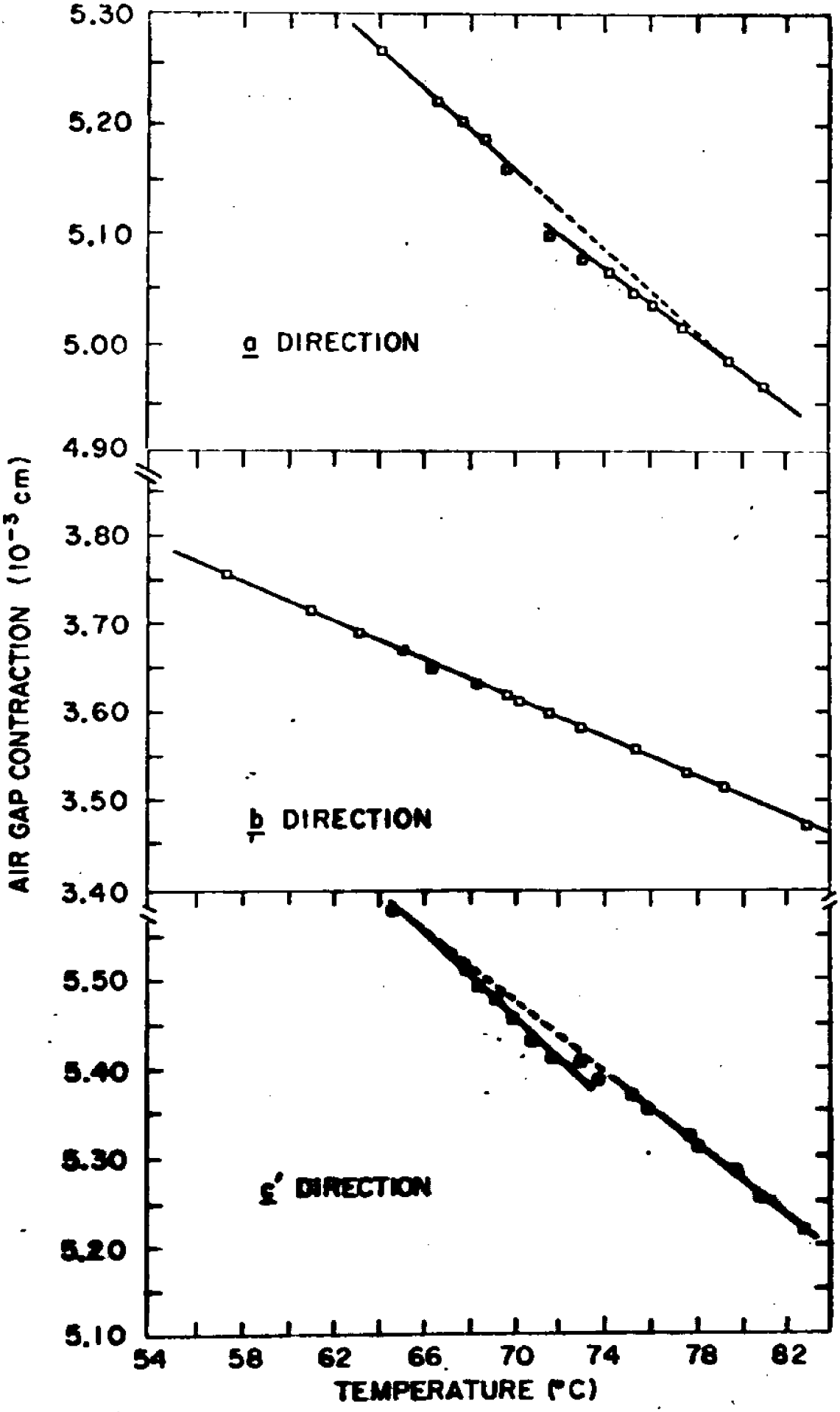

FIG.A.4. Air Gap Contraction as a Function of Temperature, Calculated From the Measured Air Gap Capacitor.

Crystal Direction	α Below, x 10^{-4}/ C	α Above, x 10^{-4}/ C
a	0.74	0.64
b	0.34	0.34
c'	2.2	1.8

Table A.1. Linear Coefficients of Thermal Expansion α of Phenanthrene in the Three Crystallographic Directions Above and Below 72 C.

Appendix B. The Anisotropic Dielectric Constant of Phenanthrene and Naphthalene

The room temperature capacitane of the crystals with the painted electrodes were determined using the capacitance bridge described in Chapter 2. The crystals were made as thin and as large in surface area as possible. Typical dimensions were 1mm x 7mm x 7mm. Special care was taken in minimizing any background capcitance. Also, residual capacitance, with the crystal sample missing was determined and subtracted from the results of the capacitance measurements.

If Eqt.A.1 is solved for ϵ, one obtains

$$\epsilon = \frac{dC}{(0.08842)A} \qquad (B.1)$$

where C is the room temperature capacitance with the residual capacitance subtracted out.

Using different crystals cut from the same boule, several measurements were made in each of the three crystallographic directions. The average value in each direction for phenanthrene is indicated in Table B.1a. The average value in each direction for naphthalene is indicated in Table B.1b. The errors represent the maximum deviations from the average value.

a)

Crystal Direction	Dielectric Constant
$\underline{a}$	4.9 ± 0.3
$\underline{b}$	2.5 ± 0.2
$\underline{c}'$	3.1 ± 0.3

PHENANTHRENE

b)

Crystal Direction	Dielectric Constant
$\underline{a}$	3.0 ± 0.2
$\underline{b}$	1.9 ± 0.2
$\underline{c}'$	4.2 ± 0.3

NAPHTHALENE

Table B.1. Dielectric Constant at 1 kHz in the Three Crystallographic Directions at Room Temperature for (a) Phenanthrene and (b) Naphthalene.

Appendix C. Anisotropic Drift Mobility Measurements on Naphthalene

C.1 Calculation of the Drift Mobilities

For space-charge free, ohmic conditions (i.e., $V \propto I$), the drift mobility is defined as:

$$\mu_D = \frac{d^2}{Vt} \qquad (C.1)$$

where d is the crystal thickness, between electrodes, in cm., t is the transit time, in seconds, and V is the applied voltage, in volts.

Space charge effects were eliminated by selecting the proper field strength. For high fields and low light intensity, space charge effects are minimized. These parameters were adjusted so that an ohmic dependence of I on V was obtained.

The effects of trapping are not significant to the analysis, since the transient currents used represent the nearly trap free case. This is because it takes a finite time for the traps to fill after a step current pulse is applied.[2]

C.2 The Experimental Procedure

The drift mobility of single crystal naphthalene was measured using a pulsed photo-injection technique described by Kepler[3]. A block diagram of the equipment is shown in Fig.C.1.

A light pulse of about 1μ sec duration was obtained from a xenon flash tube, powered by a 1μ farad capacitor, charged to about 10 kilovolts.

A Corning Glass 7-59 filter was used to allow only highly absorbed light to fall on the crystal. This is to prevent bulk injection of carriers.

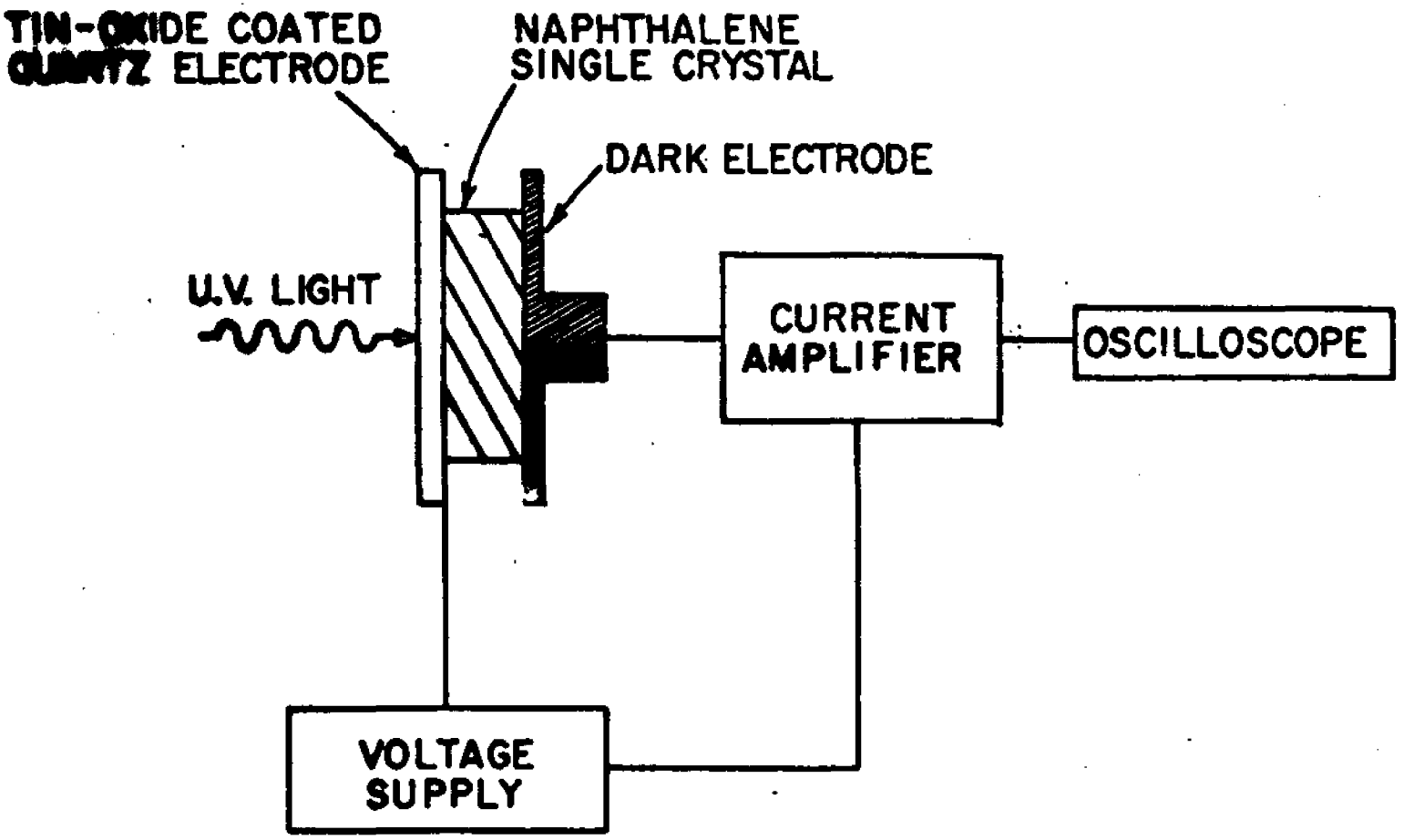

FIG. C.1

Block Diagram for the Pulsed Photoconductivity Measurement of the Drift Mobility in Naphthalene.

By adjusting the polarity of the injecting electrode, (the illuminated electrode), either holes or electrons may be made to sweep through the crystal.

A current amplifier, of about 1μ sec rise time, amplifies the resulting current pulse. An oscilloscope is then used to trace the voltage drop across a resistor in the amplifier, as a function of time. This allows for the determination of the transit time. See Fig.C.2.

Fig.C.2a shows an example of such a trace. Fig.C.2b indicates the significant intervals of the trace of the photo-current distribution as a function of time. The density of carriers is plotted vertically. At T=0 the charge carriers are created near the injecting electrode surface. After entering the crystal, the carriers move towards the dark electrode due to the applied field. Diffusive spreading of the current pulse is evident by $T=T_1$. The current having reached a maximum here, this corresponds to the beginning of the flat portion. Some time later, at $T=T_2$, the carriers are further along, and more diffusion results. Finally, at $T=T_3$, some of the carriers of the now rather diffuse pulse are reaching the dark electrode. This corresponds to the tail in Fig.C.2a. The time up to $T=T_3$ is then the transit time. So from the trace, Fig.C.2a, the transit time is the time from the start of the pulse, to the beginning of the decaying tail.

The thickness of the crystal was determined using a micrometer.

Measurements were made in the a, b, and the c' directions. The results for both holes and electrons are shown in Table C.1. The numbers are the result of several trials in each direction,

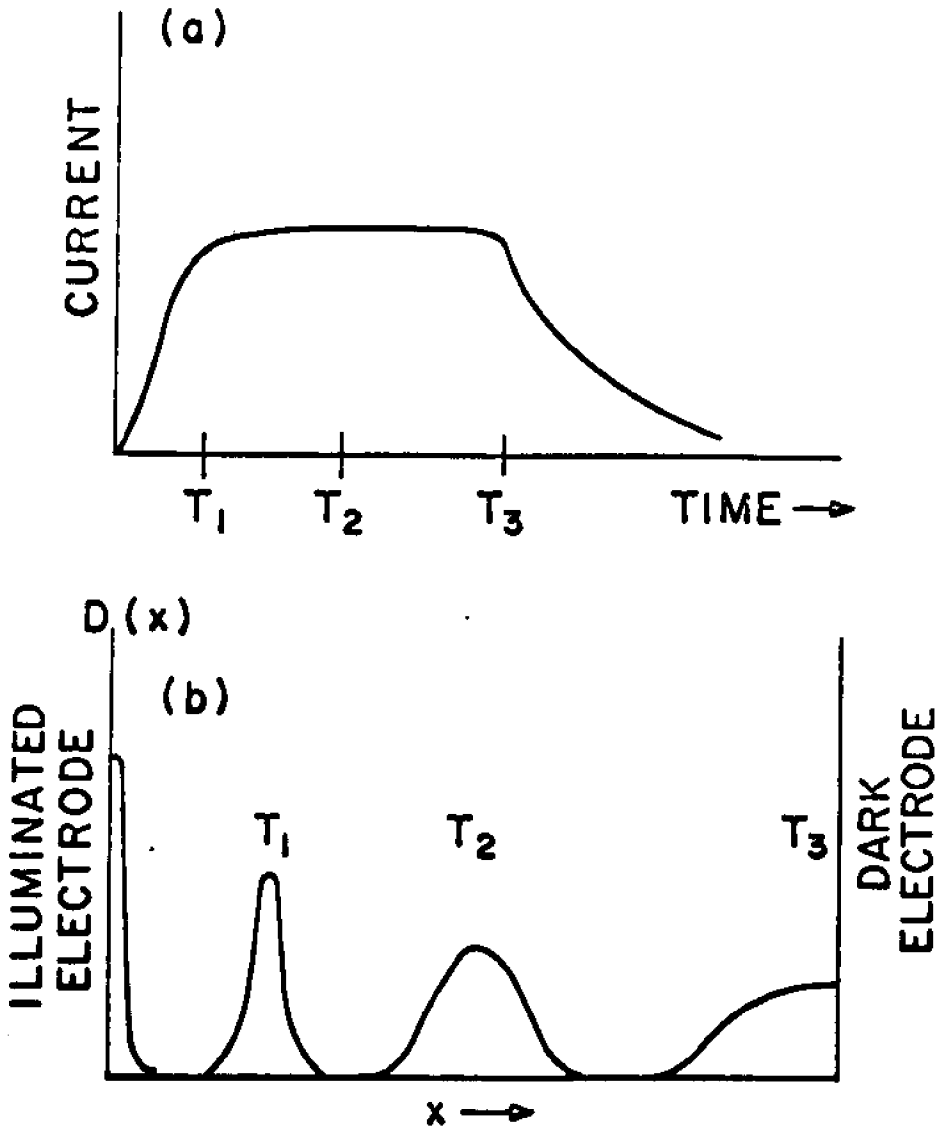

FIG. C.2

(a) The Photocurrent as a Function of Time.
(b) Distribution of the Current Pulse Along the Crystal at Various Time Intervals.

Direction		Drift Mobility (cm^2/V-sec)
a		0.80 ± 0.05
b	Holes	1.20 ± 0.10
c'		0.50 ± 0.05
a		0.60 ± 0.05
b	Electrons	0.50 ± 0.05
c'		0.60 ± 0.05

Table C.1. The Drift Mobilities for Naphthalene at Room Temperature, for Holes and Electrons Drifting in Each of the Three Crystallographic Directions.

and represent the average of the trials. The errors are the maximum deviations from the averages.

These results compare favorably with those of Silver, et al.[4]

Appendix D. The Brookhaven High Flux Beam Reactor

The Brookhaven High Flux Beam Reactor obtains a high flux by virtue of a small core and reflector. This limits the number of ports to nine compared to the fifty or so available at the Brookhaven Graphite Research Reactor. The full power rating is 40 megawatts, but has not yet been operated at this high level. The thermal flux is 7×10^{14} neutrons/sec-cm^2.

Fig.D.1 shows the cold neutron beam port, which is 12 inches wide compared to 4 inches for the other ports. As with the Graphite Reactor, the beam is filtered using polycrystalline beryllium cooled to liquid nitrogen temperature. The standard time-of-flight analysis techniques are employed at the Slow Chopper Facility with the addition of a Scientific Data System SDS-910 computer tie-in for data accumulation. The detectors were the standard BF_3 type described in Chapter 3.

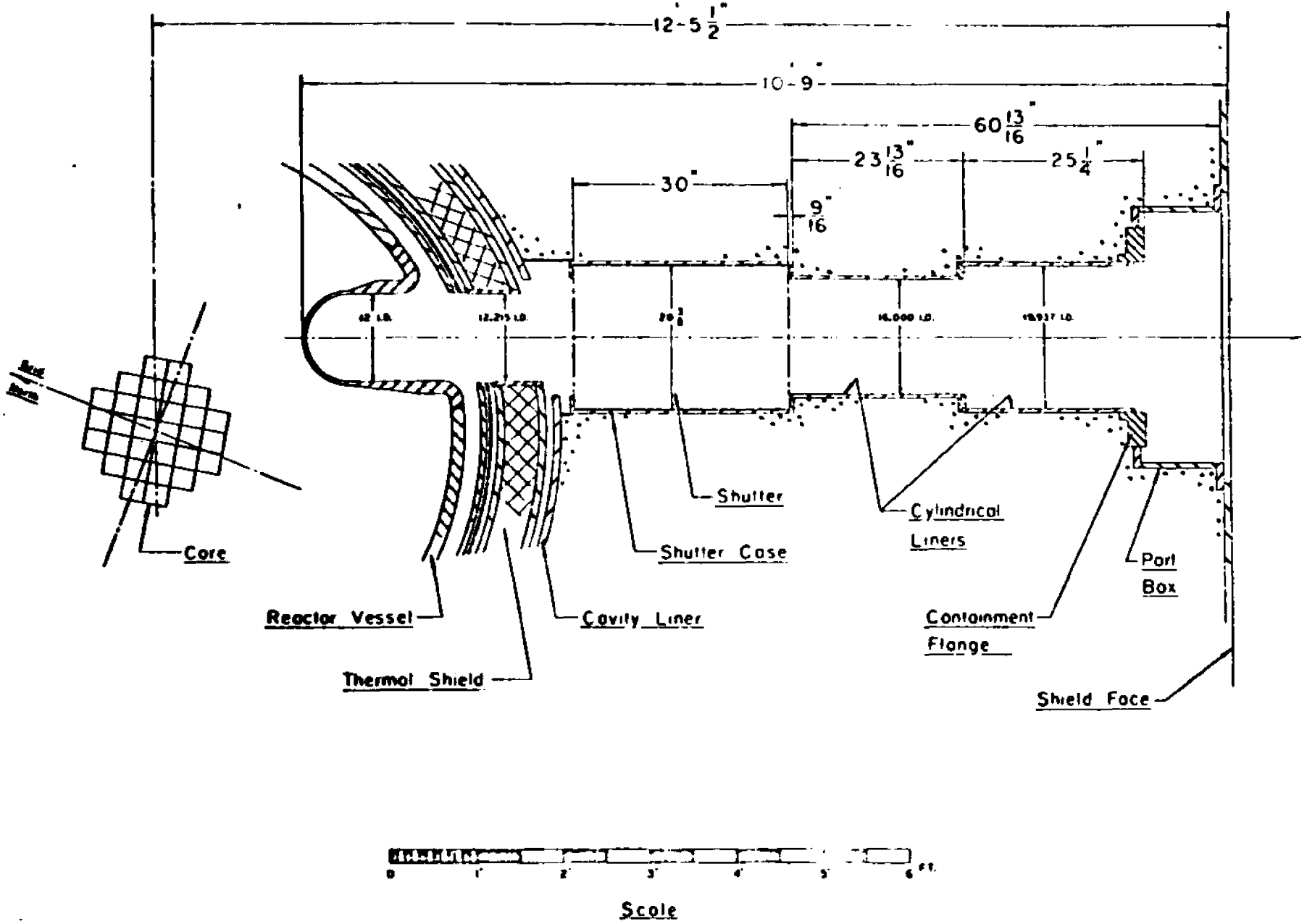

FIG.D.1. The Cold Neutron Beam Port at the High Flux Beam Reactor.

References - Appendix

1. S.Matsumoto, Bull. Chem. Soc. Japan 39, 1811 (1966).

2. P.Mark, Techniques and Interpretation of Transient Measurements, Abst. Org. Cryst. Symp.,NRC, Ottawa, Canada, Oct.,1962, p.75.

3. R.G.Kepler, Phys. Rev. 119, 1226 (1960).

4. M.Silver, J.Rho, D.Olness, and R.C.Jarnagin, J. Chem. Phys. 38, 3030 (1963).

SUMMARY

Dielectric constant measurements and cold neutron inelastic scattering measurements indicate that phenanthrene exhibits properties similar to a ferroelectric. The static dielectric constants and thermal expansion coefficients were obtained in the three crystallographic directions and reflected anomalous behavior. The prediction was made that the space group symmetry would change above the anomaly temperature.

Since the range of sensitivity of our instruments did not allow for Hall effect measurments on phenanthrene, naphthalene, a largely similar material, was chosen for the measurment. A complete set of data was obtained which allowed for the rejection of particular energy band structures.

Finally, the temperature dependence of the triplet exciton decay for hexmethylbenzene was determined. This material, having a known transition involving the onset of rotation of the methyl groups, showed that, as in previous work on phenanthrene, no anomalous behavior was apparent at the transition temperature.

AUTOBIOGRAPHY
of
DAVID H. SPIELBERG

I was born in Brooklyn in 1943, where I lived until my family moved to Queens in 1951. In public school, I was interested in art and attended a special creative projects class in the sixth grade. However, by the time I entered high school I had become interested in science. In my senior year in high school I attended a special experimental laboratory course. As an extra curricular activity, I became co-captain of the Martin Van Buren High School Gymnastics team.

When I entered Queens College as an engineering major I found my gymnastics practice toodemanding of my time. As a substitute I joined the Queens College sailing team. Sailing has remained a great source of enjoyment to me.

After my first year in college I changed to a physics major. In 1964 I recieved my B.A. degree. I was accepted to Queens College to do my graduate work. In addition, during the summer I was married. I recieved my M.A. in 1967.

While in graduate school I supplemented my wife's income by teaching general physics at Queens College . After entering the Ph.D. program of the City University of New York in 1965, I recieved a three year NASA traineeship.

While under the direction of Professor A.C.Damask, I performed the research requirements for the Ph.D. degree at Brookhaven National Laboratory.